7 Chapter 7: Development and characterization of transgelosome of standardized *Piper longum* fruit extract for melanoma therapy

7.1 Background

The anatomical architecture of the skin, mainly the stratum corneum, is a major challenge for the transdermal route of administration. The ultradeformable nanovesicular transferosomes (TFs) have been perceived as the most promising novel topical vesicular formulations for improving transdermal permeability and therapeutic activity of plant bioactives. TFs possess low viscosity, so they can be incorporated into suitable gelling agents to increase the viscosity for achieving prolonged residence time at the application site and improving topical applicability. The incorporation of TFs into gel develops transgelosome (TFG), which offers the advantage of both TFs and gel. The study aimed to develop and optimize of ultradeformable nanovesicular transgelosome of standardized *Piper longum* fruits ethanolic extract (PLFEE) via a thin-film hydration method for melanoma therapy. To our knowledge, no reports are available for the standardized PLFEE-loaded transgelosome for melanoma cancer therapy. Further, the combination of hydrogenated phosphatidylcholine (Phospholipon® 90 H) as membrane former, Tween® 80 as edge activator, and Xanthan gum as gelling agent is not explored for the development of TFG. The ultradeformable vesicular TFs formulation has been optimized using CCD-based QbD approach to obtain the best formulation with low hydrodynamic vesicular size (Z_{avg}), maximum % entrapment efficiency (% EE), and optimum flexibility. The optimized TFs were loaded into the Xanthan gum-based hydrogel to produce TFG and characterized for their physicochemical properties, pharmaceutical properties, and *in-vitro* and *in-vivo* anticancer activity in melanoma (B16F10) bearing C57BL/6 mice.

7.2 Objectives

- Development of TFs of standardized PLFEE via thin-film hydration method
- Response surface analysis and optimization using CCD using Design-Expert® software.
- Physicochemical and pharmaceutical characterizations of optimized TFs
- Development of transgelosome (TFG) of optimized TFs
- Physicochemical and pharmaceutical characterizations of optimized TFG
- *In-vitro* anticancer activity, cellular migration, and cellular uptake studies
- *Ex-vivo* skin permeation study
- *In-vivo* anticancer activity study in melanoma (B16F10) bearing C57BL/6 mice

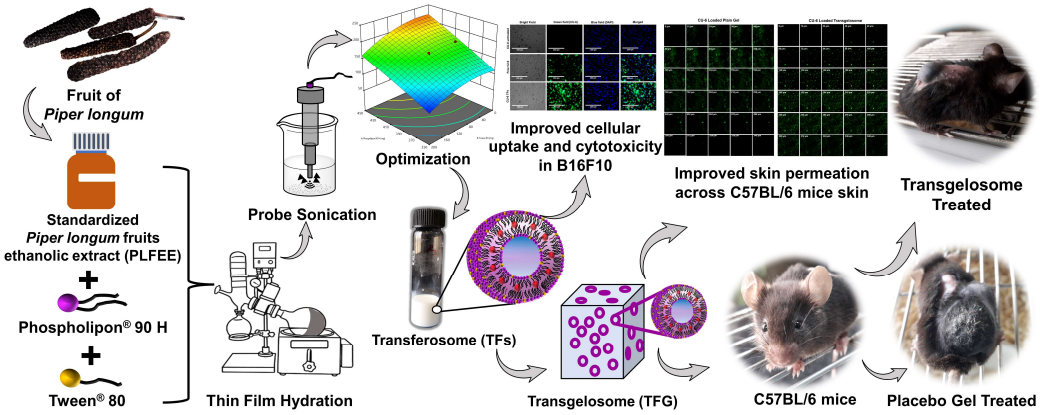

Figure 7. 1 Schematic representation of workflow of Chapter 7

7.3 Methodology

7.3.1 Formulation and Development of transferosome (TFs) of standardized PLFEE

Standardized PLFEE-loaded TFs formulations were prepared by the thin-film hydration-based rotary evaporation method. The required amount of Phospholipon® 90 H (PL-90 H), Tween® 80 (T-80), and 250 mg of standardized PLFEE was mixed with 40 mL of absolute ethanol in a 100 mL round-bottom flask and subjected to a bath sonicator for 30 min to achieve solubilization and molecular interaction of PLFEE with excipients. Afterward, the ethanol was evaporated with a rotary vacuum

evaporator at 40° C, 70 rpm, until a thin film was formed inside the walls of the flask. The residual solvent trace from the film was removed under vacuum (for 6 h) and hydrated with Type-I ultra-pure water for 1 h by shaking with an orbital shaker (REMI, RS 12 plus) to produce transferosome (TFs) vesicles. The vesicle size reduction was achieved by probe sonication (Hielscher ultrasound technology, Germany) at 80% amplitude with 1 cycle (at an interval of 120 seconds) for a different time as per the experimental design. Briefly, the TFs were poured into a screw-capped glass vial and placed in an ice-filled beaker before probe sonication to avoid degradation due to heat. The unentrapped extract was removed by centrifugation and discarding the supernatant. Then, the TFs was stored and protected from light at 4° C.

7.3.2 Response surface methodology (RSM) and optimization

RSM was used to examine the influence of CMAs, such as the quantity of PL-90 H (X_1 = mg), the quantity of edge activator or T-80 (X_2 = mg), and CPP, like probe sonication time (X_3 = min) on CQAs, such as average hydrodynamic vesicular size ($Y_1 = Z_{avg}$), entrapment efficiency of major bioactive component PIP (Y_2 = % EE), and flexibility of TFs (Y_3 = Flexibility). The RSM was studied using a 3-factor, 5-level rotatable (α value of 1.681) CCD via a Trial version of Design-Expert® software (Version-12, Stat-Ease Inc., Minneapolis, MN, USA). Preliminary experiments were conducted to identify the possible ranges of the independent variables that have a strong influence on the several dependent variables (Z_{avg}, % EE, and flexibility) chosen for this investigation. A total of 20 batches (6 replications of central points + 6-star points (axial points) + 8 cube points (factorial points) were produced by the software. The experimental results (CQAs) of 20 batches were fed into the software and analyzed by ANOVA to investigate model adequacy and significance ($p<0.005$). Statistical parameters, such as correlation coefficient (R^2), model F-value, model p-

value, lack of fit F-value, lack of fit p-value, the difference between predicted and adjusted R^2 value, and adequate precision (signal to noise ratio) were considered to investigate model adequacy. To envisage the best TFs formulation, the model was fitted to linear, two-factor (2F) interactions, quadratic, and cubic models. The software-generated polynomial equations were used to examine the factor-response relationship. The interaction effect of the CMAs and CPP on the CQAs was also observed using response surface graphs. Optimum CMAs and CPP essential for the development of desired TFs (high % EE, acceptable particle size, and optimum flexibility) were acquired by numerical and graphical optimization techniques available in the software. Finally, the predictability of the rotatable CCD model was verified by formulating checkpoint batches (n = 5) of optimized TFs formula as suggested by Design-Expert software and evaluating the corresponding CQAs. A quantitative comparison was made between the experimental values and software-based theoretical prediction by calculating the percentage prediction error by Equation 7.1.

$$\%\ Prediction\ error = \frac{Experimental\ result - predicted\ result}{Predicted\ result} \times 100 \qquad (7.1)$$

7.3.3 Characterization of TFs

7.3.3.1 Organoleptic characteristics

The prepared TFs were evaluated for color, clarity, homogeneity, transparency, etc.

7.3.3.2 pH

The pH of TFs was measured in triplicate at 25°C using a digital pH meter (PC 700, Eutech Instrument, Singapore) which was previously calibrated using pH 4, pH 7, and pH 10 buffer solutions.

7.3.3.3 Refractive index (RI)

The RI of all the TFs was estimated to verify the isotropy of the formulations by estimating and comparing the RI of samples collected from three different regions of each TFs formulation. It was determined by a digital Abbe-type refractometer (Labman Scientific Instruments Pvt. Ltd., India) equipped with a Tungsten lamp, refractometer prisms, monocular system, temperature controller, and telescopic adjustment system at 25 ± 1°C. Briefly, the prisms were cleaned thoroughly, and a few drops of the undiluted TFs were spread evenly on the surface of the lower illuminating prism for measuring the RI. The experiment was carried out in triplicates, and the average results were reported.

7.3.3.4 Entrapment Efficiency (EE) and Loading Capacity (LC)

EE for major active constituent (PIP) was estimated by the validated HPLC method. The ultracentrifugation method was used to separate the un-entrapped PIP (free drug) in supernatant from the encapsulated drug in pellet form. Briefly, each formulation was centrifuged at 100,000 g at 4°C for 1 h using an ultracentrifuge (Beckman Optima XPN-100, Palo Alto, CA, USA) with an SW 90 Ti rotor. The quantity of PIP in the supernatant after the centrifugation was estimated by the HPLC method at 342 nm after suitable dilution with HPLC-grade methanol. The EE was then calculated by Equation 7.2.

$$EE\ (\%) = \frac{PIP_T - PIP_S}{PIP_T} \times 100 \qquad (7.2)$$

Where EE is the entrapment efficiency, PIP_T is the total amount of PIP in the formulation (amount of PIP in 100 mg of PLFEE), and PIPs is the amount of free PIP in the supernatant after centrifugation.

The LC was calculated as per Equation 7.3.

$$LC\ (\%) = \frac{PIP_T - PIP_S}{Exc_T} \times 100 \qquad (7.3)$$

Where LC is the loading capacity, PIP_T is the total amount of PIP in the formulation, PIPs is the amount of free PIP in the supernatant after centrifugation, and Exc_T is the total amount of excipient used in the formulation.

7.3.3.5 Z_{avg}, PDI, and ζ

The Z_{avg}, PDI, and ζ of TFs were measured using a dynamic light scattering (DLS) instrument (Zetasizer Pro, Malvern Panalytical Ltd., UK) equipped with ZS Xplorer software (version 2.3.1) at a scattering angle of 173° at 25°C. The Z_{avg} and PDI were acquired using a polystyrene disposable cuvette (DTS0012), whereas the ζ was measured using a universal dip cell (ZEN1002) having palladium electrodes with 2 mm spacing. Each of the TFs was diluted 20 times with Type-I ultra-pure water and filtered through a 0.45 µm polyvinylidene fluoride (PVDF) syringe filter (AXIVA Sichem Pvt. Ltd.) to avoid multiple scattering effects.

7.3.3.6 Flexibility

The vesicular flexibility was measured via an in-house fabricated device (Figure 7. 2) by passing the TFs through a membrane filter (0.05 µm), connected to a vacuum pump (Axiva, chemVk V300, Haryana, India). Each formulation was diluted with 10 mL of water and passed through the membrane filter under a constant vacuum (30 mm Hg) for 5 min. The flexibility was calculated as an indicator of elasticity using Equation 7.4 [162].

$$F = J\left(\frac{r_v}{r_p}\right)^2 \qquad (7.4)$$

where F is the flexibility (mL/s), J is the amount of dispersion filtered (mL) per unit time (s), r_v is the size of vesicles after extrusion (nm), r_p is the pore size of the filter membrane (nm).

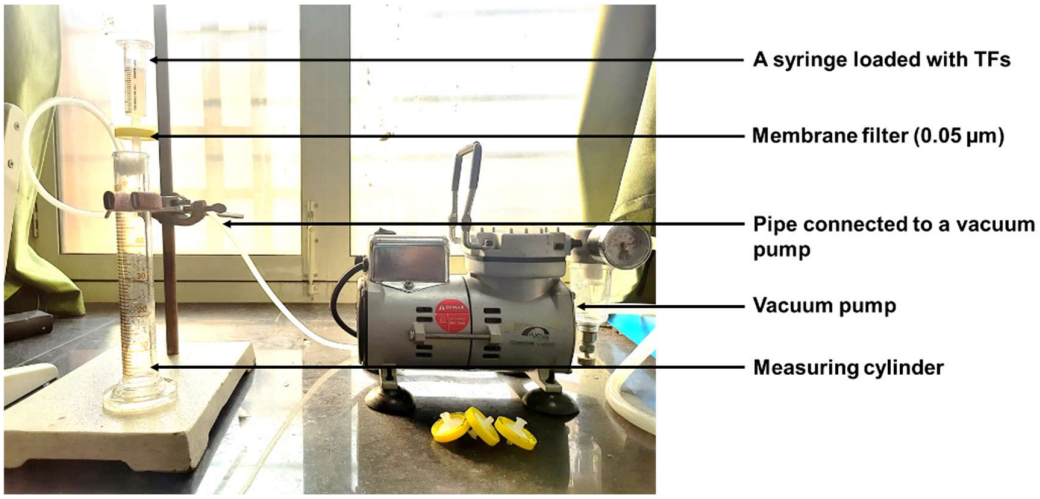

Figure 7. 2 In-house fabricated device for the flexibility determination of TFs

7.3.3.7 Optical Microscopy

Microscopic images of optimized TFs were captured (at 4X and 10X magnification) by a digital microscope (Magnus MLX Plus, Olympus Opto Systems India Pvt. Lt d., Uttar Pradesh, India) equipped with a digital camera (5.1 MP, Magcam DC 5, ½.5" CMOS Sensor) and Magvision software (version x36, 3.7.6820). The optimized TFs were dropped on a glass slide and subjected to the microscope for analyzing vesicular structure.

7.3.3.8 HRSEM

HRSEM photomicrographs of optimized TFs were taken using a high-resolution scanning electron microscope (FEI Nova^{TM} Nano SEM 450, FEI, USA) equipped with Everhart–Thornley detector (ETD) and xT Microscope software control software (version 1.0) at an accelerating voltage of 15 kV. The optimized TFs were dropped onto a clean glass slide (1 cm^2) and dried overnight at room temperature to obtain a

thin film. Before being subjected to the instrument, the sample was mounted on an aluminum stub using double-sided carbon tape followed by sputter coating by a desk sputter coater (DSR 1, Nanostructured Coating Co., Iran) with palladium and gold at a ratio of 40:60 w/w for 2 min.

7.3.3.9 Scanning probe microscopy (SPM)

The analysis was performed using an SPM instrument (NTEGRA Prima, NT-MDT Service, and Logistics Ltd.) equipped with Nova Px software (version 3.4.0). The sample was dropped onto a clean glass slide, dried naturally, and subjected to the instrument for morphological analysis.

7.3.3.10 HRTEM and SAED analysis

The HRTEM and SAED patterns of optimized TFs were examined to investigate the vesicular morphology and crystallinity. The analysis was carried out using a high-resolution transmission electron microscope (TECNAI G2 F20 TWIN, FEI, USA) equipped with high angle annular dark field (HAADF) detector and Gatan's Digital Micrograph software (version 3.7.4) at 200 kV using a carbon-coated copper grid (Ted Pella, 400 Mesh, 3.05 mm diameter). The TFs samples were diluted 20 times with Type-I ultra-pure water, filtered through a 0.45 μm syringe filter, and 20 μL of the diluted TFs was dropped onto the TEM grid and dried overnight at room temperature. The excess amount of the sample was removed by soaking it in soft tissue paper. The HRTEM photomicrographs were analyzed using ImageJ software (National Institutes of Health (NIH), Bethesda, Maryland, version 1.53e, Java 1.8.0_172), and the average size was calculated.

7.3.3.11 Drug excipient compatibility study

The drug excipient compatibility was studied by ATR-FTIR and HPTLC.

7.3.3.11.1 ATR-FTIR

ATR-FTIR analysis of standardized PLFEE, PL-90H, physical mixture, and optimized TFs was carried out to predict the possible interaction between PLFEE and excipients using an ATR-FTIR spectrophotometer (Bruker Alpha II, Bruker Optics, Ettlingen, Germany) equipped with an ATR accessory. Since the optimized TFs are liquid, it was freeze-dried for 12 h (LFD-BT-101, Labocon Scientific Limited, UK) before ATR-FTIR analysis to avoid the broad peak of water. Data acquisition was made using OPUS software (Version: 7.0) within the wavenumber of 4000-400 cm^{-1} with 4 cm^{-1} spectral resolution and 40 scans.

7.3.3.11.2 HPTLC

The compatibility of PLFEE with the TFs excipients was further analyzed by HPTLC fingerprinting. The chemical integrity of PIP and PLGN in the ethanolic extract PLFEE, physical, and optimized TFs was investigated by qualitative fingerprinting analysis with HPTLC instrument (CAMAG) equipped with WinCATS software (Version: 1.4.7.2018). Fingerprinting was carried out on 20×10 cm silica gel 60 F254 precoated aluminum plates (E. Merck, Darmstadt, Germany). Pure PIP, PLGN, PLFEE, physical mixture, and optimized TFs were dissolved in ethanol and centrifuged (10000 rpm for 5 min), and the supernatant was used for HPTLC fingerprinting. Accurately, 5 µL of each sample solution was applied in triplicate on a pre-coated aluminum plate (1^{st} band x = 15 mm, y = 8 mm) at a dosage speed of 100 nL/s with 8 mm band width by Linomat V sample applicator (CAMAG, Switzerland) attached with 100 µL CAMAG syringe. Then, the plate was developed in a pre-saturated twin trough glass chamber (CAMAG, 20 x 10 cm) up to 90 mm distance using 10 ml of mobile phase (toluene: ethyl acetate (6:4 v/v)) and dried by hair drier (Philips India Ltd., India). Then the dried plate was scanned by HPTLC scanner

(CAMAG TLC Scanner IV) at a scanning speed of 20 mm/s with a slit dimension of 6.00 × 0.45 mm micro at 254, 340, 342, and 366 nm wavelength. The values of the retardation factor (Rf) of pure phytoconstituents and the samples were compared to predict possible drug-excipient compatibility [93]. The fingerprint of the developed plate was visualized in CAMAG TLC Visualizer 2, and photographs were captured by the charge-coupled device (CCD) camera (SONY, Super HAD, HDR).

7.3.3.12 PLM

PLM images of PLFEE, PL-90H, physical mixture, and freeze-dried optimized TFs (TFs FD) were captured at 10X magnification using a polarizing microscope (Radical RXLr-5, New Delhi, India) furnished with a digital microscopic camera (Procam, 5 MP) and Radical ProCam software (Version 3.7) under the crossed polarizer analyzer arrangement at 25°C. Samples were sprinkled on a microscopic glass slide and subjected to the polarizing microscope. Samples were inspected under various setups, including plain polarized light to crossed polarized light (XPL) at various angles (from 0° to 120°) by rotating the analyzer slider fitted at the top.

7.3.3.13 XRD

The crystallinity of PLFEE, PL-90H, T-80, physical mixture, and optimized TFs were examined by a desktop X-ray diffraction system (Rigaku Miniflex 600; Tokyo, Japan) using Ni-filtered Cu Kα radiation (λ = 1.5406 A°) at current 15 mA and voltage 40 kV. The XRD pattern was recorded using MiniFlex Guidance software (Version 2.0.2.1) over a range of 2 Theta from 10° to 100° with a step size of 0.02°/step at a scan speed of 7°/min at 25°C. Since Tween® 80 is a viscous liquid, the drop cast technique was used to examine its XRD pattern by preparing a thin film of the sample on a glass plate via dropping and drying at 40°C.

7.3.3.14 DSC

DSC of PLFEE, PL-90H, physical mixture, and the optimized TFs were carried out using a DSC apparatus (DSC 60 Plus, Shimadzu, Japan) equipped with TA-60WS Collection software (Version 2.21). An empty pan was used as the blank, and the instrument was calibrated with indium (melting point of 156.6°C) before the examination. Approximately 5 mg of each sample was placed in a pierced aluminum pan and kept in the thermal chamber of the DSC. The analysis was carried out at a linear heating rate of 10°C/min from 25 to 350°C in a nitrogen atmosphere at a flow rate of 100 mL/min.

7.3.3.15 TGA

TGA analysis of PLFEE, PL-90H, physical mixture, and the optimized TFs was carried out using TGA apparatus (Shimadzu TGA-50 analyzer, Shimadzu, Japan) equipped with TA-60WS Collection software (Version 2.21). The analysis was performed under a stream of nitrogen (flow rate of 100 mL/min) by linearly heating the samples (~10 mg) from 10 to 800°C (heating rate of 10 °C/min) in a platinum pan.

7.3.3.16 Stability study

The stability testing of optimized TFs was carried out as per ICH guidelines (ICH Q1 R2). The optimized TFs were filled in the sterile glass vial and subjected to long-term stability condition (5 ± 3°C) for 12 months and accelerated condition (25 ± 2°C/60 ± 5% RH) for 6 months. Periodically (long term: at 0, 6, 9, and 12 months; accelerated condition: 0, 3, and 6 months), the formulations were evaluated for evaluating stability. Further, the stability of the optimized TFs was also evaluated under stress conditions, such as heating-cooling and freeze-thaw cycle. The stability was accessed after 3-cycles of a heating-cooling cycle (one cycle: 40°C and 4°C each for 24 h) and freeze-thaw (one cycle: -20°C and 25°C each for 24 h). Various stability-indicating

parameters, such as colloidal dispersion stability (Z_{avg}, PDI, and ZP), physical properties (color, pH, RI, structural integrity/ optical microscopy, sedimentation, precipitation, and phase separation), chemical properties (FTIR), and pharmaceutical properties (% EE, % LC, and flexibility) were accessed intermittently and at the end of the study. In addition, the lyophilization stability was evaluated for the possible change in colloidal and pharmaceutical properties. Briefly, the freshly prepared optimized TFs were subjected to pre-freezing at -20°C overnight, followed by lyophilization in a lyophilizer (LFD-BT-101, Labocon Scientific Limited, UK). The Z_{avg}, PDI, and ZP were accessed after reconstitution with water by slight agitation.

7.3.3.17 *In-vitro* cytotoxicity assay

Melanoma cell line (B16F10) and human embryonic kidney 293 cells (HEK 293) were obtained from the National Centre for Cell Science (NCCS), Pune, India. The MTT assay was performed for the *in-vitro* cytotoxicity of optimized TFs formulation along with unformulated PLFEE extract (in 0.2% DMSO) as per the previously described method (Chapter 6, section 6.4.5) with minute modifications. The cultured cells were treated with serum-free fresh media containing various concentrations of test substances (optimized TFs and PLFEE extract) and negative control (placebo-optimized TFs and 0.2% DMSO) for 24 h. The IC_{50} value was calculated using nonlinear regression analysis of log (concentration) vs. response data by GraphPad Prism 5 Software (GraphPad Software, Inc., San Diego, California). The % B16F10 cell viability at each concentration of free PLFEE and optimized TFs were compared using paired student t-test at a 95% level of significance.

7.3.3.18 *In-vitro* cellular uptake study

To examine whether the TFs can be internalized by the B16F10 cells, the uptake of Coumarin 6 (CU-6)-loaded TFs was investigated. CU-6, a hydrophobic fluorescent

dye, was used as a green fluorescent marker to track the TFs within the cancer cells. The CU-6 (1.2 mg) loaded TFs were formulated in a dark environment in a similar processing condition as that of the optimized TFs by replacing standardized PLFEE with CU-6 (for its loading in TFs, the CU-6 was solubilized in chloroform instead of ethanol as in case of PLFEE). B16F10 cell line cells were seeded into a 12-well culture plate at 1×10^5 cells per well and incubated for 24 h. After incubation, the cells were treated with media containing free CU-6 (0.055 µg/mL) and an equivalent amount of CU-6-loaded TFs and further incubated for 1 h at 37°C. The used medium, along with the treatments, was removed by washing cells with 1 mL PBS. After paraformaldehyde fixing, staining with 4′,6- diamidino-2-phenylindole (DAPI) was done for 15 min. Then, cancer cells were photomicrographed by a fluorescence microscope EVOS FLC Invitrogen fluorescence microscope (Life Technologies) at the UV excitation wavelength. The quantitative assessment of green fluorescence (i.e., total "area" and mean "gray" value) due to the free CU-6 and CU-6-TFs was carried out by processing the photomicrographs via ImageJ software. An unpaired student t-test was used to compare the results at a 95% confidence level.

7.3.3.19 Cell migration assay (*in-vitro* wound healing assay)

In-vitro cell migration assay was carried out using 2-well inserts (ibidi®, Munich, Germany) placed in 6-well plates as per the previously described method (Chapter 6, section 6.4.6). Briefly, B16F10 cells were suspended in culture media (1×10^5 cells/mL), and 100 µL of the cell suspension was added to each of the 2 wells in the cell inserts placed in 6-well plates. Then, the cells were incubated for 24 h to adhere the cells at the bottom of the wells, and cell-free gaps (wounds) were made by removing the culture inserts with the help of sterile forceps. Cellular debris and floating cells were washed off using sterile PBS. Then, the cells were treated with

sterile fresh media containing standardized PLFEE (in 0.2% DMSO) and optimized TFs each at a concentration of 50 µg/mL and incubated for 24 h. One additional plate seeded with cell suspension without any treatment was used as a control. The cell-free wound areas were photomicrographed at 0, 12, and 24 h. At each time point, 5 microphotographs were captured, and the wound areas were analyzed quantitatively using ImageJ software, and the % area of cell-free gaps (wounds) occupied by the cells due to the migration was calculated.

7.3.4 Formulation of TFG, placebo TFG, and plain gel

The TFG was prepared by incorporating the optimized TFs (containing 250 mg of PLFEE) into the Xanthan gum-based gel. Placebo TFG containing placebo-optimized TFs and plain gel containing standardized PLFEE were formulated for comparison purposes. Based on preliminary studies on the rheology, consistency, and spreadability of TFG and its comparison with the marketed gel (Omnigel, Cipla Ltd.), the percentage of the gelling agent was fixed. For TFG preparation, the Xanthan gum was gently dispersed portion-wise to the TFs formulation under continuous stirring. Propylene glycol (PG) was used as a humectant. Preservatives, such as methylparaben and propylparaben were added one by one, mixed properly, and allowed to hydrate the gel for 24 h. The placebo TFG was formulated similarly by incorporating placebo-optimized TFs into the gel and adding the remaining additives. The plain gel was prepared by directly incorporating the equivalent amount of PLFEE into a hydrated Xanthan gum-gel base, followed by the addition of humectant and preservatives. All the gel products were kept individually in screw-capped glass containers.

7.3.5 Characterization of TFG

7.3.5.1 Organoleptic properties

The color and appearance were observed visually.

7.3.5.2 Consistency and homogeneity

The consistency and homogeneity of the prepared gel formulations were inspected by visual observation, graded as +++ (Good), ++ (Fair), + (Poor) [163], and compared with the marketed gel (Omnigel, Cipla Ltd.). A small amount of each gel was placed between the thumb and the index finger, slightly rubbed, and evaluated for consistency and the existence of any masses or lumps [164].

7.3.5.3 Spreadability

Accurately, 0.5 g of gel was placed within a circle of 1 cm diameter pre-marked on a glass plate, a second plate (4 mm thick) was placed over it, and a weight of 500 g was kept on it for 5 min. The increase in diameter due to the spreading of gel was traced by marker and a minimum of 3 diameters was measured, and the average was calculated. The experiments were repeated in triplicate, and the results were presented as the average of three measurements [164, 165].

7.3.5.4 Extrudability

Extrudability in terms of weights needed to extrude a 0.5 cm ribbon of gel from a collapsible aluminum tube in 10 seconds was calculated [166].

7.3.5.5 pH

A 10% w/v dispersion of TFG, placebo gel, and plain gel was made with double distilled water, and the pH was evaluated using a digital pH meter (PC 700, Eutech Instrument, Singapore), which was previously calibrated with pH 4, pH 7 and pH 10 buffer solutions [167]. All the measurements were performed in triplicates at room temperature, and average values were reported.

7.3.5.6 Rheological studies

The rheology of gel formulations was studied by Anton Paar parallel plate rotational rheometer (MCR 72, Anton Paar GmbH, Austria) equipped with a 25 mm spindle and RheoCompass^{TM} software (version: 1.3). The rheology was studied at a constant shear rate (γ' = 50 1/s), increasing shear rate (γ'= 0.1 to 100 1/s), and amplitude sweep (γ = 0.01 to 100%, ω = 10 1/s) mode. About 0.5 g of the gel was placed between plates, and the analysis was performed by maintaining a 1 mm gap between the plates at 25 ± 1°C in triplicates. After each measurement, the plate was cleaned and dried properly.

7.3.5.7 Drug content and content uniformity determination

The drug content of TFG and the plain gel was determined by the validated HPLC method. Briefly, 200 mg of each gel was diluted with 5 mL HPLC grade methanol, vortexed, bath sonicated, centrifuged at 10000 rpm for 10 min, filtered through 0.22 µm syringe filter, and the PIP content was analyzed using the validated HPLC method. The content uniformity of each gel was estimated by quantifying the PIP content in samples taken from four different regions of the container.

7.3.5.8 Syneresis

Accurately, 200 mg of TFG, plain gel, and placebo TFG were placed individually in 2 mL of microcentrifuge tube (Eppendorf, Germany), weighed, centrifuged (10 min at 10000 rpm), and the supernatant fluid (phase separated) was discarded. The tubes were reweighed, and the percentage syneresis was calculated using Equation 7.6.

$$\% \, syneresis = \frac{W_1 - W_2}{W_1} \qquad (7.6)$$

Where, W_1 is the weight of the tube with gel before centrifugation and W_2 is the weight after centrifugation followed by decanting the fluid.

7.3.5.9 Compatibility study

The drug-excipient compatibility of the gel formulations was investigated by ATR-FTIR spectroscopy by comparing individual formulation components, physical mixture, and formulations similarly as stated under the compatibility study in TFs. To avoid the dominating broad peak due to water, the hydrogels were freeze-dried for 12 h before ATR-FTIR analysis.

7.3.5.10 *In-vitro* drug release and release kinetics

The *in-vitro* drug release with respect to PIP from the TFG-F2, plain gel, optimized TFs formulation, and PLFEE solution (in media) was carried out using the dialysis bag method. The seamless cellulose dialysis tubing (Dialysis Membrane-70, MWCO 12000-14,000 Daltons, pore size: 2.4 nm, average flat width 28.46 mm, average diameter: 17.5 mm, capacity approx.: 2.41 mL/cm, Himedia, Laboratories, Pvt. Ltd., Mumbai, India) was soaked overnight in deionized water to remove the preservatives and to swell the bag. Phosphate-buffered saline (PBS pH=7.4) containing 0.5% of T-80 was used as release media for *in-vitro* release study [168]. Accurately, 25 mg of PLFEE in solution form (in release media), an equivalent amount of optimized TFs, plain gel, and TFG-F2 were taken in a dialysis bag, hermetically sealed at both ends by threads and placed into a beaker containing 80 mL of release media. The receptor medium was maintained at 37 ± 0.5°C with continuous stirring at 150 rpm by a temperature-controlled magnetic stirrer with a hot plate (IKA C-MAG HS 7). At predetermined time intervals (0, 0.083, 0.25, 0.5, 0.75, 1, 2, 3, 4, 5 6, 8, 10, 12, 14, 16, 18, 20, 22, 24, 26, 28, 30, 32, 34, 36, 38, and 48 h), 1 mL of the aliquot was withdrawn from receptor medium and immediately replenished with the same volume of fresh blank medium to maintain sink condition. The amount of drug released was estimated

by the validated HPLC method. The results were expressed in terms of the cumulative percentage of PIP released as a function of time.

The data of the *in-vitro* drug release study was fitted to various mathematical kinetic models (zero order, first order, Korsmeyer-Peppas, Higuchi, and Hixson-Crowel cube root) to predict the release kinetics of PIP from TFs formulation. The linear regression analysis was performed to analyze the release data, and the correlation coefficient (R^2) in each case was estimated to predict the best-fitting model. The mechanism of drug release was investigated by fitting the 1st 60% of the *in-vitro* drug release data to the Korsmeyer-Peppas model and estimating the release exponent (n). The mathematical Equations (Equation 5.8-5.12) described under Chapter 5, section 5.3.4.14 are used for kinetic analysis.

7.3.5.11 Stability Studies

The stability testing was carried out as per ICH guidelines (ICH Q1 R2). The gel formulations were filled in the sterile collapsible aluminum tubes and subjected to long-term stability conditions (5 ± 3°C) for 12 months and accelerated conditions (25 ± 2°C/60 ± 5% RH) for 6 months. Periodically at 0, 6, 9, and 12 months for long-term stability study and 0, 3, and 6 months for accelerated condition, the formulations were evaluated for organoleptic properties, consistency, homogeneity, spreadability, extrudability, pH, viscosity, drug content, syneresis, and drug-excipient compatibility.

7.3.6 Approved protocol for standard experimental animals' conditions

The guidelines of the CPCSEA were strictly followed for care and animal experiments. The experiments were carried out following an approved protocol from the Institutional Animal Ethics Committee (IAEC Approval Number: IIT(BHU)/IAEC/2022/001). Female C57BL/6 mice: 7-8 weeks old, 18 ± 1.865 g body

weight) were housed in cages with free access to standard food (Laboratory animal feeds, VRK Nutritional Solutions, Maharashtra, India) and water. All the animals were kept in a room (25 ± 1°C, 55 ± 5% RH) with 12 h of dark/light cycle and accustomed to the laboratory conditions over 1 week before experiments.

7.3.7 *Ex-vivo* skin permeation study and permeability kinetics

The skin of C57BL/6 female mice was collected from the healthy group of the dermal toxicity study. The skin permeability study was carried out using OECD 428 guidelines (*in-vitro* skin absorption). To investigate the *in-vitro* transdermal permeability of a drug, a nonoccluded open skin hydration setup was followed to maintain a transepidermal aqueous gradient that acts as a driving force for the skin penetration of transfersomes [169]. The hair from the dorsal side was removed precisely using an electric clipper, the skin was isolated, and the adhering fatty material was removed by isopropyl alcohol using a cotton swab. The skin was wrapped in aluminum foil and stored at - 20°C until further use. The stored skin was thawed to room temperature and hydrated with water for 2 h to attain the equilibrium. The *ex-vivo* skin permeability was carried out using a vertical Franz diffusion cell (Kshitij International Equipment, India) with a 20 mL receptor volume and diffusional area of 2.545 cm^2. The skin was sandwiched between the donor and receptor compartments with the epidermis towards the donor compartment and exposed to the receptor compartment containing fresh phosphate-buffered saline (pH 7.4 containing 0.5% T-80). Sodium azide (0.0025% w/v) was added to the medium to avoid the growth of microbes [170]. The receptor media was stirred continuously at 150 rpm using temperature controlled magnetic stirrer (IKA C-MAG HS 7, IKA, Germany), and the temperature of the receptor compartment was maintained at 37 ± 1°C to achieve the physiological skin temperature of 32 ± 1°C [171]. The 4.658 mg PLFEE containing

plain gel (0.2 g) and an equivalent amount of TFG-F2 (0.218 g) formulations were applied to the skin uniformly. Aliquots of 1 mL were collected at regular intervals (0, 0.083, 0.25, 0.5, 1, 2, 3, 4, 5 6, 8, 10, 12, 14, 16, 18, 20, 22, 24, 26, 28, 30, 32, 34, 36, and 38 h) from receptor compartment and replenished with the same volume of fresh release medium to maintain the sink condition. Collected samples were diluted with suitably with HPLC grade methanol, centrifuged, filtered through the 0.22 µm membrane filter, and the supernatant was analyzed for the drug permeated by validated HPLC method. The cumulative amount of PIP permeated through a unit area of skin at a predetermined time was calculated using Equation 7.7 [172].

$$Cumulative\ amount(Qi) = \frac{C_i V + \sum_1^{i-1} C_{i-1} \times V_i}{A} \qquad (7.7)$$

Where, Qi is the cumulative amount of drug permeated through the skin, A is the effective diffusional area (2.545 cm^2), V represents the volume of the receptor medium (20 mL); Ci represents the drug concentration at a predetermined time (i) in receptor medium, V_i represents the volume after each sampling time; $\sum_1^{i-1} C_{i-1}$ denotes the summed total of the previously measured concentrations. The permeability results were kinetically analyzed by various mathematical models as described in *in-vitro* release study.

The permeability coefficient (k_p) was calculated using Equation 7.8 [173].

$$Permeability\ coefficient\ (k_p) = \frac{\frac{dQ}{dt}}{A.C_d} \qquad (7.8)$$

Where, A is diffusion area, dQ/dt = amount of drug/time, and C_d is the drug concentration in the donor compartment

The drug permeation rate (flux) at steady state (Jss) was calculated by dividing the slope of the linear portion of the graph by the area of the diffusion cell (Equation 7.9) [174].

$$Steady\ state\ Flux\ (J_{ss}) = \frac{\frac{dQ}{dt}}{A} = k_p \times C_d \qquad (7.9)$$

Where, dQ/dt is the slope of the linear portion, and A is the diffusion area.

The maximum flux (J_{max}) was calculated using Equation 7.10.

$$Maximum\ Flux\ (J_{max}) = \frac{\frac{dQ}{dt_{max}}}{A} \qquad (7.10)$$

Where, dQ/dt_{max} represents the maximum amount of drug permeated at the end of the study and A is the diffusional area.

The enhancement ratio (E_r) was estimated using Equation 7.11 [174].

$$Enhancement\ ratio\ (E_r) = \frac{J_{ss}\ of\ Transgelosome}{J_{ss}\ of\ Control\ Gel} \qquad (7.11)$$

7.3.8 Depth of skin penetration via confocal laser scanning microscopy (CLSM) microscopy

CLSM was used to study the depth of permeation of plain gel and TFG F2 across the skin using CU-6 as a fluorescent marker in place of standardized PLFEE. Each formulation was applied nonocclusively to the dermal side of the C57BL/6 mice skin and subjected to the vertical diffusion apparatus similarly (as in the case of *ex-vivo* permeability study) for 8 h. Then, the skin samples were removed carefully and washed thrice in running tap water to remove sample residue. The skin samples from the diffusion area were carefully removed and optically scanned and sliced (12 µm thickness) by the Z-stacking option of a confocal laser microscope (CLSM 900, Carl

Zeiss Microscopy, GMBH, Germany), using an argon beam at an excitation wavelength of 457 nm. The photomicrographs were captured using Zen (Blue edition) software (version: 3.6). All the system parameters were kept constant during the measurements to compare the photomicrographs.

7.3.9 Acute dermal toxicity of standardized PLFEE

Acute dermal toxicity study of standardized PLFEE was carried out on nulliparous and non-pregnant C57BL/6 female mice as per OECD 402 guideline (Acute Dermal Toxicity: Fixed Dose Procedure). The dermal toxicity of the standardized PLFEE was investigated by conducting a "range-finding study" followed by a "main study". Prior to the toxicity study, the mice were caged individually to avoid oral ingestion of the test sample by other animals in the cage. All fur from the dorsal region (~ 10% of the total body surface area) of C57BL/6 mice was removed by clipping before topical application with special attention to avoid abrading the skin. For better contact with the skin, the dried PLFEE was slightly moistened with distilled water. A starting dose (200 mg/kg) of the standardized PLFEE followed by 1000 mg/kg and 2000 mg/kg was uniformly applied topically as a very thin layer on a single animal/group in the range-finding study followed by repeating the aforementioned doses on 2 animals/ group in the main study. For statistical analysis, the obtained final safe dermal dose was applied to 4 animals/group. The animals topically applied with distilled water served as a control group for comparison purposes. The prolonged (24-h) skin retention of standardized PLFEE and avoidance of ingestion by the animals were ensured by means of a porous gauze dressing. Each animal was carefully observed initially just after administration, after the first 30 min, with special attention at first 2-6 h, periodically during the first 24 h, and daily afterward for up to 14 days for detecting any sign of toxicity (changes in skin, fur, eyes, mucous membranes), survival or

behavioral, and body weight changes. At the end of the exposure period (24 h), the residual standardized PLFEE was removed. The treatment site was thoroughly observed at 24, 48, and 72 h after the removal of the test chemical using the Draize criteria. After 14 days, the mice were thoroughly observed, weighed, and anesthetized with isoflurane, and blood was collected by cardiac puncture for hematological and biochemical studies as per the manufacturer's instructions.

Then, the animals were humanly sacrificed, and the vital organs (heart, liver, kidney, spleen, and lungs) were carefully isolated, washed with ice-cold phosphate-buffered saline, and stored in 10% aqueous formalin for 12 h for histopathological studies. Paraffin organ sections (~ 4 μm thick) were cut and stained with eosin and hematoxylin and mounted in a non-aqueous mounting medium (DPX). The photomicrographs of the sections were captured at 10x magnification using a light microscope (Magnus MLX Plus, Olympus Opto Systems India Pvt. Ltd., Uttar Pradesh, India) furnished with a digital microscopic camera (Magcam DC 5, 5.1 MP) and Magvision software (version: x36, 3.7.6820). Based on all the observations, the dermal toxicity of standardized PLFEE was reported as per the Globally Harmonised System (GHS) category (category 1- 5/Unclassified).

7.3.10 Skin irritation study

The Draize patch test was used to assess the skin irritation potential of prepared gel formulations. Briefly, the study was performed on female C57BL/6 mice. Carefully 10% of hair was removed from the dorsal side by an electric clipper 24 h before the test, washed with distilled water, and applied uniformly with 0.5 g of placebo TFG-F2 (vehicle control), TFG-F2, plain gel, and aqueous formalin solutions (0.8% v/v) as a positive control. The skin surface was inspected for signs of erythema and edema at

24, 48, and 72 h after application. The responses were examined as reactions on the skin surface, the scores in terms of "primary irritation index (PII)" were assigned, and the irritability potential of the formulations was interpreted using the "Grading values and response categories".

7.3.11 *In-vivo* anticancer activity in melanoma (B16F10) bearing C57BL/6 mice

The *in-vivo* anticancer activity was investigated in solid tumor/melanoma (B16F10) bearing C57BL/6 female mice. The tumor induction was carried out as per the previously described method (Chapter 6). After 8 days, mice bearing palpable tumor (volume: 35 ± 3 mm^3) were topically applied with a placebo gel, plain gel (at a dose of 200 mg/kg PLFEE), and an equivalent quantity of TFG-F2 daily for up to 30 days. DTIC, as a standard anticancer drug, was administered at a dose of 5 mg/kg intraperitoneally (i.p.) every 2 days for up to 30 days [103]. The treatments comprising DTIC with standardized PLFEE-loaded plain gel or TFG-F2 were also provided to evaluate their efficacy as supportive therapy. Body weight and tumor size were evaluated throughout the treatment period.

7.3.11.1 Experimental design

A total of 70 adult female C57BL/6 mice were divided into 7 groups as follows:

- **Group-I (Normal control)**: Non-tumor-bearing mice
- **Group-II (Tumor control)**: Tumor-bearing mice, topically applied with placebo gel (0.196 g/ animal) daily
- **Group-III (Standard drug/ DTIC group)**: Tumor-bearing mice, receiving DTIC (5 mg/kg) i.p. every 2 days.

- **Group-IV (PLFEE-loaded plain gel group)**: Tumor-bearing mice, applied with standardized PLFEE-loaded plain gel (0.180 g/animal, at a dose of 200 mg/kg) daily

- **Group-V (PLFEE-loaded Transgelosome group)**: Tumor-bearing mice, applied with standardized PLFEE-loaded transgelosome (0.196 g, i.e., equivalent to 0.180 g of plain gel/animal, at a dose of 200 mg/kg) daily

- **Group-VI (DTIC + PLFEE loaded plain gel group)**: Tumor-bearing mice applied with standardized PLFEE loaded plain gel (0.180 g/animal) daily and DTIC (5 mg/kg b.wt.) i.p. every 2 days.

- **Group-VII (DTIC + Transgelosome group)**: Tumor-bearing mice, applied with standardized PLFEE loaded transgelosome (0.196 g/animal) daily, and DTIC (5 mg/kg b.wt) i.p. every 2 days.

7.3.11.2 Tumor regression analysis

The tumor regression analysis (TV, VDT, %TGI, tumor weight, and % ILS) and histopathology were carried out as per the described method under Chapter 6, section 6.3.5.9.1.

7.3.12 Statistical analysis

The mean and standard deviation (SD) for all experiments were calculated and expressed as mean ± SD. Statistical analysis was performed by one-way analysis of variance (ANOVA) followed by Tukey's test (for 3 groups or more) or students t-test (between two groups) at $p<0.05$ using GraphPad Prism 5 (GraphPad Software, Inc., San Diego, California).

7.4 Results and Discussion

7.4.1 Formulation development of TFs

The detailed formulation scheme of TFs using PL-90 H and T-80 by rotary evaporation-based thin film hydration is graphically represented in Figure 7. 3. The

TFs formulations were found to be homogeneous liquids with milky white in color (Figure 7. 4). The PL-90 H (hydrogenated phosphatidylcholine from soybean lecithin containing phosphatidylcholine of more than 90%) was used as a membrane-forming agent and the hydrophilic surfactant i.e., Tween® 80 was used as an edge activator (EA) to provide the membrane flexibility. Rotatory evaporation-based thin film hydration (Figure 7. 3) is a widely used lab scale technique for the formulation of TFs that allows the easy monitoring of processing variables like rpm and temperature. Further, this method allows the development of a thin film on a large surface area and proper hydration of the vesicles, which enhances entrapment efficiency [164, 175].

The hydrogenated phosphatidylcholine (PL-90 H), as a membrane-forming agent, is known for its high stability, purity, biocompatibility, and biodegradability. Tween® 80 is widely preferred EAs over others, such as sodium cholate (SC) and sodium deoxycholate (SDC), which produce low flexibility and high vesicle size owing to their bulkier steroidal structure than the hydrocarbon chains of Tween® 80 [162, 167]. Hydrophobic EAs, like Span 80®-based TFs show lower flexibility owing to their high hydrophobicity, decreased formation of transient hydrophilic holes, and amphiphilic behavior of bilayers liable for membrane fluidity [162]. EAs with a higher hydrophilic-lipophilic balance (HLB) value interact more strongly with the aqueous phase and result in smaller vesicles [176]. The high HLB value of Tween® 80 (15) over Span 80® (HLB: 4.3) is responsible for its smaller vesicle size. Further, hydrophobic EAs compete with a hydrophobic drug candidate for the limited hydrophobic bilayer space of TFs. Considering the above facts, the hydrophobic nature of the standardized PLFEE, and some of the preliminary outcomes on vesicle size and flexibility, the Tween® 80 was used as EA along with PL-90H as membrane former for the development of TFs.

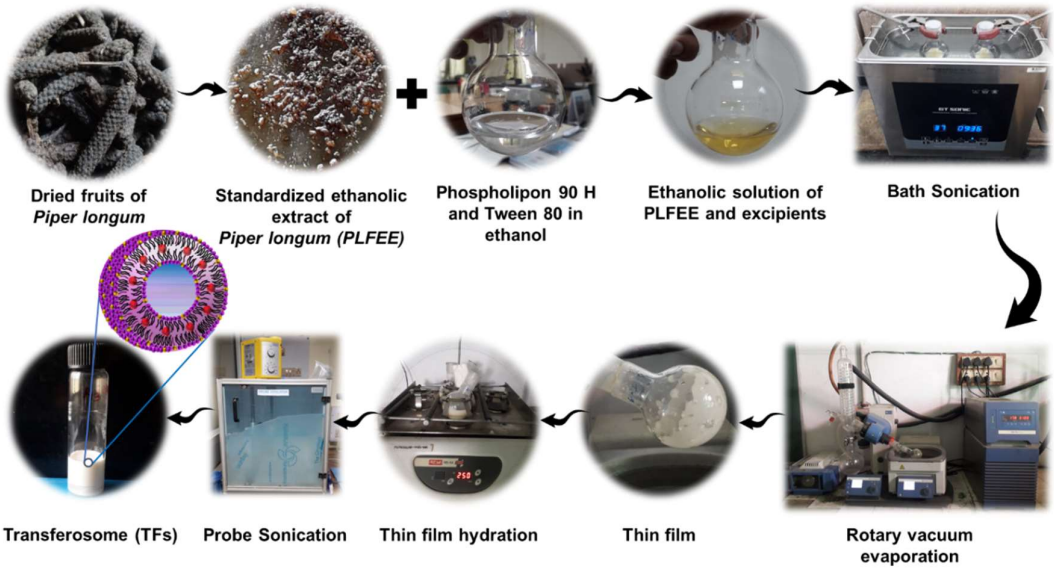

Figure 7. 3 Formulation methodology of standardized PLFEE-loaded TFs by thin film hydration method.

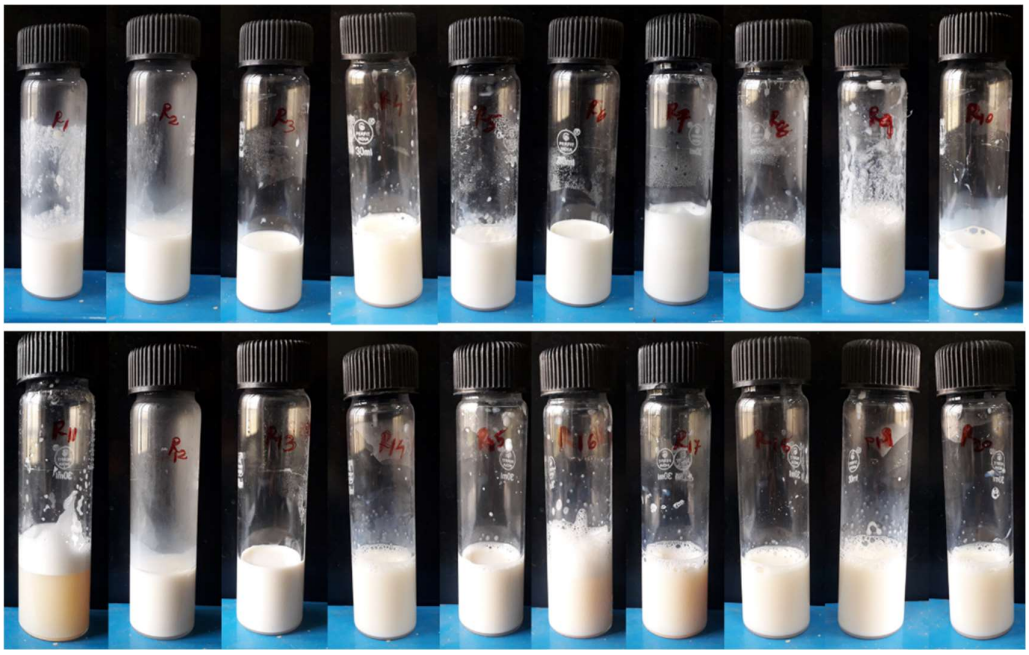

Figure 7. 4 Twenty formulations of standardized PLFEE-loaded TFs as per the design of experiment

7.4.2 Optimization

A CCD-based optimization approach was utilized to get an optimal composition for TFs [177]. The levels of three independent variables and the response as per the CCD model are displayed in Table 7. 1. As per the CCD, 20 TFs were formulated (6

replications of central points, 6-star points (axial points), and 8 cube points (factorial points)) using various levels of independent variables, such as PL-90 H, Tween® 80, and probe sonication time. The ranges of the independent variables that have a strong influence on the several dependent variables (Z_{avg}, % EE, and flexibility) were chosen based on the preliminary experiments. The results of chosen responses (Z_{avg} (Y_1), % EE (Y_2), and flexibility (Y_3) are represented in Table 7. 2. The outcomes of other evaluated parameters of the prepared TFs formulations are represented in Table 7. 3.

Table 7. 1 Coded levels, real values of each factor, and Critical Quality Attributes (CQA)

	Levels Coded Values				
	-1.681	**-1**	**0**	**+1**	**+1.681**
Independent variables (CMAs and CPP)	**Real values**				
Phospholipon® 90 H (X_1, mg)	315.91	350	400	450	484.089
Tween® 80 (X_2, mg)	15.91	50	100	150	184.089
Probe Sonication Time (X_3, min)	0.954	3	6	9	11.045
Dependent variables (CQAs)	**Goal**				
Vesicle Size (Y_1, nm)	To minimize				
Entrapment Efficiency (Y_2, %)	To maximize				
Flexibility (Y_3, **mL/s**)	To maximize				

CQAs: critical quality attributes; CMAs: critical material attributes and CPP: critical process parameter

Table 7. 2 CCD-based TFs formulations with respective responses

	Factor 1 (X_1)	Factor 2 (X_2)	Factor 3 (X_3)	Response 1 (Y_1)	Response 2 (Y_2)	Response 3 (Y_3)
Formulation	**A: Phospholipon 90 H (PL-90 H)**	**B: Tween® 80**	**C: Probe Sonication Time**	**Vesicle Size (Zavg)**	**Entrapment Efficiency (EE)**	**Flexibility**
	mg	**mg**	**min**	**nm**	**%**	**mL/s**
1	450	50	9	197.254 ± 3.215	86.545 ± 2.346	14.124 ± 2.245
2	450	50	3	231.253 ± 2.452	92.385 ± 3.457	13.254 ± 1.117
3	400	100	6	160.667 ± 3.554	62.846 ± 5.46	16.242 ± 2.623
4	350	50	9	110.334 ± 2.346	48.254 ± 4.489	14.215 ± 1.157
5	400	184.08975	6	129.334 ± 4.424	52.354 ± 3.247	12.213 ± 0.985
6	400	15.91035	6	171.667 ± 1.252	72.892 ± 1.278	10.244 ± 1.136
7	400	100	6	165.68 ± 2.246	65.254 ± 2.457	17.243 ± 2.016
8	400	100	11.0454	140.334 ± 3.423	56.235 ± 3.349	17.242 ± 0.896
9	484.09	100	6	238.333 ± 5.131	72.2865 ± 2.248	5.265 ± 1.273
10	400	100	6	161.213 ± 2.178	66.243 ± 4.478	16.242 ± 0.784
11	400	100	6	162.235 ± 1.546	63.234 ± 3.118	15.874 ± 0.858
12	315.91	100	6	75.5667 ± 2.147	38.152 ± 2.427	12.875 ± 1.346
13	350	150	9	97.1333 ± 3.279	45.545 ± 1.468	19.242 ± 1.023
14	400	100	6	167.548 ± 4.127	65.572 ± 3.314	16.124 ± 2.063
15	450	150	3	195.35 ± 2.179	66.356 ± 1.248	8.645 ± 0.965
16	400	100	6	168.235 ± 2.136	65.243 ± 1.118	16.578 ± 1.143
17	350	150	3	101.23 ± 1.746	65.246 ± 2.147	18.236 ± 2.034
18	400	100	0.954622	165.667 ± 3.364	80.324 ± 3.217	16.989 ± 0.864
19	350	50	3	120.243 ± 2.547	48.248 ± 2.211	8.345 ± 1.145
20	450	150	9	176.631 ± 1.578	42.213 ± 1.875	6.245 ± 1.368

Results were represented as mean ± standard deviation (n = 3)

Table 7. 3 Polydispersity index (PDI), Zeta potential (ζ), loading capacity (LC), pH, and refractive index (RI) of TFs

	Other Parameters				
Formulation	**Polydispersity Index (PDI)**	**Zeta Potential (ζ)**	**Loading Capacity (LC)**	**pH**	**Refractive Index (RI)**
		mV	**%**		
1	0.211 ± 0.014	-18.5 ± 0.275	9.606 ± 1.231	4.756 ± 0.012	1.335 ± 0.0001
2	0.358 ± 0.006	-17.8 ± 0.312	10.254 ± 1.543	4.743 ± 0.016	1.334 ± 0.0003
3	0.184 ± 0.005	-18.2 ± 0.242	6.975 ± 2.131	4.703 ± 0.024	1.337 ± 0.0004
4	0.214 ± 0.014	-11.8 ± 1.024	6.695 ± 1.546	4.81 ± 0.016	1.337 ± 0.0014
5	0.192 ± 0.048	-17.2 ± 0.234	4.974 ± 3.071	4.733 ± 0.016	1.343 ± 0.0004
6	0.389 ± 0.006	-18.2 ± 0.178	9.726 ± 1.067	4.52 ± 0.037	1.334 ± 0.0002
7	0.237 ± 0.006	-19.2 ± 0.123	7.243 ± 2.214	5.51 ± 0.035	1.338 ± 0.0003
8	0.201 ± 0.021	-18.1 ± 1.214	6.242 ± 1.473	6.72 ± 0.016	1.34 ± 0.0007
9	0.128 ± 0.004	-17.2 ± 0.542	6.868 ± 2.105	6.85 ± 0.028	1.337 ± 0.0008
10	0.216 ± 0.024	-19.4 ± 0.097	7.352 ± 1.136	4.78 ± 0.014	1.336 ± 0.0008
11	0.221 ± 0.018	-18.3 ± 0.132	7.018 ± 2.082	5.17 ± 0.008	1.335 ± 0.0001
12	0.216 ± 0.073	-5.38 ± 0.245	5.091 ± 1.142	5.58 ± 0.021	1.334 ± 0.0001
13	0.183 ± 0.028	-15.5 ± 0.312	5.055 ± 3.472	5.49 ± 0.008	1.335 ± 0.0002
14	0.197 ± 0.029	-19.2 ± 0.324	7.278 ± 2.140	4.79 ± 0.021	1.335 ± 0.0012
15	0.276 ± 0.033	-19.3 ± 0.547	6.137 ± 1.224	4.756 ± 0.012	1.338 ± 0.0003
16	0.213 ± 0.028	-17.2 ± 0.467	7.241 ± 0.985	4.756 ± 0.004	1.335 ± 0.0004
17	0.249 ± 0.028	-15.2 ± 0.247	7.242 ± 1.105	4.486 ± 0.055	1.337 ± 0.0002
18	0.401 ± 0.008	-18.3 ± 0.176	8.915 ± 1.432	4.75 ± 0.008	1.337 ± 0.0002
19	0.34 ± 0.042	-9.32 ± 0.364	6.694 ± 2.017	4.63 ± 0.016	1.336 ± 0.0002
20	0.212 ± 0.007	-18.5 ± 1.081	3.904 ± 1.036	4.76 ± 0.018	1.335 ± 0.0001

Results were represented as mean ± standard deviation (n = 3)

The statistical model fit summary of all responses is represented in Table 7. 4. For all responses (CQAs), the quadratic model was selected among various models (liner, 2FI, and cubic models) considering the low sequential p-value (<0.05), high model R^2 values (0.9973 for Y_1, 0.9961 for Y_2, and 0.9877 for Y_3), the permissible difference (<0.2) between adjusted and predicted R^2 values, insignificant lack of fit value (>0.05), low standard deviation ("Std. Dev."), and a low "Predicted Residual Sum of Squares" (PRESS) value.

The ANOVA results of the statistical analysis by the Design-Expert software for Y_1, Y_2, and Y_3 are represented in Table 7. 5, Table 7. 6, and Table 7. 7, respectively. Very low model p values (<0.0001), all model terms below 0.05, and adequate precision (signal-to-noise ratio>4) demonstrate the suitability of the model for response surface analysis and prediction of optimized formula.

The diagnostic plots for Y1, Y2, and Y3 are represented in Figure 7. 5-Figure 7. 7, Figure 7. 8-Figure 7. 10, and Figure 7. 11-Figure 7. 13, respectively. The linearity in the "normal plot of residual," optimum lambda value in the "Box-Cox plot," constant range of residuals in the "externally studentized residual v/s predicted plot," and random scattering within the control limits in the "externally studentized residual v/s run plot," and "residual v/s factor plot" of various diagnostic plots reflected the goodness of fit of the proposed model.

Table 7. 4 Statistical model fit summary

Fit summary statistics: Vesicle Size (Y_1)								
Source (Models)	**Sequential p-value**	**Lack of Fit p-value**	**Adjusted R^2**	**Predicted R^2**	**R^2 value**	**Std. Dev.**	**PRESS**	
Linear	<0.0001	0.0202	0.9677	0.9580	0.9728	7.63	1437.14	
2FI	0.1288	0.0287	0.9739	0.9579	0.9821	6.85	1439.42	
Quadratic	**0.0002**	**0.6756**	**0.9950**	**0.9892**	**0.9973**	**3.01**	**368.84**	**Suggested**
Cubic	0.5261	0.6788	0.9947	0.9840	0.9983	3.08	546.14	Aliased
Fit summary statistics: Entrapment Efficiency (Y_2)								
Source (Models)	**Sequential p-value**	**Lack of Fit p-value**	**Adjusted R^2**	**Predicted R^2**	**R^2 value**	**Std. Dev.**	**PRESS**	
Linear	0.0005	0.0001	0.6006	0.3786	0.6636	9.05	2419.08	
2FI	<0.0001	0.0049	0.9174	0.8887	0.9435	4.11	433.45	
Quadratic	**<0.0001**	**0.6796**	**0.9925**	**0.9847**	**0.9961**	**1.24**	**59.41**	**Suggested**
Cubic	0.4899	0.9719	0.9924	0.9964	0.9976	1.25	13.98	Aliased
Model summary statistics: Flexibility (Y_3)								
Source	**Sequential p-value**	**Lack of Fit p-value**	**Adjusted R^2**	**Predicted R^2**	**R^2 value**	**Std. Dev.**	**PRESS**	
Linear	0.2254	< 0.0001	0.0884	-0.3209	0.2324	3.89	416.53	
2FI	0.0410	0.0001	0.3925	0.1731	0.5843	3.18	260.75	
Quadratic	**<0.0001**	**0.1805**	**0.9766**	**0.9275**	**0.9877**	**0.6226**	**22.86**	**Suggested**
Cubic	0.3877	0.0931	0.9787	0.3092	0.9933	0.5950	217.84	Aliased

Table 7. 5 ANOVA for quadratic model and fit statistics for vesicle size

ANOVA: Vesicle Size (Y_1)						
Source	**Sum of Squares**	**df**	**Mean Square**	**F-value**	**p-value**	
Model	34089.46	9	3787.72	417.79	<0.0001	significant
X_1	30509.87	1	30509.87	3365.29	<0.0001	
X_2	1868.03	1	1868.03	206.05	<0.0001	
X_3	871.83	1	871.83	96.16	<0.0001	
$X_1 X_2$	75.56	1	75.56	8.33	0.0162	
$X_1 X_3$	189.99	1	189.99	20.96	0.0010	
$X_2 X_3$	54.18	1	54.18	5.98	0.0346	
X_1^2	83.96	1	83.96	9.26	0.0124	
X_2^2	317.52	1	317.52	35.02	0.0001	
X_3^2	209.20	1	209.20	23.07	0.0007	
Residual	90.66	10	9.07			
Lack of Fit	35.74	5	7.15	0.6507	0.6756	not significant
Pure Error	54.92	5	10.98			
Cor Total	34180.12	19				

Fit statistics						
Standard deviation (SD)	**Mean**	**C.V (%)**	**R^2**	**Adjusted R^2**	**Predicted R^2**	**Adequate precision**
3.01	156.78	1.92	0.9973	0.9950	0.9892	74.6713

Table 7. 6 ANOVA for quadratic model and fit statistics for entrapment efficiency

ANOVA: Entrapment Efficiency (Y_2)						
Source	**Sum of Squares**	**df**	**Mean Square**	**F-value**	**p-value**	
Model	3877.68	9	430.85	281.11	<0.0001	significant
X_1	1386.66	1	1386.66	904.71	<0.0001	
X_2	601.21	1	601.21	392.25	<0.0001	
X_3	595.62	1	595.62	388.61	<0.0001	
$X_1 X_2$	895.70	1	895.70	584.39	<0.0001	
$X_1 X_3$	13.23	1	13.23	8.63	0.0148	
$X_2 X_3$	180.60	1	180.60	117.83	<0.0001	
X_1^2	163.59	1	163.59	106.74	<0.0001	
X_2^2	8.14	1	8.14	5.31	0.0439	
X_3^2	22.45	1	22.45	14.65	0.0033	
Residual	15.33	10	1.53			
Lack of Fit	6.00	5	1.20	0.6439	0.6796	not significant
Pure Error	9.32	5	1.86			
Cor Total	3893.01	19				

Fit statistics						
Standard deviation (SD)	**Mean**	**C.V (%)**	**R^2**	**Adjusted R^2**	**Predicted R^2**	**Adequate precision**
1.24	62.77	1.97	0.9961	0.9925	0.9847	61.7251

Table 7. 7 ANOVA for quadratic model and fit statistics for flexibility

ANOVA: Flexibility (Y_3)						
Source	**Sum of Squares**	**df**	**Mean Square**	**F-value**	**p-value**	
Model	311.47	9	34.61	89.28	<0.0001	significant
X_1	68.42	1	68.42	176.51	<0.0001	
X_2	2.41	1	2.41	6.23	0.0317	
X_3	2.44	1	2.44	6.29	0.0310	
$X_1 X_2$	93.89	1	93.89	242.20	<0.0001	
$X_1 X_3$	8.83	1	8.83	22.79	0.0008	
$X_2 X_3$	8.27	1	8.27	21.33	0.0010	
X_1^2	87.84	1	87.84	226.61	<0.0001	
X_2^2	41.93	1	41.93	108.17	<0.0001	
X_3^2	2.03	1	2.03	5.25	0.0449	
Residual	3.88	10	0.3876			
Lack of Fit	2.73	5	0.5466	2.39	0.1805	not significant
Pure Error	1.14	5	0.2287			
Cor Total						

Fit statistics						
Standard deviation (SD)	**Mean**	**C.V (%)**	**R^2**	**Adjusted R^2**	**Predicted R^2**	**Adequate precision**
0.6226	13.77	4.52	0.9877	0.9766	0.9275	30.6408

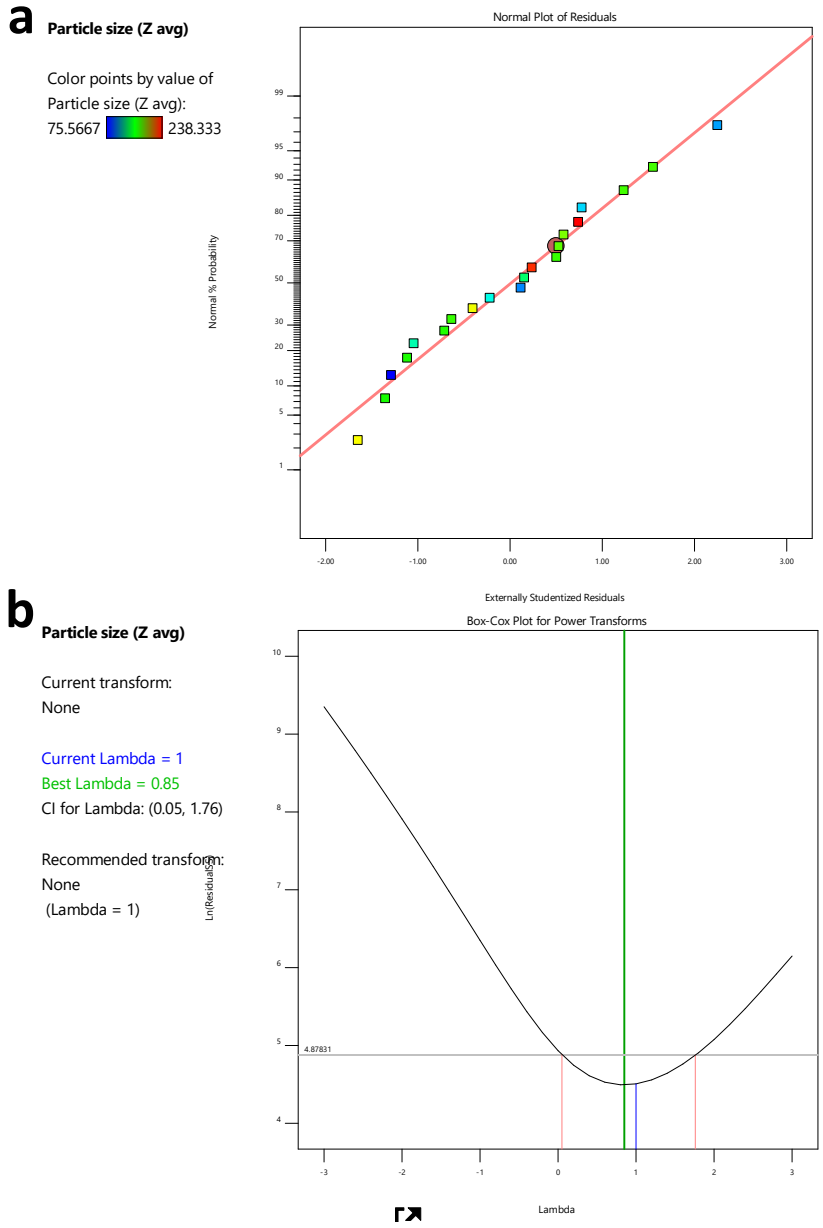

Figure 7. 5 Diagnostic plots for response Y_1: Vesicle Size (Z_{avg}) (a) normal plot of residuals and (b) Box-Cox plot

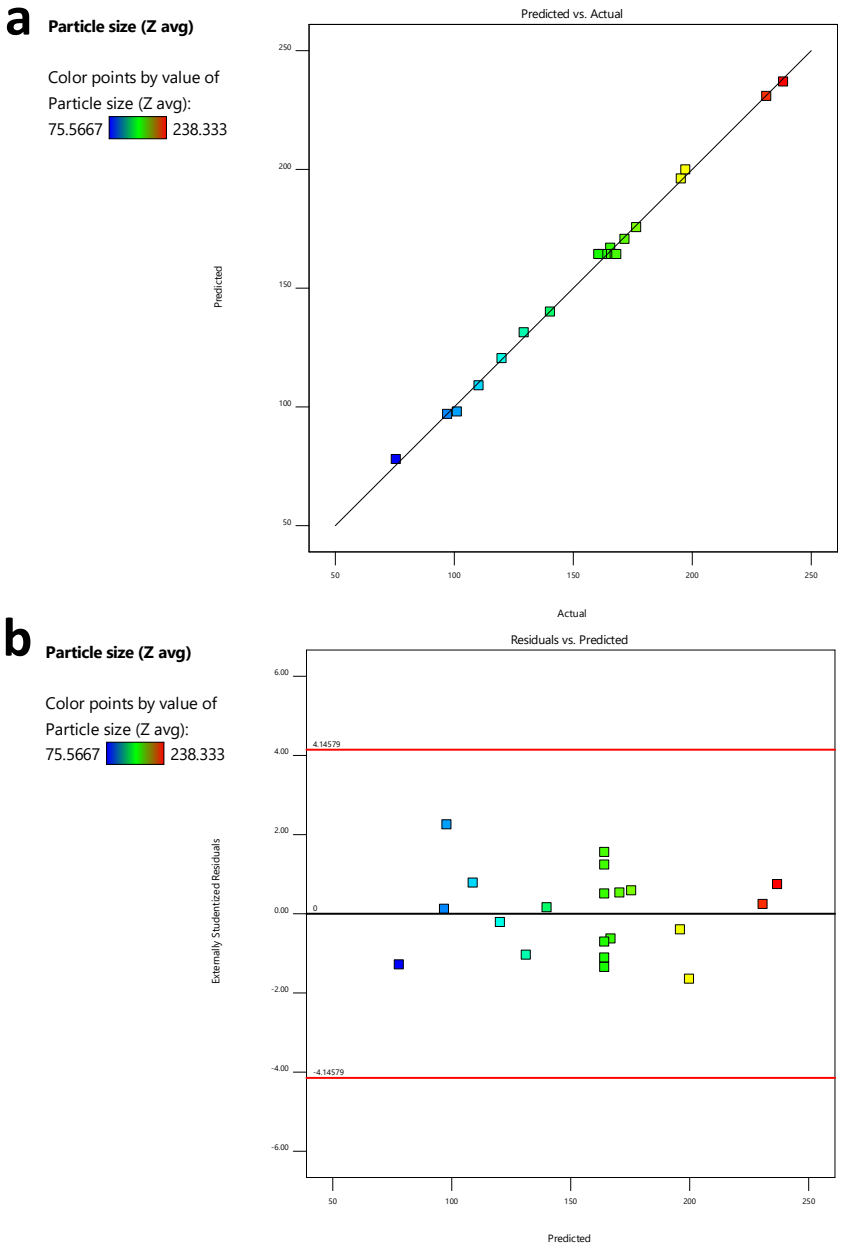

Figure 7. 6 Diagnostic plots for response Y_1: Vesicle Size (Z_{avg}) (a) predicted vs. actual plot and (b) residual vs. predicted plot

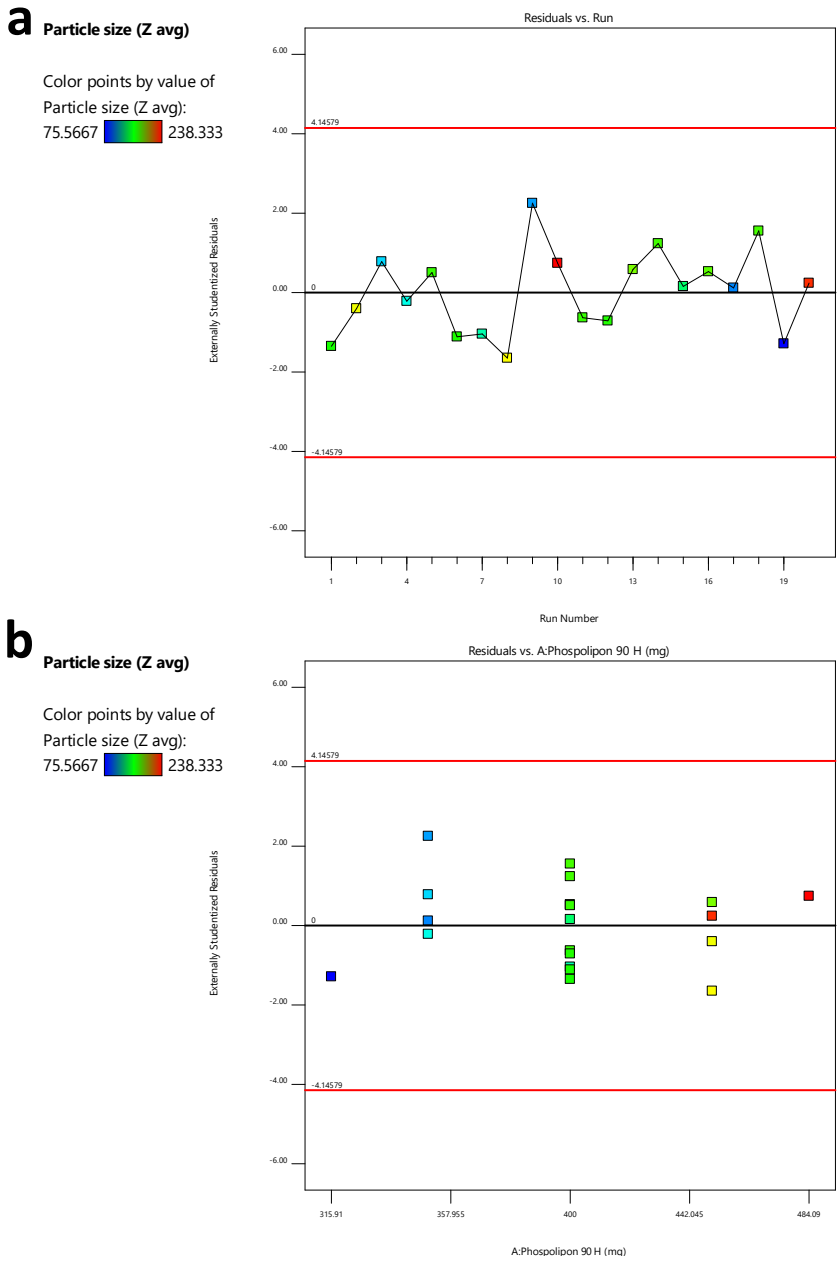

Figure 7. 7 Diagnostic plots for response Y_1: Vesicle Size (Z_{avg}) (a) residual vs. run and (b) residual vs. factor plot

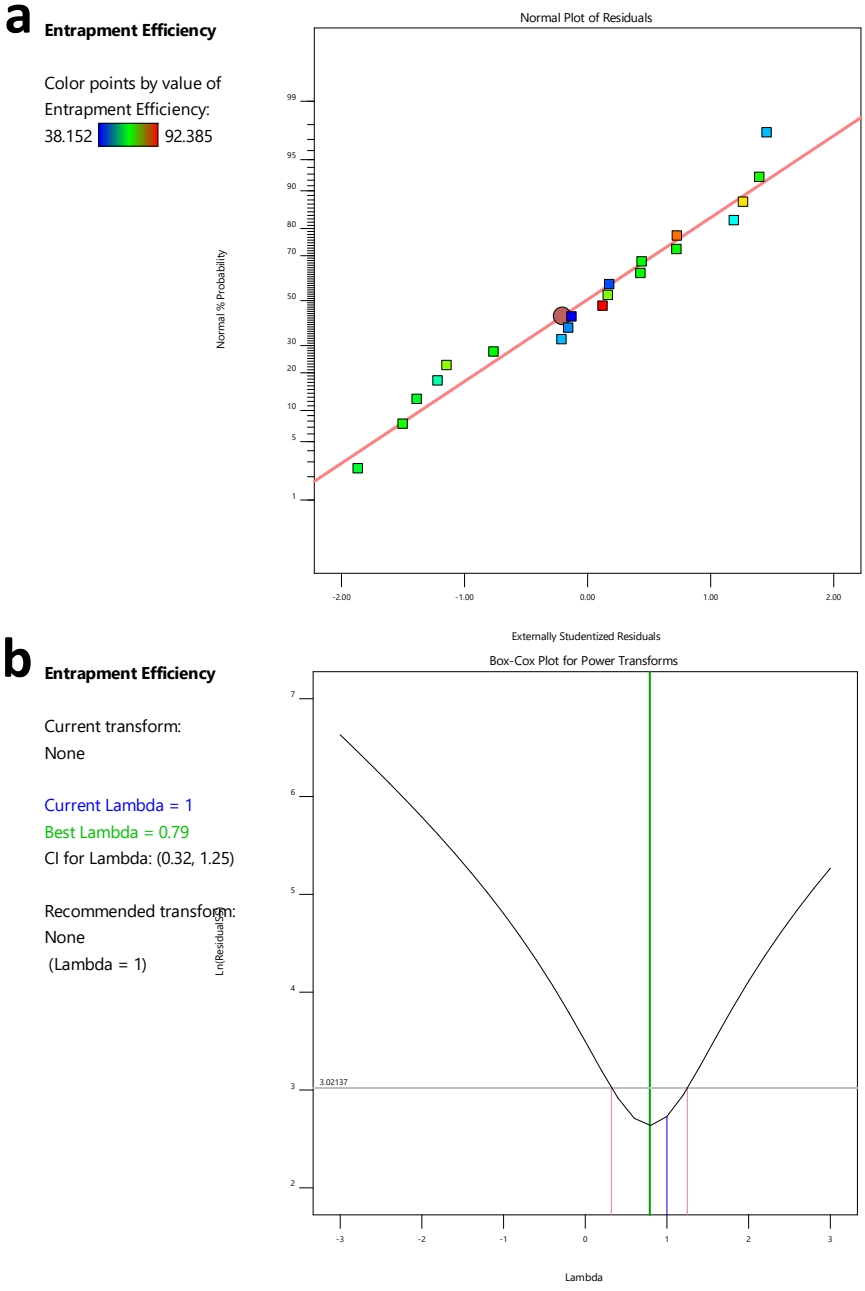

Figure 7. 8 Diagnostic plots for response Y_2: % Entrapment Efficiency (% EE) (a) normal plot of residuals, and (b) Box-Cox plot

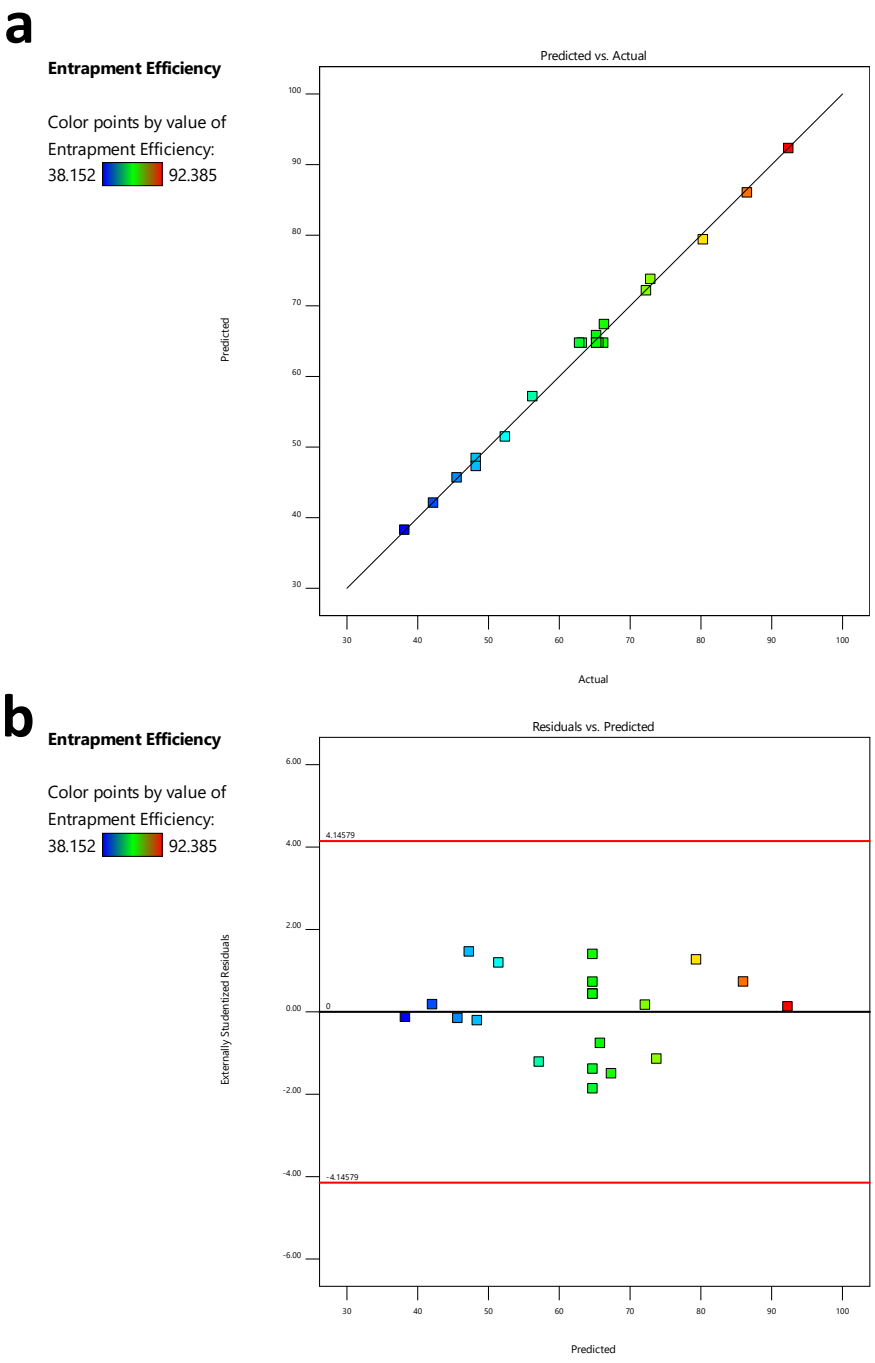

Figure 7. 9 Diagnostic plots for response Y_2: % Entrapment Efficiency (% EE) (a) predicted vs. actual plot and (b) residual vs. predicted plot

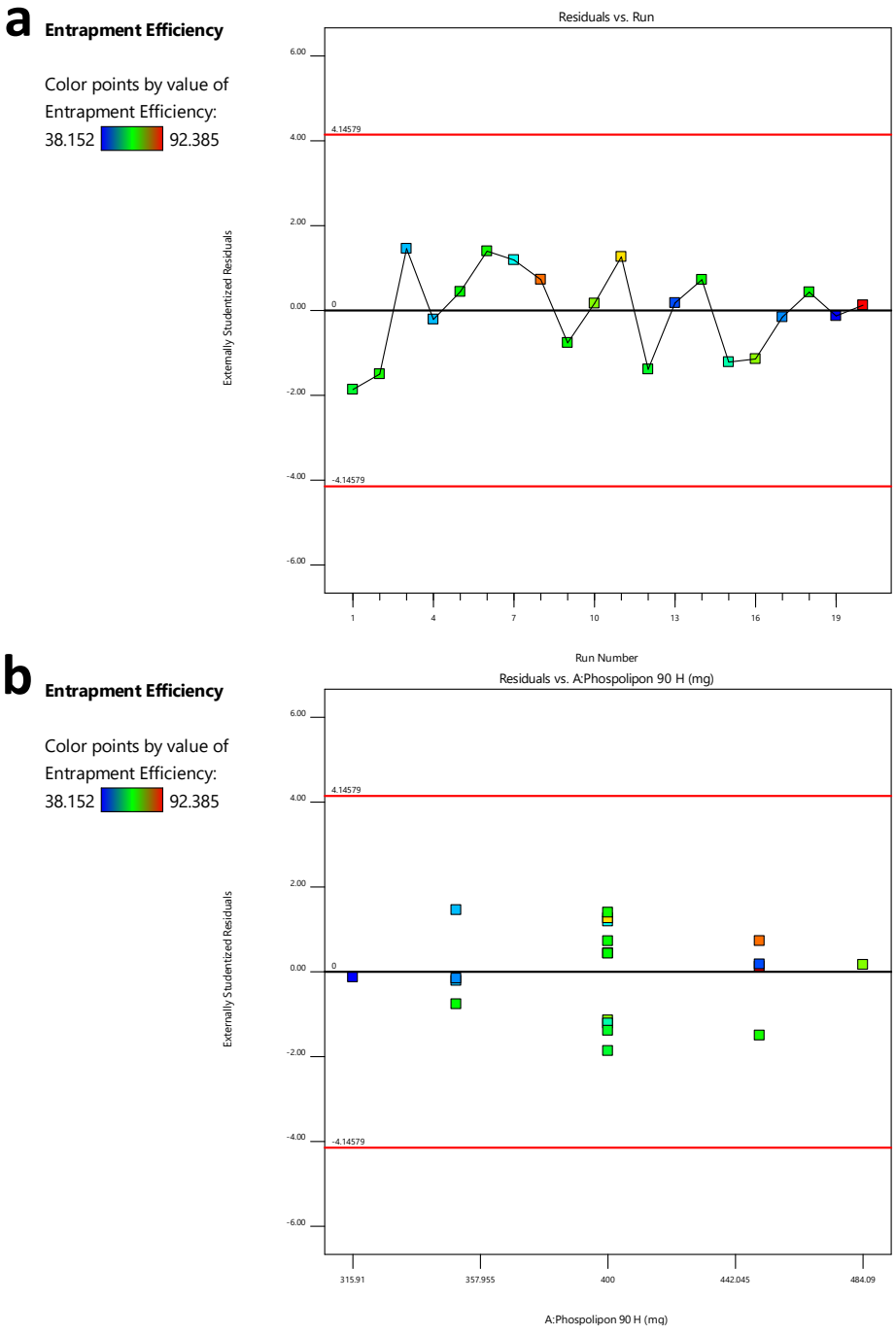

Figure 7. 10 Diagnostic plots for response Y_2: % Entrapment Efficiency (% EE) (a) residual vs. run and (b) residual vs. factor plot

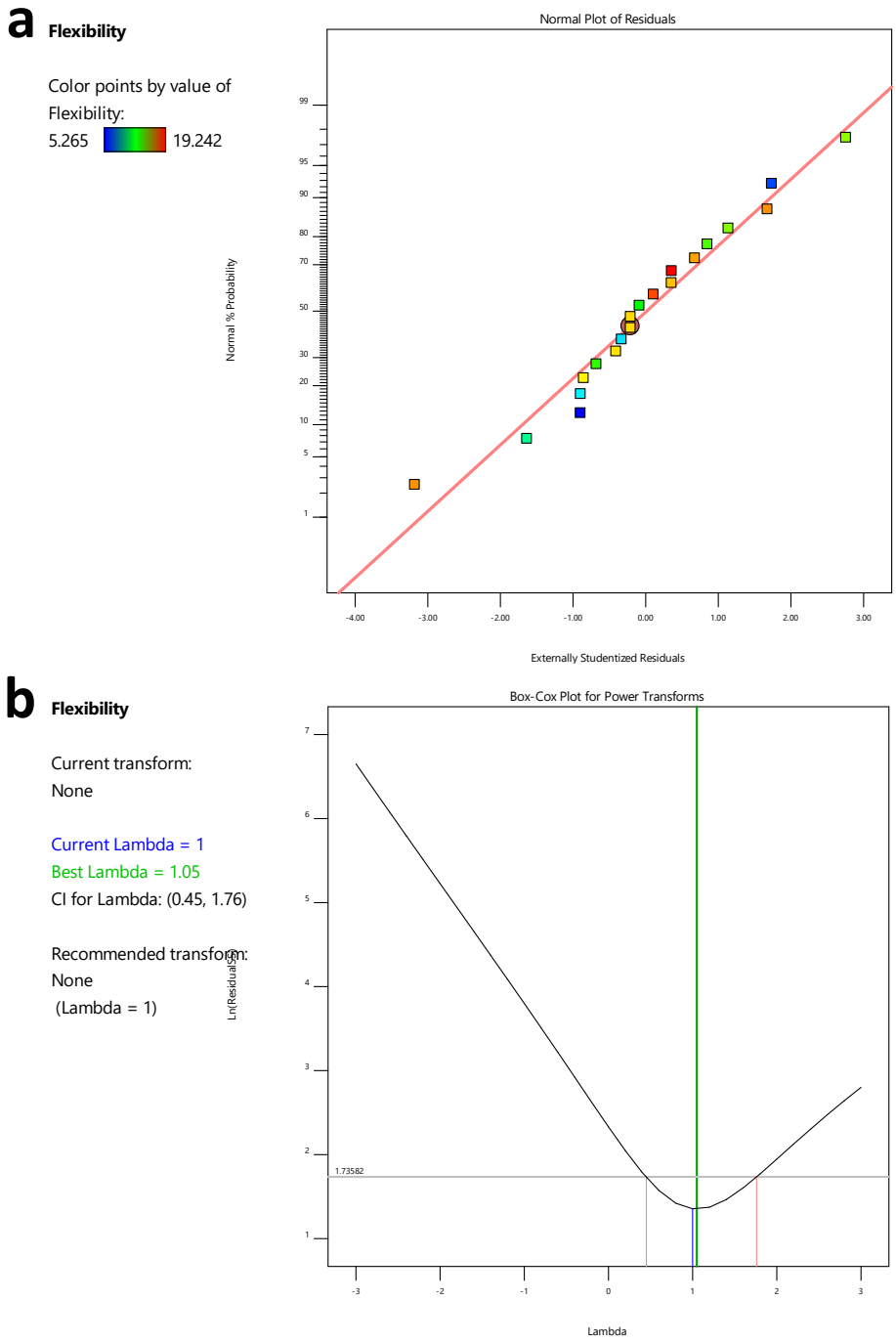

Figure 7. 11 Diagnostic plots for response Y_3: Flexibility (a) normal plot of residuals, and (b) Box-Cox plot

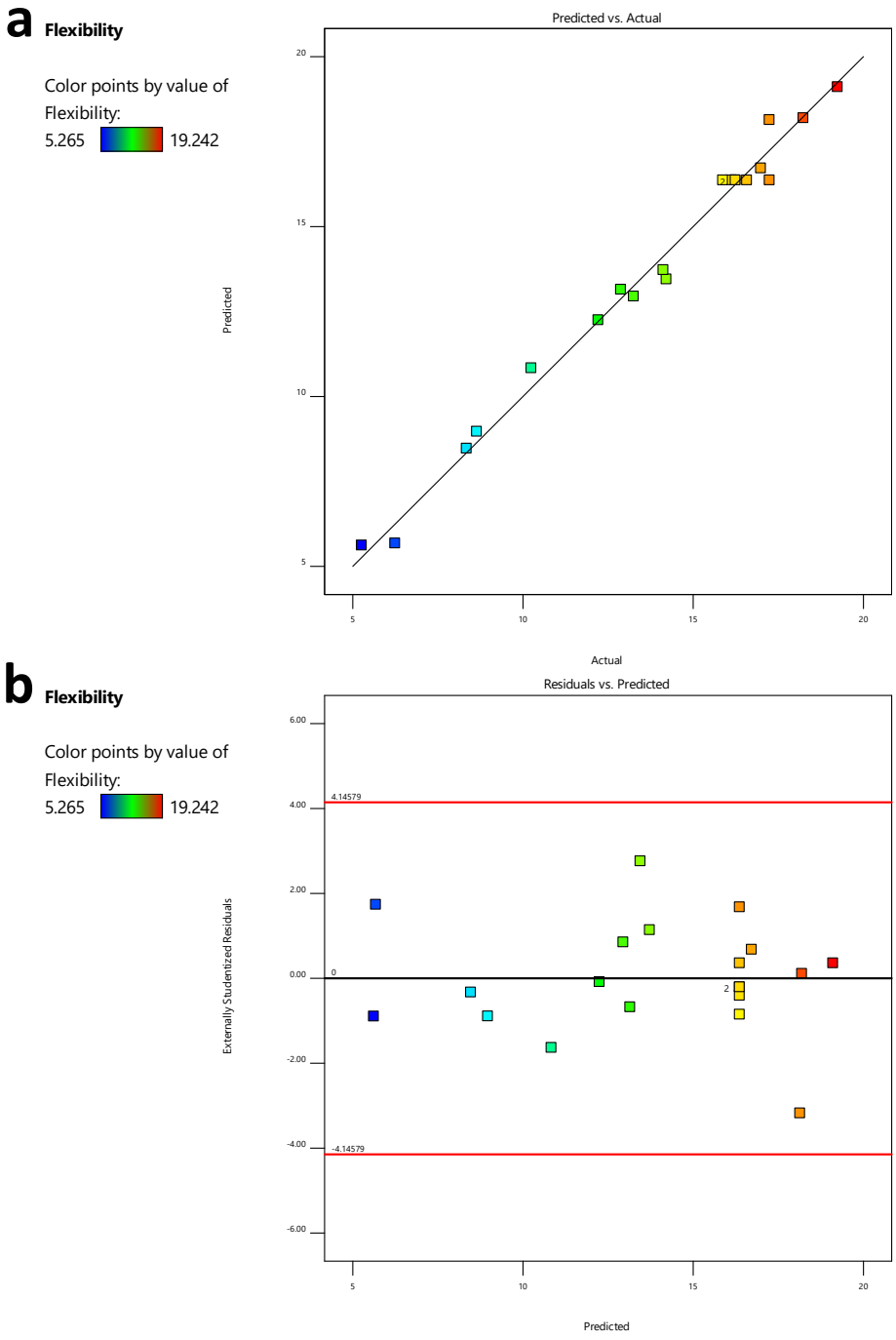

Figure 7. 12 Diagnostic plots for response Y_3: Flexibility (a) predicted vs. actual plot and (b) residual vs. predicted plot

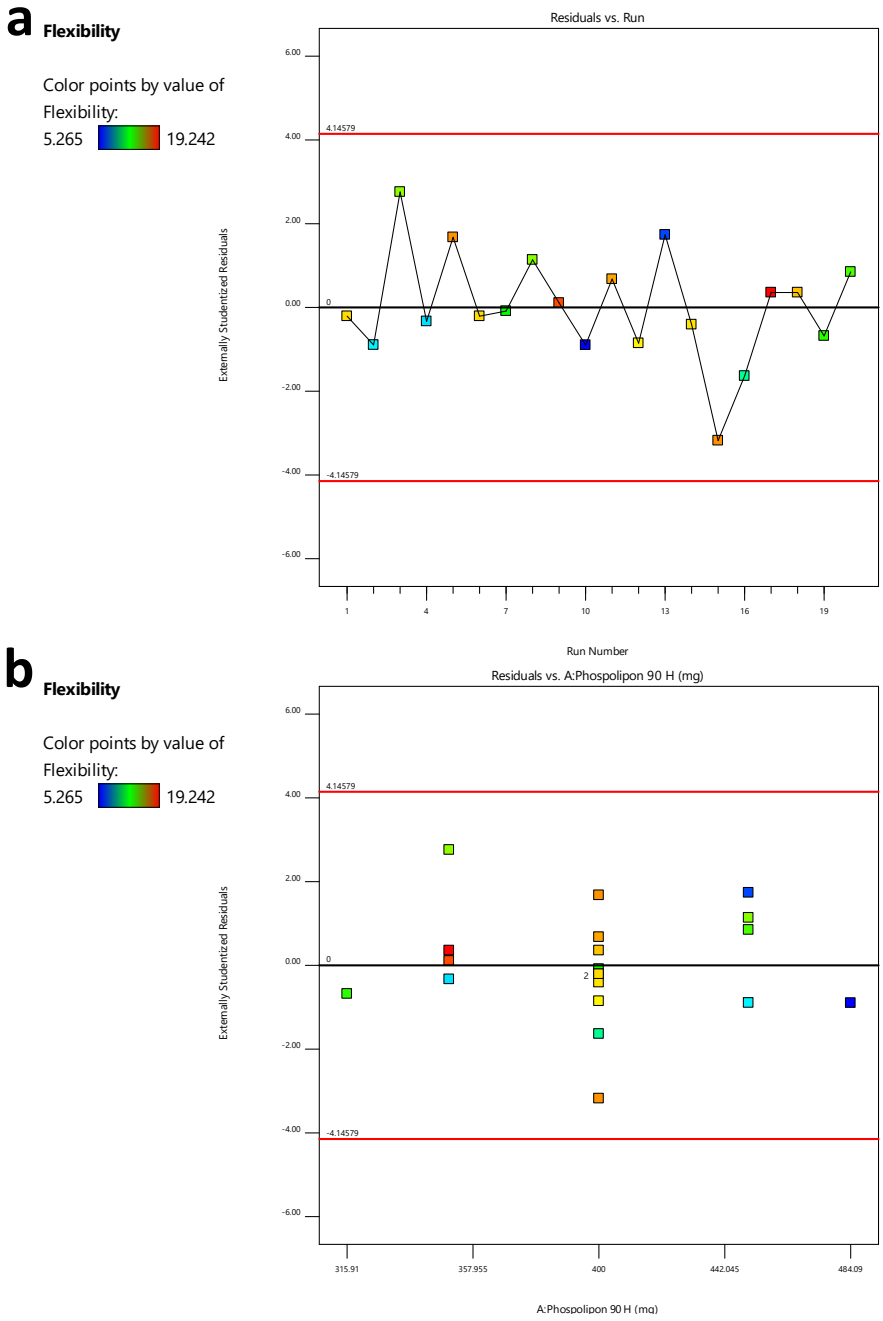

Figure 7. 13 Diagnostic plots for response Y_3: Flexibility (a) residual vs. run and (b) residual vs. factor plot

The anticipated model polynomial coded equations for Y_1, Y_2, and Y_3 are presented in Equation 7.12, Equation 7.13, and Equation 7.14, respectively. In the model-coded equations, the values and signs of the coefficients related to each factor reflect the magnitude and direction of the effect, respectively [162]. The coefficients with a + ve sign indicate a synergistic effect on the response (Y), whereas the -ve sign indicates an inverse effect on the response [162, 177].

Model coded equations

$$Vesicle\ Size\ (Y_1) = 164.24 + 47.27\ X_1 - 11.70\ X_2 - 7.99\ X_3 - 3.07\ X_1X_2 - 4.87\ X_1X_3 - 0.0047\ X_2X_3 - 2.41\ X_1^2 - 4.69\ X_2^2 - 3.81\ X_3^2 \quad (7.12)$$

$$Entrapment\ Efficiency\ (Y_2) = 64.73 + 10.08\ X_1 - 6.63\ X_2 - 6.60\ X_3 - 10.58\ X_1X_2 - 1.29\ X_1X_3 - 4.75\ X_2X_3 - 3.37\ X_1^2 - 0.7516\ X_2^2 + 1.25\ X_3^2 \quad (7.13)$$

$$Flexibility\ (Y_3) = 16.37 - 2.24X_1 + 0.4204\ X_2 + 0.4225\ X_3 - 3.43\ X_1X_2 - 1.05\ X_1X_3 - 1.02\ X_2X_3 - 2.47\ X_1^2 - 1.71\ X_2^2 + 0.3757\ X_3^2 \quad (7.14)$$

The perturbation plots are presented in Figure 7. 14. The plots represent the higher influence of PL-90H on Z_{avg}, % EE, and flexibility of the TFs due to its higher slope as compared to the remaining factors.

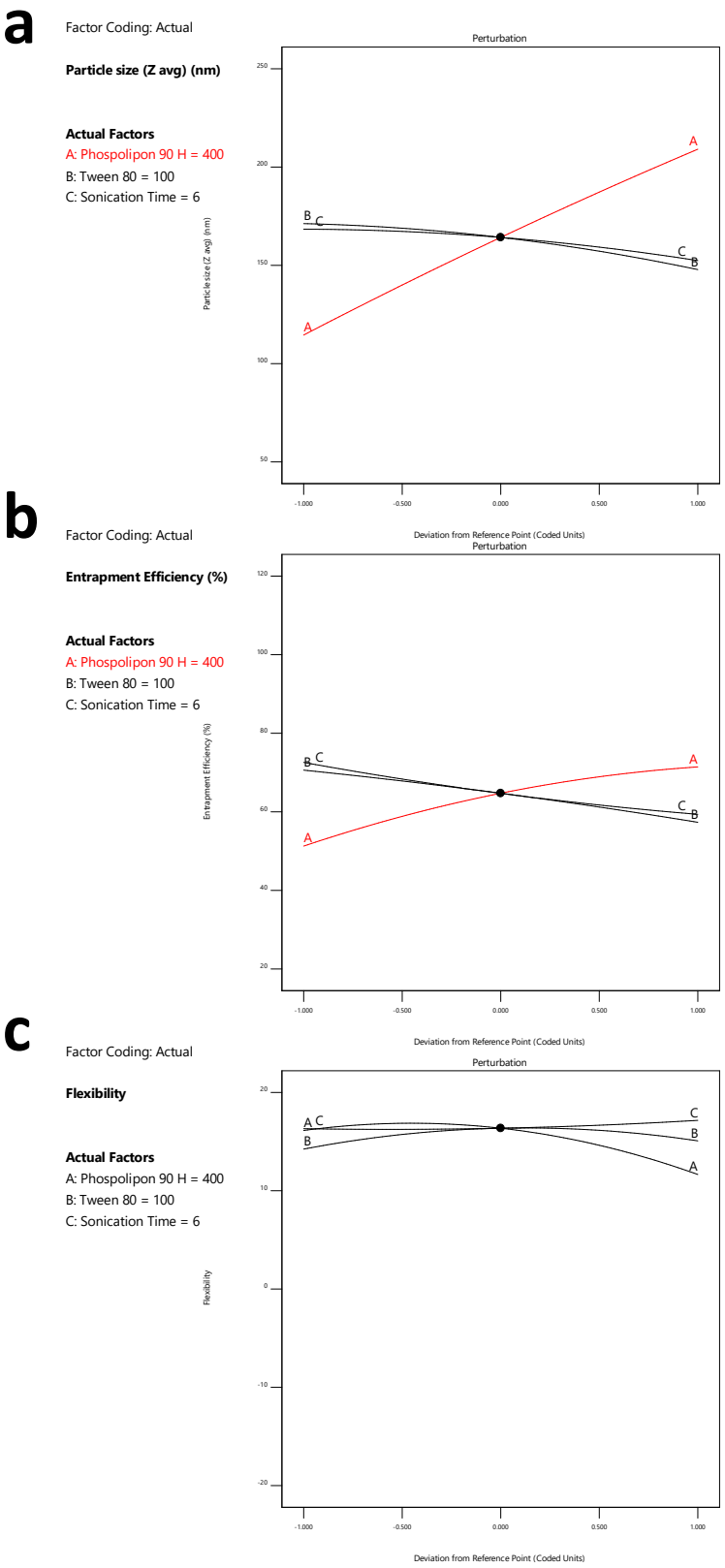

Figure 7. 14 Perturbation plots (a) perturbation plot for Y_1, (b) perturbation plot for Y_2, and (c) perturbation plot for Y_3

The relationships among the investigated factors and responses are represented in 3D response surface plots (Figure 7. 15, Figure 7. 16, and Figure 7. 17). The Z_{avg} was found to be decreased with decreasing the PL-90H concentration, increasing the Tween® 80 concentrations, and sonication time Figure 7. 15 (a-c). The result is in good agreement with the previous report [166]. PL-90H is the major component of the vesicular bilayer and forms a larger vesicle at a higher concentration. The decreased vesicle size at a higher concentration of Tween® 80 is attributed to the reduction of interfacial tension, enhancement of the fluidity, bending ability of the bilayer, and enhanced dispersion of the system in the aqueous medium [164, 166, 172]. An increase in the sonication time causes the disruption of the vesicles and converts the multilamellar vesicles into unilamellar, leading to a decrease in the Z_{avg}. The PDI values of most of the formulations are below 0.3 (Table 7. 3), reflecting the homogeneous and narrow size distribution of the formulations [175, 178]. The larger the magnitude of zeta potential (ζ), the higher the repulsive force among the vesicles, and the better the colloidal stability. Also, the ζ is crucial for transdermal formulations since it affects the rate of permeation across the skin. TFs with a high negative charge effectively improve their skin permeability [179]. The negative ζ values of most of the prepared TFs reflected their potential for transdermal applications (Table 7. 3).

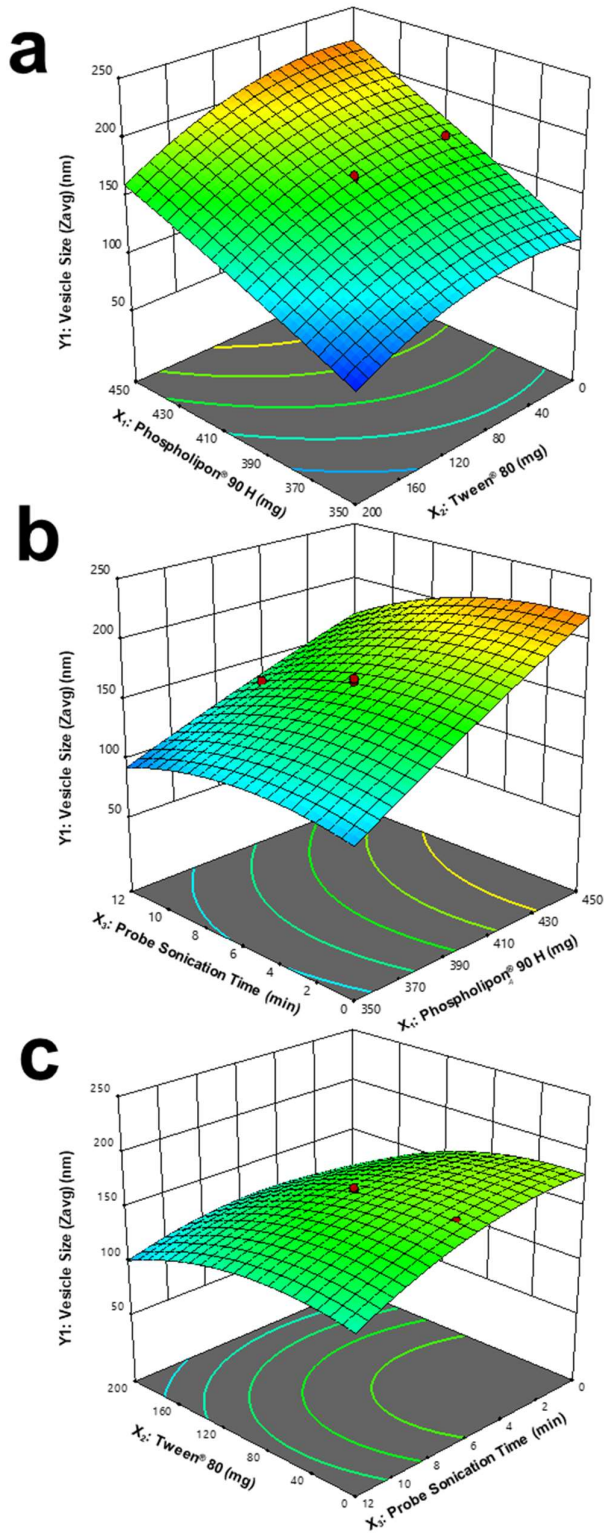

Figure 7. 15 3D response surface plots for vesicle size (a) effect of Tween® 80 and PL-90H on vesicle size, (b) effect of PL-90H and probe sonication time on vesicle size, and (c) effect of Tween® 80 and probe sonication time on vesicle size

The EE was found to be increased with increasing the concentration of PL-90H and decreasing the concentration of Tween® 80 and the sonication time Figure 7. 16 (a-c). An increase in the % EE at a higher concentration of PL-90H is attributed to the complete dispersion of the drug in the bilayer. Lipophilicity also played a crucial role in trapping the lipophilic drug in the lipid phase [166]. In addition, at high concentrations of PL-90H, the vesicle size is larger, leading to a higher % EE. Since the extract (mainly the phytoconstituents) is lipophilic, the lipid bilayer should entrap it; however, in case of small vesicular size, the bilayer is insufficient to accommodate the maximum amount of the drug [179]. At low concentrations of Tween® 80, TFs vesicle formation occurred, whereas, at higher concentrations, the formation of pores in the bilayer and the existence of mixed micelles with the vesicles occurred, leading to a decrease in % EE [175, 180]. The decrease in the % EE with an increase in the sonication time is ascribed to the formation of smaller vesicles at high sonication time.

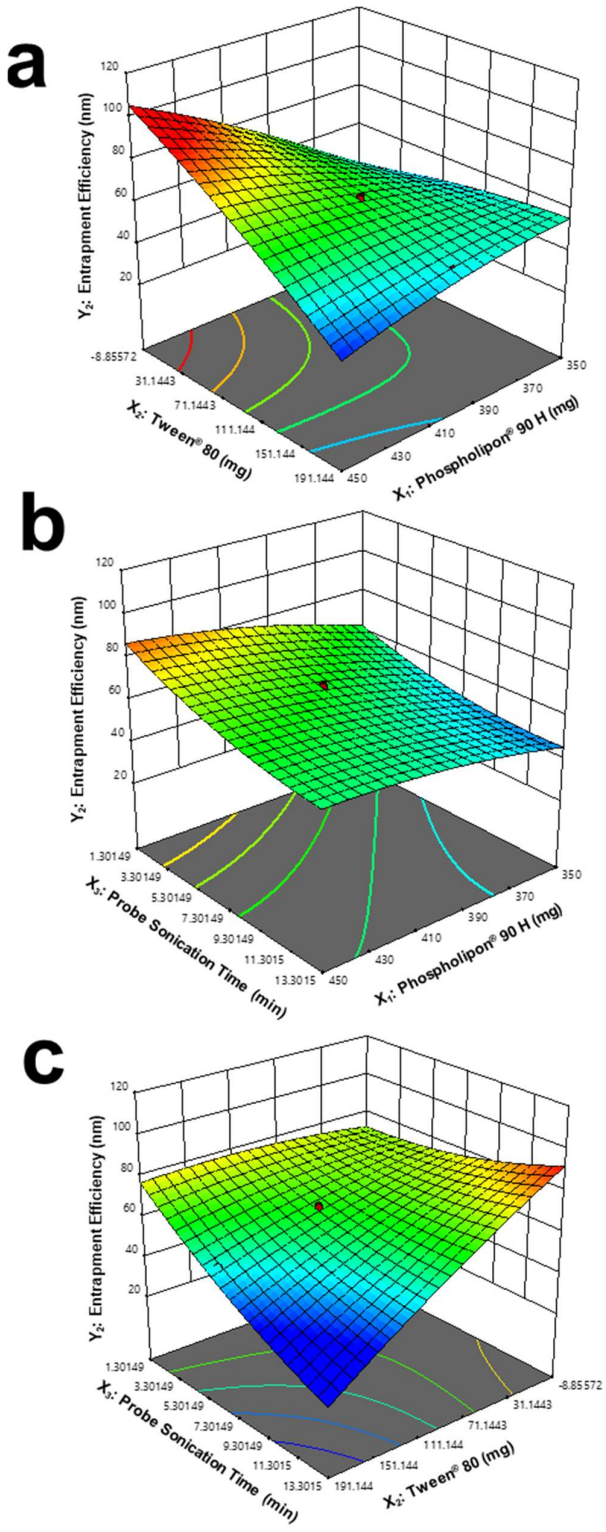

Figure 7. 16 3D response surface plots for entrapment efficiency (a) effect of Tween® 80 and PL-90H on entrapment efficiency, (b) effect probe sonication time and PL-90H on entrapment efficiency, and (c) effect of probe sonication time and Tween® 80 on entrapment efficiency

The flexibility was found to be increased with increasing the concentration of Tween® 80, increasing the probe sonication time, and decreasing the concentration of PL-90H Figure 7. 17 (a-c). Phospholipids offer rigidity to the vesicular membrane, leading to a decrease in flexibility at higher concentrations. The Tween® 80 destabilizes the vesicular bilayer and improves the flexibility by lowering interfacial tension, and results in a reduction of vesicular size [181]. Up to an optimal concentration of Tween® 80 (50 mg~10%), the flexibility was found to be increased; afterward, a further increase in the Tween® 80 concentrations decreased the flexibility, which is due to the formation of micellar suspension or mixed micelles. Such micelles behave as fatty droplets under nonocclusive conditions and are predominantly confined to the topmost layer of the SC due to their less sensitivity towards the trans-epidermal aqueous gradient than TFs [175, 182]. Increased flexibility at high sonication time is attributed to the formation of smaller unilamellar vesicles at high sonication time.

An optimal formulation with the desired responses was established using numerical and graphical optimization tools and the desirability approach. The overlay plot (Figure 7. 18) represents the desired region for constraining variables within the yellow design space with a flag mark representing the optimized batch (i.e., 450 mg of X_1, 50 mg of X_2, and 8.9863 min of X_3). Table 7. 8 represents the validation outcomes of the checkpoint batch. The low percentage prediction error (<5%) for various responses of the checkpoint batch validated the predictive capacity and accuracy of the design model. Besides the evaluated responses (Y_1-Y_3), a very close RI value from 3 different regions of the TFs represented the isotropic nature of the prepared TFs (Table 7. 3). The pH of the TFs was found to be acidic (Table 7. 3). The LC of the formulations was found to be within 3.904 ± 1.036 to 10.254 ± 1.543%.

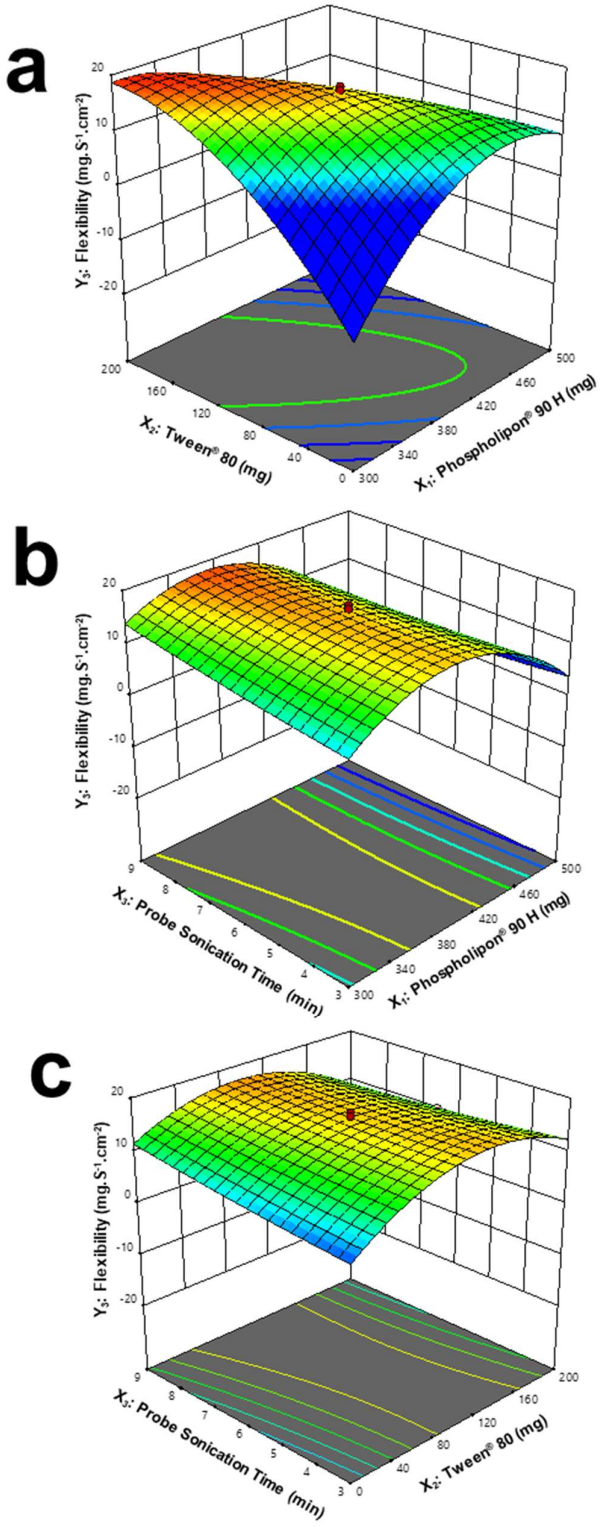

Figure 7. 17 3D response surface plots for flexibility (a) effect of Tween® 80 and PL-90H on flexibility, (b) effect probe sonication time and PL-90H on flexibility, and (c) effect of probe sonication time and Tween® 80 on flexibility

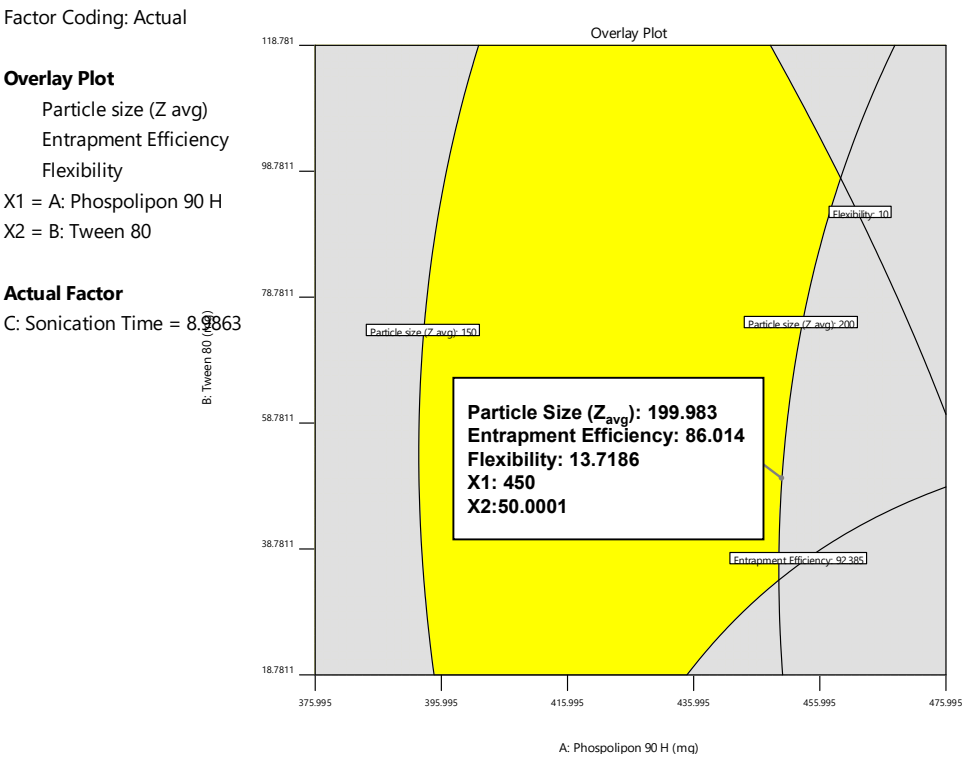

Figure 7. 18 Overlay plot indicating the optimized formula

Table 7. 8 Validations results of checkpoint batch (n = 5)

Responses	**Predicted result**	**Experimental result**	**% Prediction error (% Bias)**
Vesicle Size (Y_1, nm)	199.983	198.223 ± 1.701	- 0.879
Entrapment Efficiency (Y_2, %)	86.014	83.875 ± 1.602	- 2.486
Flexibility (Y_3, mL/s)	13.718	13.187 ± 0.544	- 3.869

7.4.3 Characterization of TFs

7.4.3.1 Z_{avg}, PDI, and ζ

The DLS results of optimized TFs showed a Z_{avg} of 197±1.234 nm and a PDI value of 0.185±0.001 (Figure 7. 19a). The nanometric Z_{avg} of optimized TFs represented the formation of nanovesicles. The PDI was found to be 0.185±0.001 (<0.3), reflecting the monodispersity and narrow size distribution of the vesicles [175, 178]. The width of the correlogram and the middle point of the fall represent the PDI and size of

vesicles, respectively (Figure 7. 19b). A sudden fall in the correlogram also represents the vesicles having low PDI and narrow size distribution.

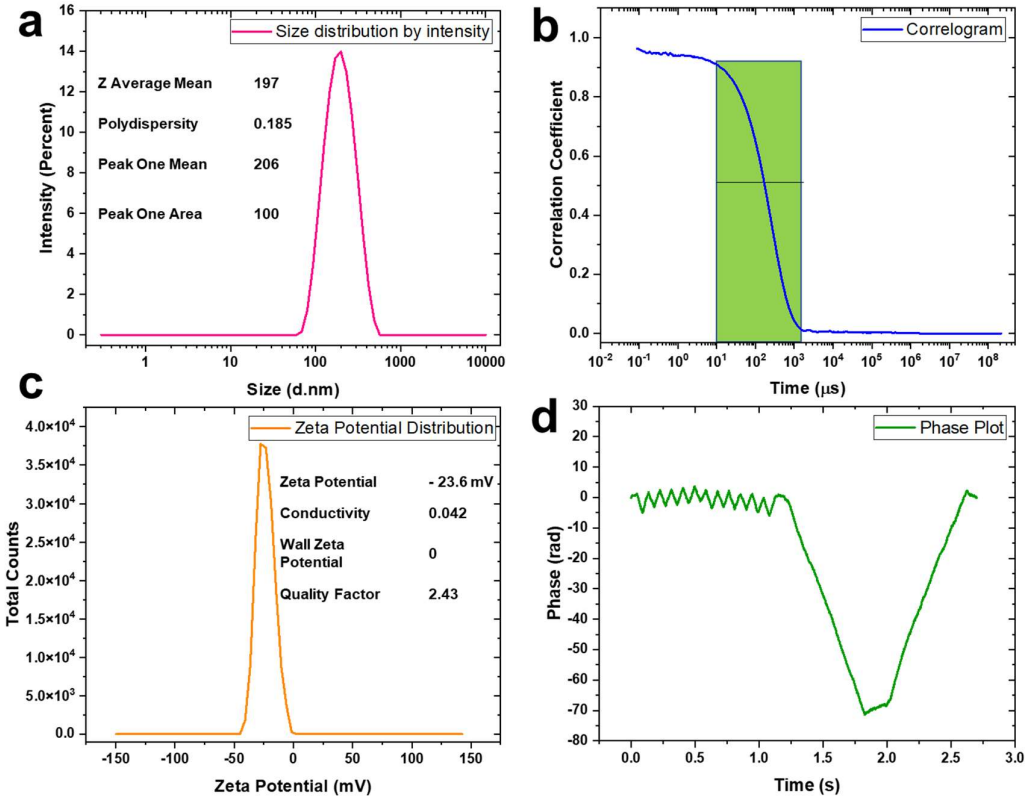

Figure 7. 19 Vesicle size (Z_{avg}), polydispersity index (PDI), and zeta potential (ζ) of optimized TFs (a) Z_{avg}, PDI, (b) correlogram, (c) ζ, and (d) phase plot

The electrostatic surface charge on the vesicles is crucial for formulation stability as it creates a repulsion that prevents particle aggregation [169]. The ζ of most of the nanoformulations range from -30 to +30 mV, where the value from ± 0-10 mV signifies highly unstable, ± 10-20 mV signifies relatively stable, ± 20-30 mV represents moderately stable, and > ± 30 mV represent highly stable product [96]. The ζ result and phase plot are shown in Figure 7. 19c and Figure 7. 19d, respectively. The ζ of the optimized TFs (Figure 7. 19c) was found to be - 23.6±1.243 mV, representing a moderately stable nature with an inverse phase plot showing a negative value (Figure 7. 19d). The -ve ζ is imparted by the -ve charges on the phosphate groups of

phosphatidylcholine moieties [183]. The - ve surface charge on TFs will enhance the permeation across the skin due to the electrostatic repulsion between the like charges (slightly negative) on the skin surface and optimized TFs [167, 170]. TFs with a high negative charge successfully improve their skin permeability [179, 184].

7.4.3.2 Morphology of TFs vesicles

7.4.3.2.1 Optical microscopy

The results of optical microscopy of TFs are shown in Figure 7. 20a-c. The TFs vesicles before probe sonication (Figure 7. 20a) were found to be heterogeneous with the presence of smaller and larger vesicles (>500 nm). In contrast, the optimized TFs showed spherical homogeneous vesicles with a diameter of ~200 nm when photomicrographed at 10X (Figure 7. 20b) and 4X magnifications (Figure 7. 20c). The morphology via optical photomicrograph is in accordance with the reported optical microscopy results TFs [169, 185, 186].

7.4.3.2.2 HRSEM

The HRSEM photomicrograph of optimized TFs is shown in Figure 7. 20d. The TFs are found to be spherical-shaped homogeneous vesicles with smooth surfaces, and most of the particles nearer to 200 nm. The result of HRSEM is in accordance with the outcomes of DLS and optical microscopy. Also, the results of HRSEM are similar to the reported results [162, 167].

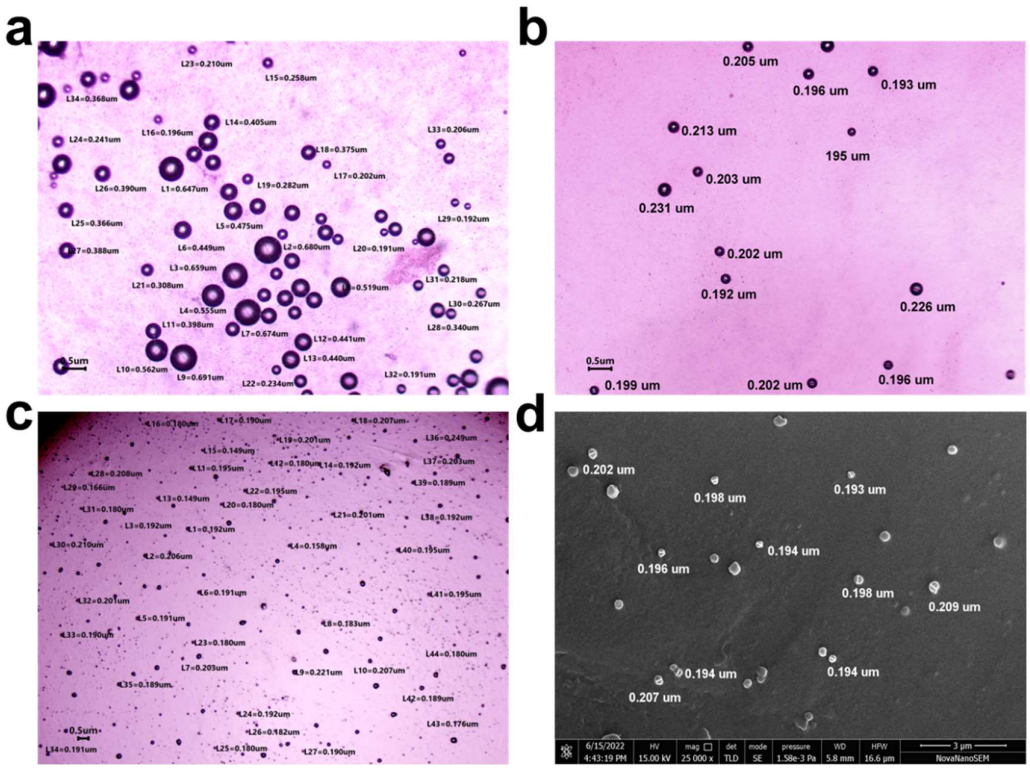

Figure 7. 20 Morphology analysis through optical microscopy and HRSEM (a) optical photomicrograph of TFs before probe sonication at 10X magnification, (b) optical photomicrograph of optimized TFs at 10X magnification, (c) optical photomicrograph of optimized TFs at 4X magnification, and (d) HRSEM photomicrograph of optimized TFs

7.4.3.2.3 Scanning probe microscopy (SPM)

The 2D and 3D SPM photomicrographs of optimized TFs are shown in Figure 7. 21a and Figure 7. 21b, respectively. The optimized TFs were found to be smooth, spherical-shaped, uniformly dispersed vesicles with size within 200 nm (Figure 7. 21a). The 3D SPM photomicrograph of optimized TFs (Figure 7. 21b) also revealed the height of the vesicles within 200 nm. A similar morphology of TFs through SPM was reported previously [187].

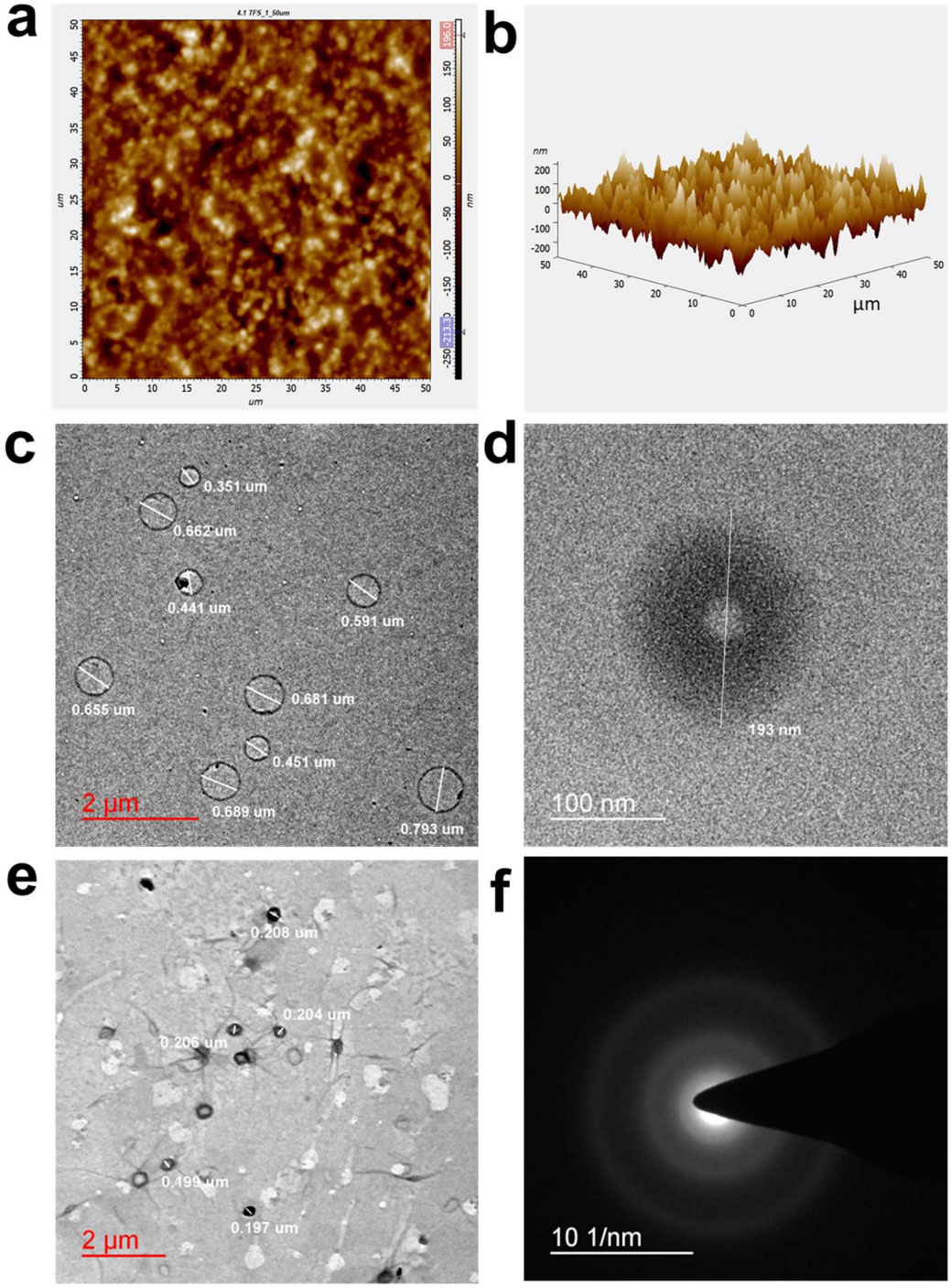

Figure 7. 21 Morphology analysis through SPM and HRTEM (a) 2D SPM photomicrograph of optimized TFs, (b) 3D SPM photomicrograph of optimized TFs, (c) HRTEM photomicrograph of TFs before probe sonication at 2 µm scale, (d) HRTEM photomicrograph of optimized TFs at 100 nm scale, (e) HRTEM photomicrograph of optimized TFs at 2 µm scale, and (f) SAED pattern of optimized TFs

7.4.3.2.4 HRTEM and SAED analysis

The TFs were found to be smooth and spherical, with a clear appearance of phospholipid bilayers and a large aqueous core (Figure 7. 21c-e). Similar morphology of TFs through TEM was reported previously [176, 178, 180, 185, 188]. The TFs vesicles before probe sonication (Figure 7. 21c) were found to be heterogeneous with the presence of smaller and very large vesicles (>500 nm). However, the optimized TFs showed spherical homogeneous vesicles with a diameter of ~ 200 nm (Figure 7. 21d and Figure 7. 21e). The results are in accordance with DLS, optical microscopy, HRSEM, and SPM results. The diffused SAED pattern of (Figure 7. 21f) represents the amorphous nature of the optimized TFs.

7.4.3.3 Drug excipient compatibility study

7.4.3.3.1 ATR-FTIR

The drug-excipient compatibility by ATR-FTIR was verified from the alterations (shifting or vanishing) of the characteristic vibrational spectra. The ATR-FTIR spectra of standardized PLFEE, PL-90H, Tween® 80, their physical mixture, and freeze-dried optimized TFs (TFs FD) are shown in Figure 7. 22.

The PLFEE displayed characteristic peaks at 2929.78 cm^{-1} and 2856.58 cm^{-1} (C-H stretching), 1635.35 cm^{-1} (-C=O-N= stretching), 1612.75 cm^{-1} (aliphatic diene stretching), 1444.24 cm^{-1} (C=C aromatic stretching), 1247.45 cm^{-1} (=C-O-C asymmetrical stretching), 1036.73 cm^{-1} (=C-O-C symmetrical stretching), 998.34 cm^{-1} (C–H bending), and 928.25 cm^{-1} (C-O stretching of methylenedioxy group). The spectra are similar to that of PIP [137, 189] due to its presence in higher amounts.

PL-90H showed peaks at 2917.05 cm^{-1} and 2852.71 cm^{-1} (C–H stretching of fatty acid chain), 1738.75 cm^{-1} (esteric C=O stretching of fatty acid), 1239.53 cm^{-1} (P=O

stretching), 1091.47 cm^{-1} (P-O-C stretching), and 969.76 cm^{-1} ($-N^{+}(CH_3)_3$ stretching) [190].

Tween® 80 showed vibrational peaks at 3507.25 cm^{-1} (alcoholic -O-H stretching), 2922.73 (-C-H asymmetric stretching), 2858.38 cm^{-1} (-C-H symmetric stretching), 1735.62 cm^{-1} (esteric -C=O stretching) [138, 164], 1647.12 cm^{-1} (amidic C=O stretching), 1455.24 cm^{-1} and 1348.32 cm^{-1} (-C-H bending of alkane), and 1297 cm^{-1} to 1092.5 cm^{-1} (C-O stretching esters, alcohols, or ethers).

The ATR-FTIR spectrum of the physical mixture is a superposition of standardized PLFEE, PL-90H, and Tween® 80, representing the retention of the characteristic functional groups of PLFEE and its chemical compatibility with the used excipients.

The freeze-dried optimized TFs (TFs FD) predominantly showed the peaks of excipient (mainly the PL-90H) and all the characteristic peaks of PLFEE with reduced intensity. The presence of all the characteristic peaks of PLFEE in TFs FD with reduced intensity is due to the encapsulation and dilution by the excipients. A similar observation was reported previously [185]. These outcomes demonstrated the absence of any chemical interactions between the excipients and PLFEE in the optimized TFs [164, 185, 191].

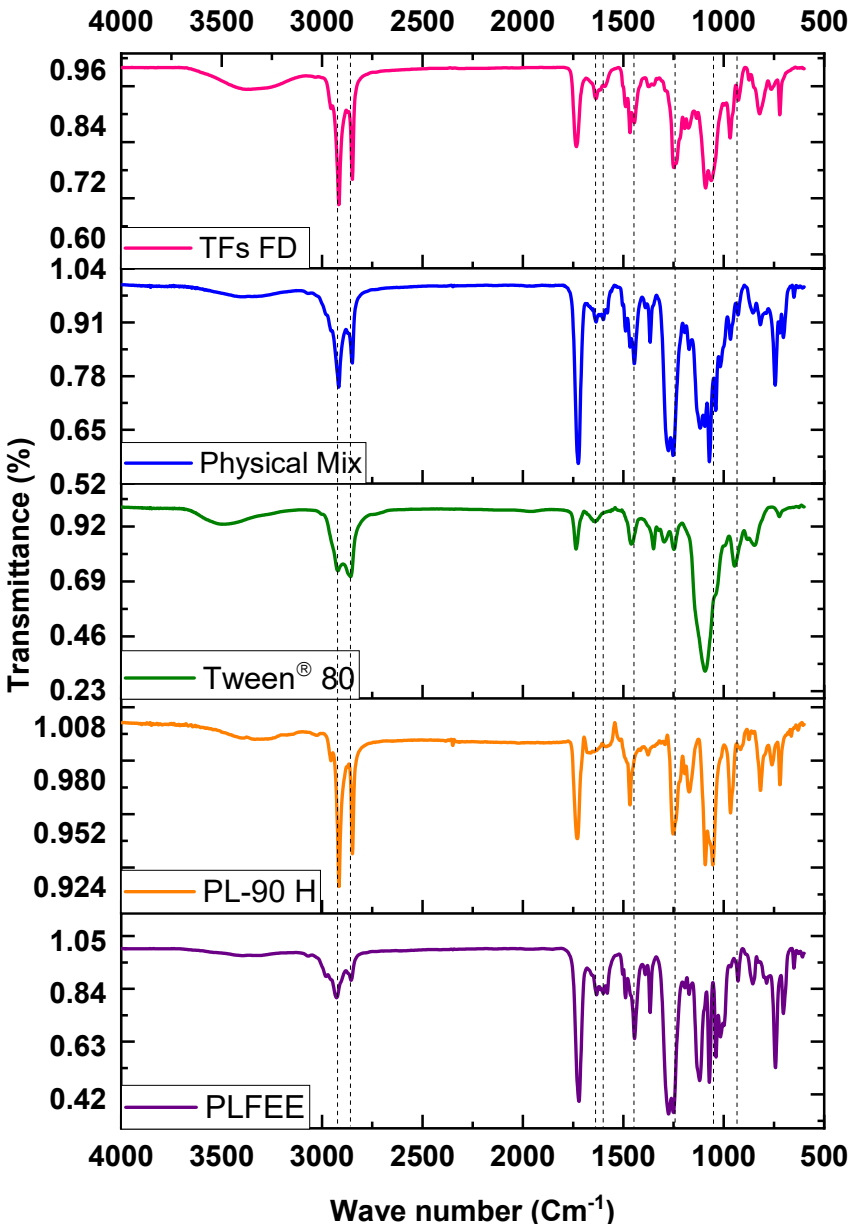

Figure 7. 22 Drug-excipient compatibility analysis in optimized TFs by ATR-FTIR (a) fingerprint under 254 nm, (b) fingerprint under 366 nm, and (c) fingerprint under visible light

7.4.3.3.2 HPTLC

The HPTLC fingerprints of PLFEE, physical mixture, and optimized TFs under UV light (245, 366 nm), and visible light are shown in Figure 7. 23. The obtained retardation factor (Rf) was found to be 0.39 ± 0.0003, and 0.45 ± 0.005 for PIP and

PLGN, respectively. The fingerprints of PLFEE, physical mixture, and optimized TFs showed the chromatographic bands for pure PIP and PLGN at their respective Rf values, reflecting their integrity in the extract, physical mixture, and TFs formulation. All the other bands of PLFEE are also available in the physical mixture and optimized TFs, signifying the absence of any drug-excipient interaction.

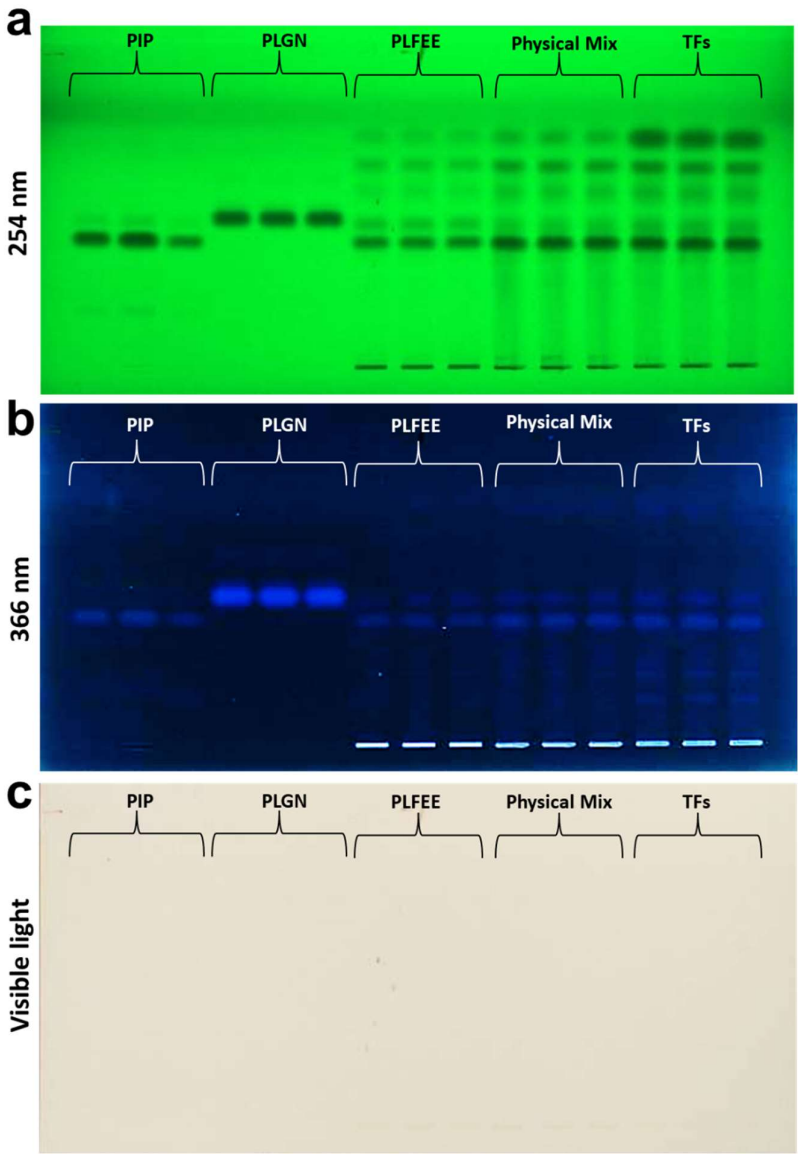

Figure 7. 23 Drug-excipient compatibility analysis in optimized TFs by HPTLC (a) fingerprint under 254 nm, (b) fingerprint under 366 nm, and (c) fingerprint under visible light

7.4.3.4 PLM

The PLM results of PLFEE, PL-90H, their physical mixture, and TFs FD at 0° and 90° are shown in Figure 7. 24. The PLFEE and physical mixture showed intense birefringence, whereas the PL-90H and TFs FD showed no birefringence. Optical anisotropy and birefringence are the characteristics of crystalline materials. In contrast, amorphous materials are optically isotropic and do not possess birefringence. The intense birefringence in the case of PLFEE and physical mixture is due to their crystalline properties. In contrast, the absence of any birefringence in the case of TFs FD is ascribed to its amorphous nature and entrapment of PLFEE in the excipient.

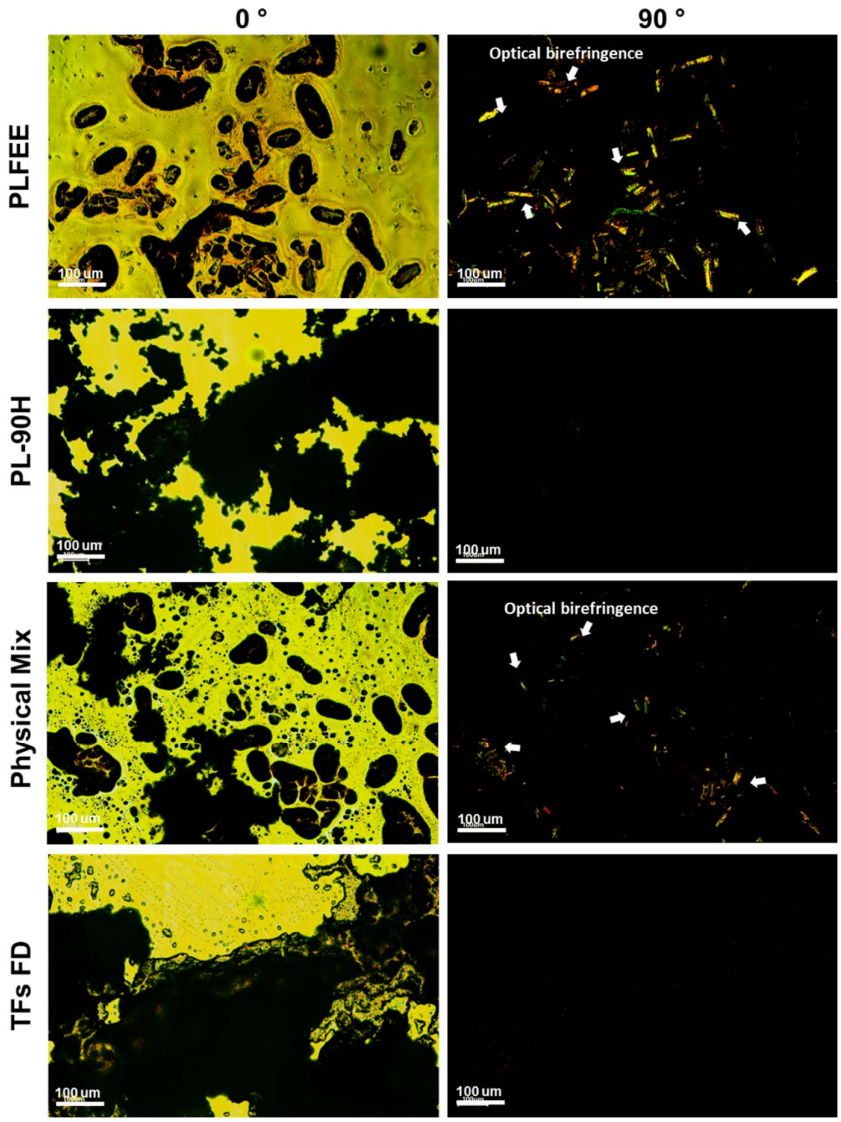

Figure 7. 24 PLM photomicrographs of PLFEE, PL-90H, physical mixture, and TFs FD at 10X magnification

7.4.3.5 XRD

In Figure 7. 25, the PLFEE displayed a series of well-defined sharp diffraction peaks within the diffraction range of 10 to 50°, suggesting its crystalline property. PL-90H exhibited a single broad, intense diffraction peak at 2θ of 21.2° which is well consistent with the previous report [190, 192]. Tween® 80 showed a typical halo diffraction with a diffused peak, owing to its amorphous nature. The diffractogram of the physical mixture showed superimposed diffraction patterns of PLFEE and

excipients. The appearance of the superimposed diffraction pattern of PLFEE and excipients in the physical mixture reflects the retention of crystallinity. However, the less intense diffractions of PLFEE in the physical mixture are due to the dilution/dominating effect of the excipients [180]. TFs FD showed a complete disappearance of the characteristic crystalline peaks of PLFEE. The complete disappearance of the characteristic crystalline peaks of PLFEE in TFs FD is ascribed to its amorphous state or molecular level dispersion or entrapment of PLFEE inside the excipients. Similar results were reported previously [180, 190]. The XRD result is in agreement with SAED and PLM results.

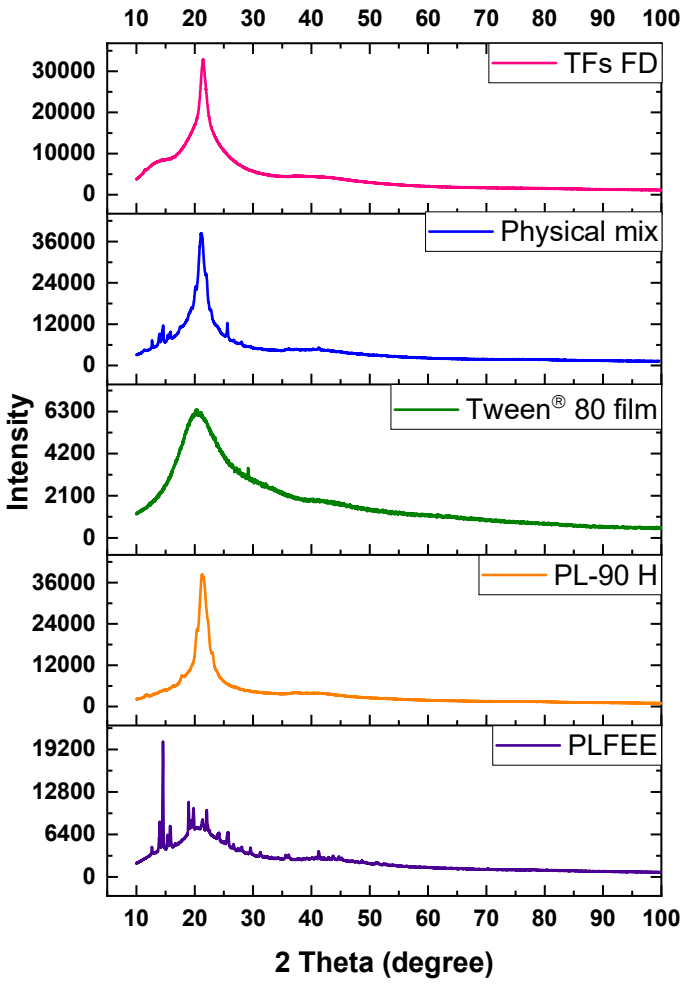

Figure 7. 25 XRD diffractograms of optimized freeze-dried TFs (TFs FD), formulation components (PLFEE, PL-90H, Tween® 80), and physical mixture

7.4.3.6 DSC

DSC was used to investigate the physical state of the drug in the lipid vesicle [164]. From the DSC thermograms (Figure 7. 26), the PLFEE showed a sharp endothermic peak at 121.047°C, representing its crystallinity. PL-90H showed three endothermic peaks at 109.035°C, 125.046°C, and 182.53°C. The peak at 125.046°C is ascribed to the melting of phospholipid, and the peak at 182.53°C is ascribed to phase transition from gel to a liquid-crystalline state, and there may have been additional isomeric or crystal modifications to the carbon chain of phospholipid [190]. The physical mixture showed the crystalline peak of PLFEE, whereas the TFs FD showed a broad endothermic peak with a complete disappearance of the PLFEE peak. The physical mixture retained the characteristic peak of PLFEE (Figure 4B). However, the intensity was reduced due to the dilution effect [193] or molecular level mixing and partial formation of PLFEE-excipients complex at elevated temperatures during the study [190]. The thermogram of TFs FD showed a completely different broad fused endotherm with a complete absence of PLFEE peak, representing the amorphous state of the PLFEE in the lipid vesicle [164], increased PLFEE salvation [180], molecular dispersion in the nano-carrier [167], and complete incorporation into the vesicular compartment [193].

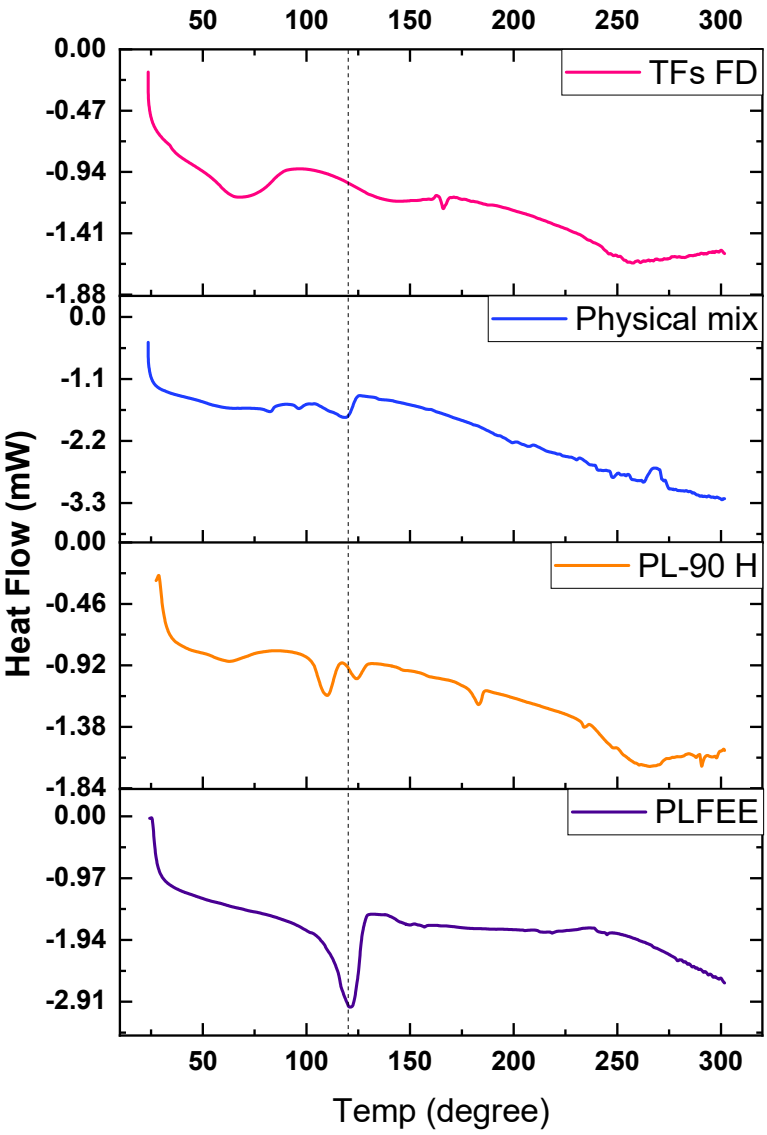

Figure 7. 26 DSC thermogram of optimized freeze-dried TFs (TFs FD), formulation components (PLFEE, PL-90H), and physical mixture

7.4.3.7 TGA

The PLFEE exhibited two-step degradation patterns (Figure 7. 27), with an initial weight loss of 64.555 % from 201.978 to 383.346°C, followed by 23.18% weight loss from 383.346 to 800 C. PL-90H showed 3-step degradation at 221.35 to 319.73°C (18.027%), 319.73 to 376.67 (65.071%), and 376.67 to 800°C (6.964%). The physical mixture also showed 3-step thermal degradation at 137.37 to 216.88 (8.813%), 216.88 to 367.14 (67.489%), and 367.14 to 800°C (11.584%). The TFs FD showed

degradation of 28.971% from 201.42 to 313.46°C, 56.746% from 313.46 to 358.36°C, and 8.277 % from 358.36 to 800°C. The TFs FD showed an entirely different TGA thermogram than that of PLFEE, PL-90H, and physical mixture, possibly due to the molecular level interaction and entrapment of PLFEE inside the vesicle.

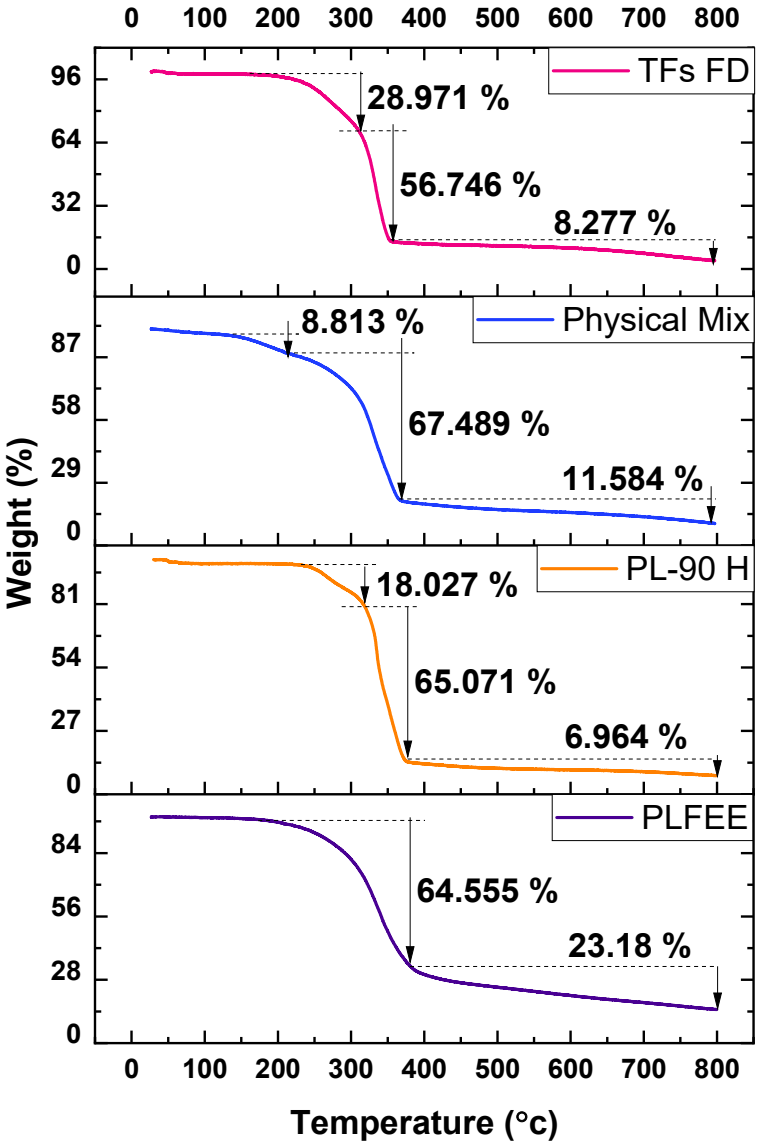

Figure 7. 27 TGA thermogram of optimized freeze-dried TFs (TFs FD), formulation components (PLFEE, PL-90H), and physical mixture

7.4.3.8 Stability study

The stability study results of optimized TFs under long-term (5 ± 3°C) are presented in Table 7. 9. The results of accelerated stability, freeze-thaw, and heating-cooling cycle are presented in Table 7. 10. The results of lyophilization stability are presented in Table 7. 11.

7.4.3.8.1 Physical stability

The results of physical stability represented no substantial changes in the physical properties under refrigerated conditions for up to 12 months. In contrast, the TFs showed slight sedimentation and phase separation after 6 months at accelerated stability conditions and the end of the heating-cooling cycle.

7.4.3.8.2 Colloidal dispersion stability

The Z_{avg} and PDI were found to be maintained for up to 6 months under refrigerated conditions (Table 7. 9) and at the end of the freeze-thaw cycle (Table 7. 10), whereas it was found to be drastically increased with a lapse of time when evaluated under accelerated conditions and at the end of the heating-cooling cycle due to agglomeration of vesicles (Table 7. 10). Under long-term stability conditions (up to 9 months) and after the freeze-thaw cycle, the obtained PDI values are within 0.3, representing the homogeneity; afterward, the polydisperse vesicles were found. In the case of long-term stability (up to 9 months) and at the end of the freeze-thaw cycle, the ζ on the TFs vesicles were found to be maintained and are within the range of ± 20-30 mV, representing moderately stable [96]. In contrast, under accelerated stability conditions and after the heating-cooling cycle, a substantial decrease in the ζ value was observed, ascribed to the agglomeration of vesicles, slight sedimentation, and phase separation.

7.4.3.8.3 Pharmaceutical properties

The % EE, % LC, and flexibility were found to be slightly decreased while evaluated at 6 months under refrigerated conditions (Table 7. 9) and at the end of freeze-thaw cycles (Table 7. 10). However, in the case of accelerated conditions and at the end of the heating-cooling cycle, the values were found to be drastically decreased which might be due to the aggregation, coalescence, and rupture of vesicles, leading to the formation of large-sized rigid multilamellar vesicles, loss of contained drug and flexibility.

7.4.3.8.4 Chemical stability

The retention of all characteristic vibrational peaks of standardized PLFEE at the end of each stability study reflected no signs of chemical incompatibility.

7.4.3.8.5 Lyophilization stability

The results of lyophilization stability are presented in Table 7. 11. The $Z_{avg,}$ PDI, and ZP after reconstitution of the lyophilized TFs were found to be 198.357 ± 1.004 nm, 0.193 ± 0.002, and -23.14 ± 0.097 mV, respectively which is close to the value of optimized TFs in liquid form, representing the lyophilization stability and long-term storage ability of the dried form. The RI, % EE, and LC were found to be close to the initial values. Further, the maintenance of structural integrity, drug-excipient compatibility, and absence of sedimentation & precipitation reflected the lyophilization stability of the optimized TFs.

The overall outcomes of the stability study (Table 7. 9, Table 7. 10, and Table 7. 11) of optimized TFs revealed the retention of physicochemical properties, colloidal dispersion stability, pharmaceutical properties, and drug-excipient compatibility under

refrigerated conditions (5 ± 3°C) for up to 6 months. Further, the optimized TFs also showed freeze-thaw stability and lyophilization stability.

Table 7. 9 Long-term stability study of optimized TFs

Parameters	**Initial results**	**Long-term stability study (5°C ± 3°C)**		
	0 month	**6 months**	**9 months**	**12 months**
Color	Milky white	Milky white		
pH	4.756 ± 0.012	4.735 ± 0.038	4.894 ± 0.057	4.882 ± 0.044
RI	1.335 ± 0.0001	1.334 ± 0.003	1.335 ± 0.002	1.334 ± 0.007
Structural integrity	Spherical bilayered structure	Spherical bilayered structure		
Sedimentation	No	No		
Precipitation	No	No		
Phase separation	No	No		
Z_{avg} (nm)	196.368 ± 1.123	204.334 ± 1.368	221.56 ± 1.546	237.567 ± 2.357
PDI	0.185 ± 0.001	0.194 ± 0.004	0.284 ± 0.002	0.467 ± 0.004
ζ (mV)	- 23.6 ± 1.355	-22.13 ± 1.275	-20.461 ± 0.873	-17.462 ± 1.225
EE (%)	88.545 ± 2.134	85.463 ± 1.841	78.361 ± 2.134	73.253 ± 2.066
LC (%)	9.506 ± 0.223	9.171 ± 0.537	8.408 ± 0.667	7.860 ± 0.571
Flexibility (mL/s)	13.719 ± 1.613	12.876 ± .0.542	10.572 ± 0.879	10.135 ± 0.753
Drug-excipient compatibility	Compatible	Yes		

Results are presented as Mean ± SD

Table 7. 10 Accelerated stability study, freeze-thaw, and heating-cooling stability study of optimized TFs

Parameters	**Initial results**	**Accelerated stability study (25°C ± 2°C/60% RH ± 5% RH)**		**Freeze-thaw (one cycle: -20 °C and 25 °C each for 24 h) and Heating-cooling cycle (one cycle: 40° C and 4° C each for 24 h)**	
	0 month	**3 months**	**6 months**	**Freeze-thaw cycle**	**Heating-cooling cycle**
Color	Milky white	Milky white		Milky white	
pH	4.756 ± 0.012	4.772 ± 0.021	4.898 ± 0.057	4.822 ± 0.039	4.86 ± 0.015
RI	1.335 ± 0.0001	1.335 ± 0.0001	1.334 ± 0.003	1.335 ± 0.002	1.335 ± 0.004
Structural integrity	Spherical bilayered structure	Spherical bilayered structure		Spherical bilayered structure	
Sedimentation	No	No	Slight sedimentation	No	Slight sedimentation after 3rd cycle
Precipitation	No	No		No	No
Phase separation	No	No	Slight separation	No	Yes (after 3rd cycle)
Z_{avg} (nm)	196.368 ± 1.123	228.327 ± 1.159	246.354 ± 2.374	197.616 ± 1.141	219.346 ± 2.352
PDI	0.185 ± 0.001	0.335 ± 0.003	0.573 ± 0.004	0.187 ± 0.003	0.273 ± 0.004
ζ (mV)	- 23.6 ± 1.355	-18.772 ± 1.053	-15.357 ± 1.361	-23.214 ± 0.996	-17.354 ± 1.007
EE (%)	88.545 ± 2.134	67.151 ± 2.165	53.243 ± 1.273	87.165 ± 2.263	77.434 ± 3.631
LC (%)	9.506 ± 0.223	7.205 ± 0.356	5.712 ± 0.673	9.352 ± 0.584	8.308 ± 1.546
Flexibility (mL/s)	13.719 ± 1.613	9.152 ± 2.613	7.167 ± 0.786	12.435 ± 2.443	11.053 ± 0.873
Drug-excipient compatibility	Compatible	Yes		Yes	

Results are presented as Mean ± SD

Table 7. 11 Lyophilization stability of optimized TFs

Parameters	Before lyophilization	After lyophilization (reconstitution)
RI	1.335 ± 0.0001	1.334 ± 0.0002
Structural integrity	Spherical bilayered structure	Spherical bilayered structure
Sedimentation	No	No
Precipitation	No	No
Phase separation	No	No
Z_{avg} (nm)	196.368 ± 1.123	198.357 ± 1.004
PDI	0.185 ± 0.001	0.193 ± 0.002
ζ (mV)	- 23.6 ± 1.355	-23.14 ± 0.897
EE (%)	88.545 ± 2.134	86.359 ± 1.364
LC (%)	9.506 ± 0.223	9.266 ± 0.643
Flexibility (mL/s)	13.719 ± 1.613	13.214 ± 0.316
Drug-excipient compatibility	Compatible	Compatible

Results are presented as Mean ± SD

7.4.3.9 *In-vitro* cytotoxicity assay

The cytotoxicity results of PLFEE and optimized TFs against metastatic melanoma cells (B16F10) and human embryonic kidney 293 cells (HEK293) cells after 24 h are shown in Figure 7. 28a, and Figure 7. 28b, respectively. The log of concentration v/s % cell viability of free PLFEE and optimized TFs against B16F10 were presented in inset Figure 7. 28a. The obtained IC_{50} values of free PLFEE and optimized TFs against B16F10 were found to be 87.41 ± 2.149 µg/mL (R^2 = 0.998) and 45.65 ± 1.396 µg/mL (R^2 = 0.994), respectively. The cytotoxicity by optimized TFs against B16F10 melanoma cells was found to be significantly higher ($p<0.05$) than neat PLFEE (Figure 5A). The higher cytotoxicity of optimized TFs compared to neat PLFEE might be ascribed to its nanostructure, better penetration, and partitioning ability into the cells. The PLFEE and optimized TFs were found to be non-toxic to normal HEK293 cells (Figure 7. 28b). The negligible toxicity of PLFEE and TFs towards normal HEK293 cells represents its selective cancer cell cytotoxicity without harming the normal cells.

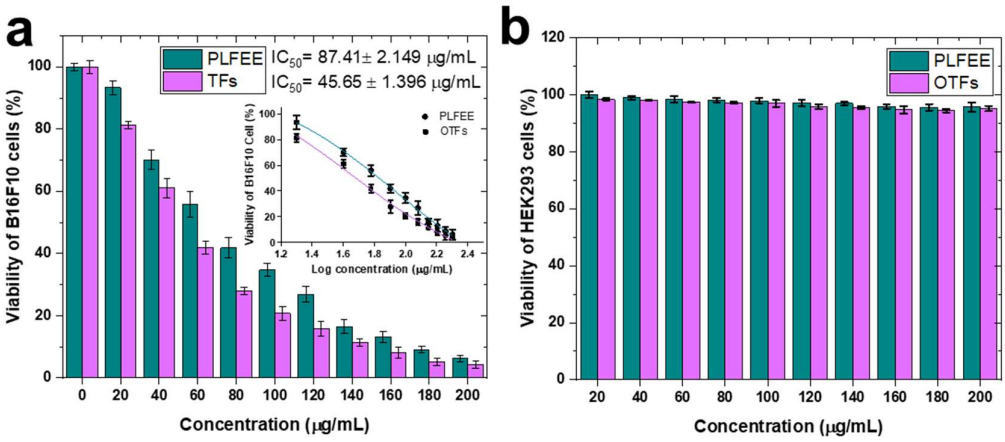

Figure 7. 28 Cytotoxicity studies (a) cytotoxicity of PLFEE and optimized TFs against B16F10 after 24 h with the inset figure showing the log of concentrations v/s % cell viability, (b) cytotoxicity of PLFEE and optimized TFs against HEK293 after 24 h

7.4.3.10 *In-vitro* cellular uptake study

Coumarin-6 (CU-6) was utilized as a model dye [95] for the qualitative cellular uptake study of the TFs. The cellular uptake of free CU-6 and CU-6 loaded optimized TFs (CU-6-TFs) against B16F10 after 1 h is shown in Figure 7. 29a. The CU-6 treated cells showed green-colored fluorescence. In contrast, there was no fluorescence in the CU-6 untreated cells. Nuclear counterstaining with DAPI indicated healthy cells with intact nuclei and uptake of CU-6 to the cytoplasmic region. The fluorescent intensity (Figure 7. 29a and Figure 7. 29b) was found to be higher in the case of CU-6-TFs than CU-6, reflecting better uptake of CU-6 TFs as compared to free CU-6. The increased effective surface area, higher partitioning into the cellular region, and nanostructure of CU-6-TFs may be responsible for the improved uptake of the drug.

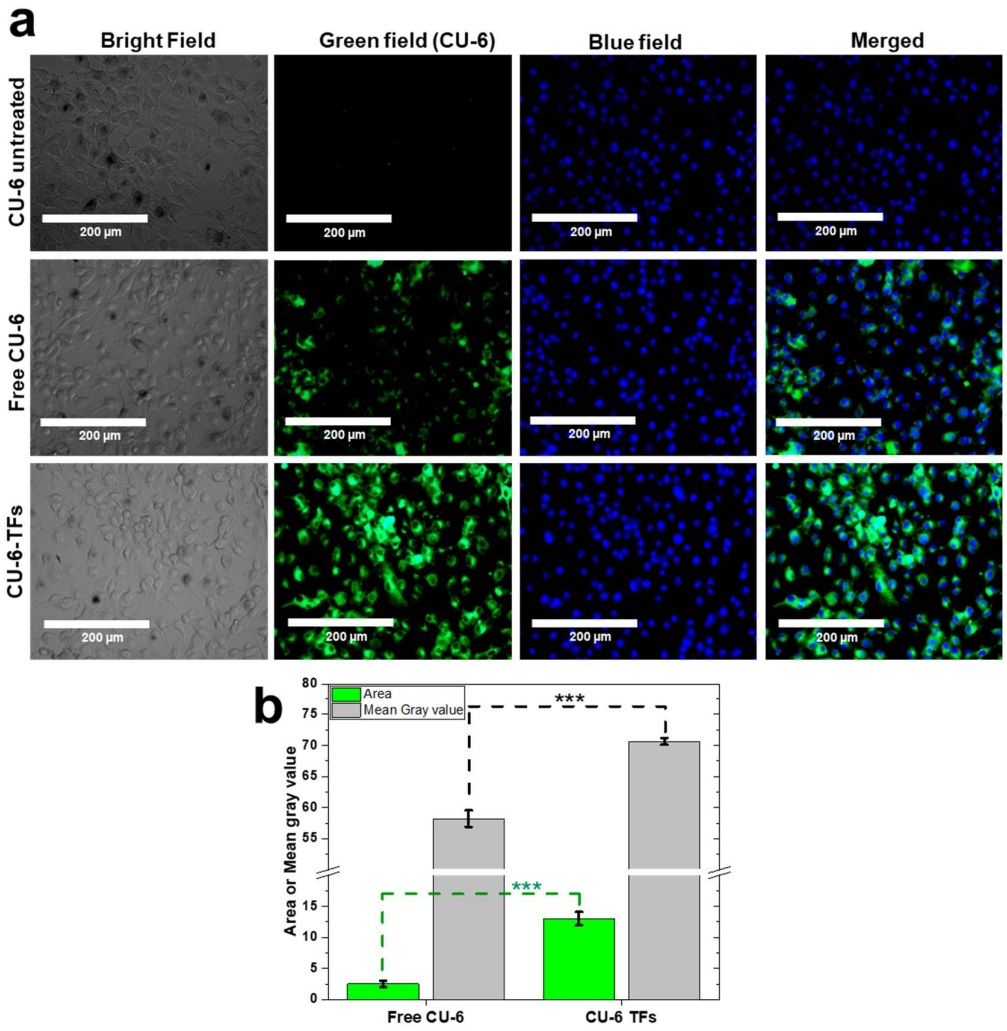

Figure 7. 29 Cellular uptake studies (a) cellular uptake of CU-6 and CU-6-TFs in B16F10 cells after 1 h and (b) quantitative graph of fluorescence intensity of CU-6 and CU-6-TFs in B16F10 cell line in terms of total area and mean gray value statistically analyzed by unpaired t-test at 95% significance level

7.4.3.11 Cell migration assay

The photomicrographs of *in-vitro* cell migration assay (*in-vitro* wound healing assay) are represented in Figure 7. 30a, and the % cell migration is represented in Figure 7. 30b. After 12 h, the control group showed 88.054 ± 3.7625 % of wound area occupied (% migration) by the cells, and after 24 h, it completed occupied the wound area. In contrast, the standardized PLFEE showed 57.736 ± 5.233 % and 78.843 ± 4.357 % of the wound areas occupied by cells at 12 and 24 h, respectively. Further, the optimized

TFs showed a relatively low migration area of 25.468 ± 3.786 % and 67.344 ± 3.346 % at 12 and 24 h, respectively, indicating suppression of cell motility. The standardized PLFEE and optimized TFs significantly ($p<0.05$) inhibited the motility of B16F10 cells compared to the control group at 12 and 24 h (Figure 7. 30b). Further, the optimized TFs also significantly inhibited the % of cell migration compared to the standardized PLFEE. Being a highly metastatic variant of melanoma, the B16F10 rapidly migrated toward the wound area and occupied 100 % of the area after 24h. However, in the case of standardized PLFEE, the migration is inhibited due to its inherent cytotoxic activity. The significant inhibition of the B16F10 cell migration by optimized TFs is ascribed to the increased effective surface area, higher partitioning into the cellular region, better cellular uptake, and nanostructure.

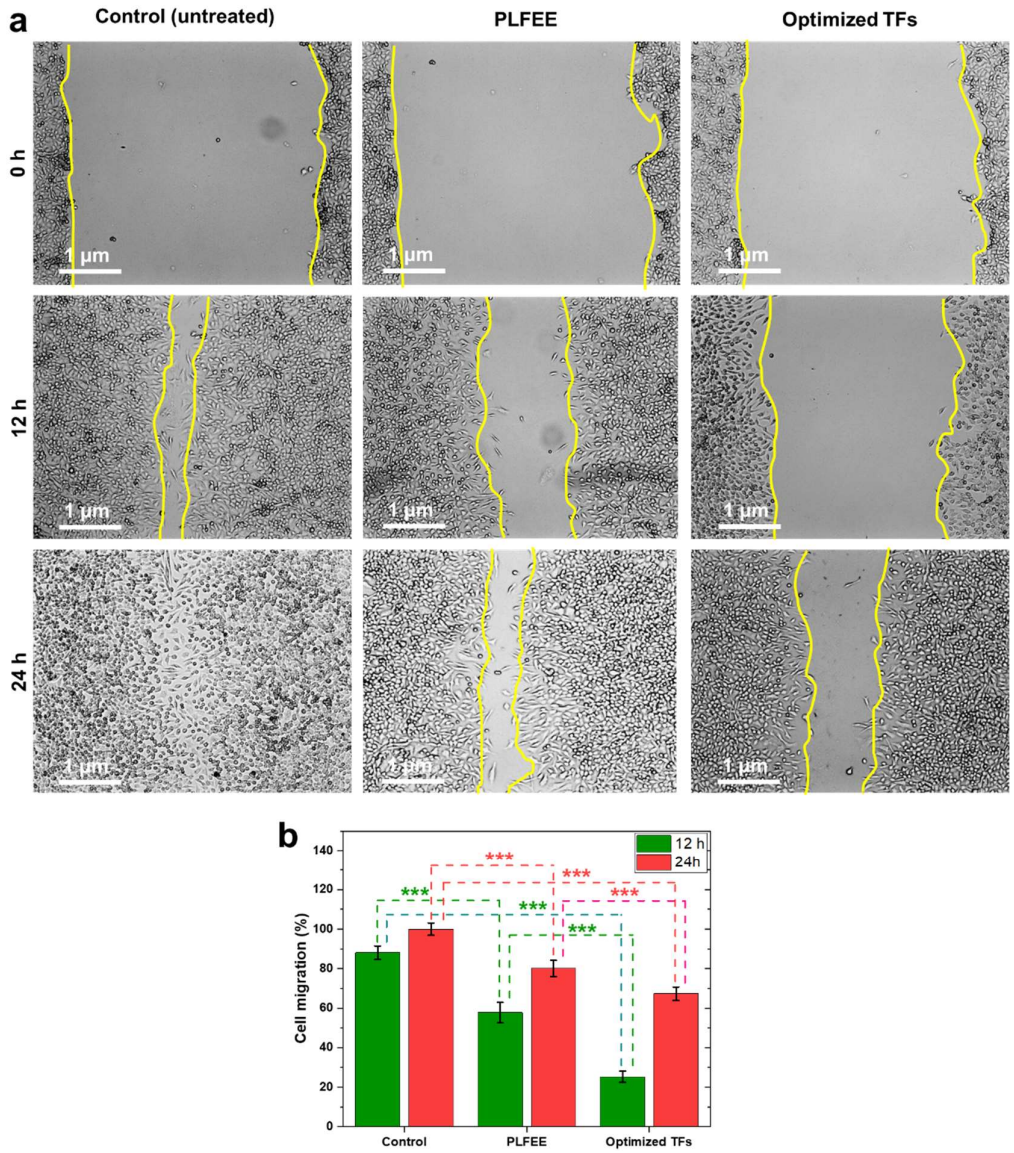

Figure 7. 30 *In-vitro* cell migration assay (a) inhibitory effect of PLFEE and optimized TFs on the motility of B16F10 cells and (b) percentage cell migration in the presence of PLFEE and optimized TFs. Each data point represents the mean ± SD of three independent experiments. The statistical analysis was carried out using one-way ANOVA followed by Tukey's multiple comparison test at $p<0.05$

7.4.3.12 Formulation of transgelosome, placebo transgelosome, and plain gel

Since optimized TFs possess very low viscosity and viscosity has an important role in prolonging drug retention at the application site and better topical applicability, optimized TFs was converted into transgelosome using Xanthan gum. The composition of transgelosomes (TFG F1-F3), placebo transgelosome (Placebo TFG F2), and plain gel is shown in Table 7. 12. Xanthan gum is a GRAS-listed high molecular weight polysaccharide widely used in the pharmaceutical industry as gelling agent for topical products. It is nontoxic, nonirritant, compatible with the majority of drugs, and exhibits excellent viscosity and stability characteristics over a broad pH (pH 4-10) and temperature (10-60°C) range [194].

Table 7. 12 Composition of transgelosomes, placebo transgelosome, and plain gel

Ingredients	**Formulations**				
	TFG F1	**TFG F2**	**TFG F3**	**Placebo TFG F2**	**Plain Gel**
PLFEE (mg)	--	--	--	--	250
Xanthan Gum (% w/v)	1	3	5	3	3
Methyl Paraben (% w/w)	0.1	0.1	0.1	0.1	0.1
Propyl Paraben (% w/w)	0.05	0.05	0.05	0.05	0.05
Propylene glycol (% w/w)	12.5	12.5	12.5	12.5	12.5
250 mg PLFEE-loaded optimized TFs (mL)	10	10	10	--	--
Placebo optimized TFs (mL)	--	--	--	10	--
Water (mL)	--	--	--	--	10

7.4.4 Characterization of gel

Table 7. 13 represents the characterization outcomes of the prepared gel formulations.

Table 7. 13 Characterization of transgelosome, plain gel, and placebo transgelosome

Formulations	TFG F1	TFG F2	TFG F3	Placebo TFG F2	Plain Gel	Omnigel
Appearance	White color	White color	White color	White color	Pale yellow	White color
Consistency and homogeneity	Gel like consistency with smooth and homogeneous properties	Gel like consistency with smooth and homogeneous properties	Gel like consistency with smooth and homogeneous properties	Gel like consistency with smooth and homogeneous properties	Gel like consistency with smooth and homogeneous properties	Gel like consistency with smooth and homogeneous properties
Spreadability (cm)	5.467 ± 0.047	5.034 ± 0.048	4.547 ± 0.031	5.103 ± 0.091	5.23 ± 0.089	4.941 ± 0.417
Extrudability (g)	141.217 ± 2.157	154.372 ± 1.428	164.739 ± 2.357	150.367 ± 1.445	146.125 ± 2.147	155.847 ± 1.665
pH	6.725 ± 0.051	6.736 ± 0.018	6.682 ± 0.023	6.279 ± 0.041	6.652 ± 0.035	6.67 ± 0.035
Viscosity (mPa.s) at Shear rate of 25.1/sec	101.203 ± 2.117	450.042 ± 3.464	847.16 ± 3.837	426.31 ± 2.643	407.73 ± 2.137	464.19 ± 2.432
Drug content (%)	98.356 ± 1.258	98.647 ± 1.124	97.899 ± 2.237	0	98.436 ± 1.159	--
Syneresis (%)	1.834 ± 0.012	0.671 ± 0.001	0.554 ± 0.0.004	0.832 ± 0.002	0.941 ± 0.003	0.604 ± 0.001

Results were represented as mean ± standard deviation (n = 3)

7.4.4.1 Organoleptic properties

All gel formulations were found to be gel-like and opaque in nature. The TFGs were white in color, while the plain gel was found to be pale yellow (Figure 7. 31). The white color of TFGs is imparted by the phospholipid, which entrapped the PLFEE in the bilayer.

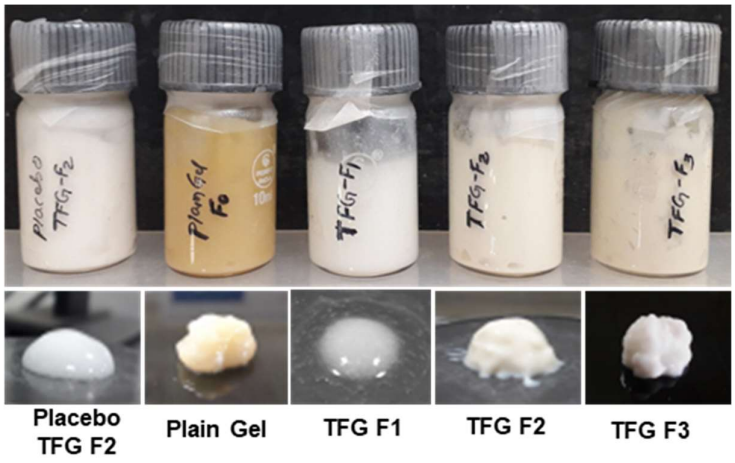

Figure 7. 31 Photographs of prepared gels (placebo TFG F2, plain gel, TFG F1, TFG F2, and TFG F3)

7.4.4.2 Consistency and homogeneity

For better patient acceptance, consistency and homogeneity are of utmost importance. All the gels presented a pleasant appearance, semisolid gelling consistency, and homogeneous (+++) properties without any gritty particles and lumps (Figure 7. 31).

7.4.4.3 Spreadability

For better patient compliance, a gel should be able to be applied comfortably. It is more comfortable to apply the formulation topically to damaged or inflamed skin if the gel spreads readily and has maximum ‘‘slip’’. Additionally, gel shouldn't be very slippery because this affects its ability to retain at the application site. More viscous gel possesses poor spreadability. Hence, optimum spreadability is desired for topical applicability. All the prepared gel showed good spreadability. The spreadability of

TFG F2 (5.034 ± 0.048 cm) was found to be well comparable to the spreadability value (4.941 ± 0.417 cm) of marketed gel (Omnigel, Cipla Ltd.) (Figure 7. 32a and Figure 7. 32b), reflecting its potential topical applicability.

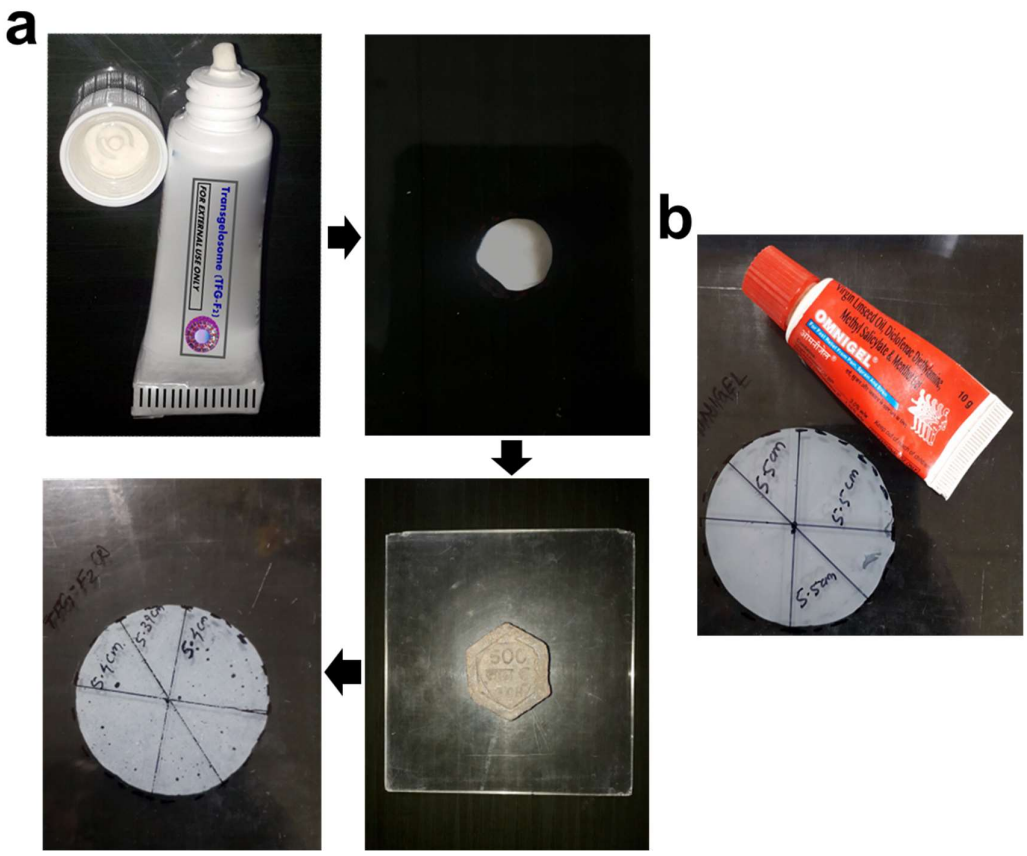

Figure 7. 32 Spreadability study of gels (a) spreadability of TFG F2 and (b) spreadability of marketed gel (Omnigel, Cipla Ltd.)

7.4.4.4 Extrudability

Extrudability of the gel is the power required to push out from the collapsible tube. The extrudability of TFG F2 in terms of weight desired to extrude 0.5 cm ribbon was found to be 154.372 ± 1.428 g, which is close to the values of marketed Omnigel (155.847 ± 1.665), representing the ability of the gel to extrude easily with thumb pressure.

7.4.4.5 pH

The pH of gel meant for dermal/transdermal applications is crucial, as formulations with a higher acidity or alkalinity affect the natural environment of the skin [163, 164]. All the gel formulations possess pH values (6.279 ± 0.041 to 6.736 ± 0.018) close to the pH value (6.67 ± 0.035) of reference marketed gel (Omnigel, Cipla Ltd.) (Table 7. 13) and are within the acceptable normal physiological range to avoid skin irritation, reflecting their topical applicability [163, 164, 166, 195].

7.4.4.6 Rheological studies

The viscosities of evaluated hydrogels at a shear rate of 25.1/sec are shown in Table 7. 13. The viscosity of TFG F2 (450.042 ± 3.464 mPa.s) is higher than the plain gel (407.73 ± 2.137 mPa.s) and is closure to the viscosity of marketed gel (464.19 ± 2.432 mPa.s) signifying the attainment of optimum viscosity and expected to enable retention of gel at topical site. The higher viscosity of the TFG F2 than the plain gel was ascribed to the presence of phospholipid and edge activator [174].

All the gel formulations showed non-Newtonian behavior and exhibited a shear-thinning pseudoplastic type of flow, reflecting the decrease in viscosity with an increase in the shear rate [196]. Similar results were reported previously with vitamin C-enriched adapalene-loaded TFG [195] and ketoconazole-loaded TFG [196]. During the increase in the shear stress (Figure 7. 33), the disarranged molecules of the gelling agent are caused to align their long axes in the direction of flow. Such orientation decreases the internal resistance of the material and reduces the viscosity. The rheogram of TFG F2 is superimposable with that of reference marketed gel, representing the possession of optimal consistency for topical application.

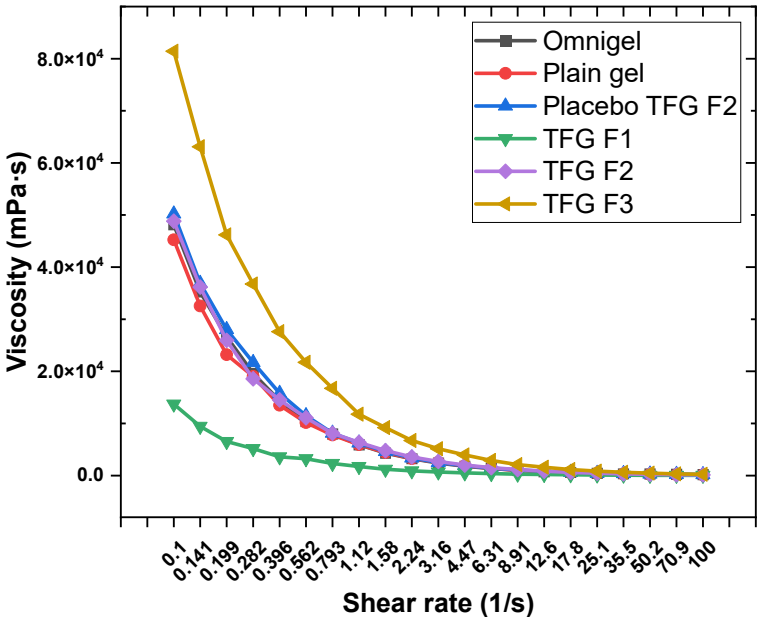

Figure 7. 33 Rheogram of various gel

The amplitude sweep curves (Figure 7. 34a-f) of various gels represent their deformation behavior (gel to fluid transition) under a particular shear strain (%). The point of inflection represents the yield value, i.e., the deformation point of the gel. Low yield value represents the requirement of relatively low shear strain to spread the gel at the topical site. The values of the evaluated gels were in the order of TFG F1 < plain gel < placebo TFG F2 < TFG F2 < Omnigel < TFG F3.

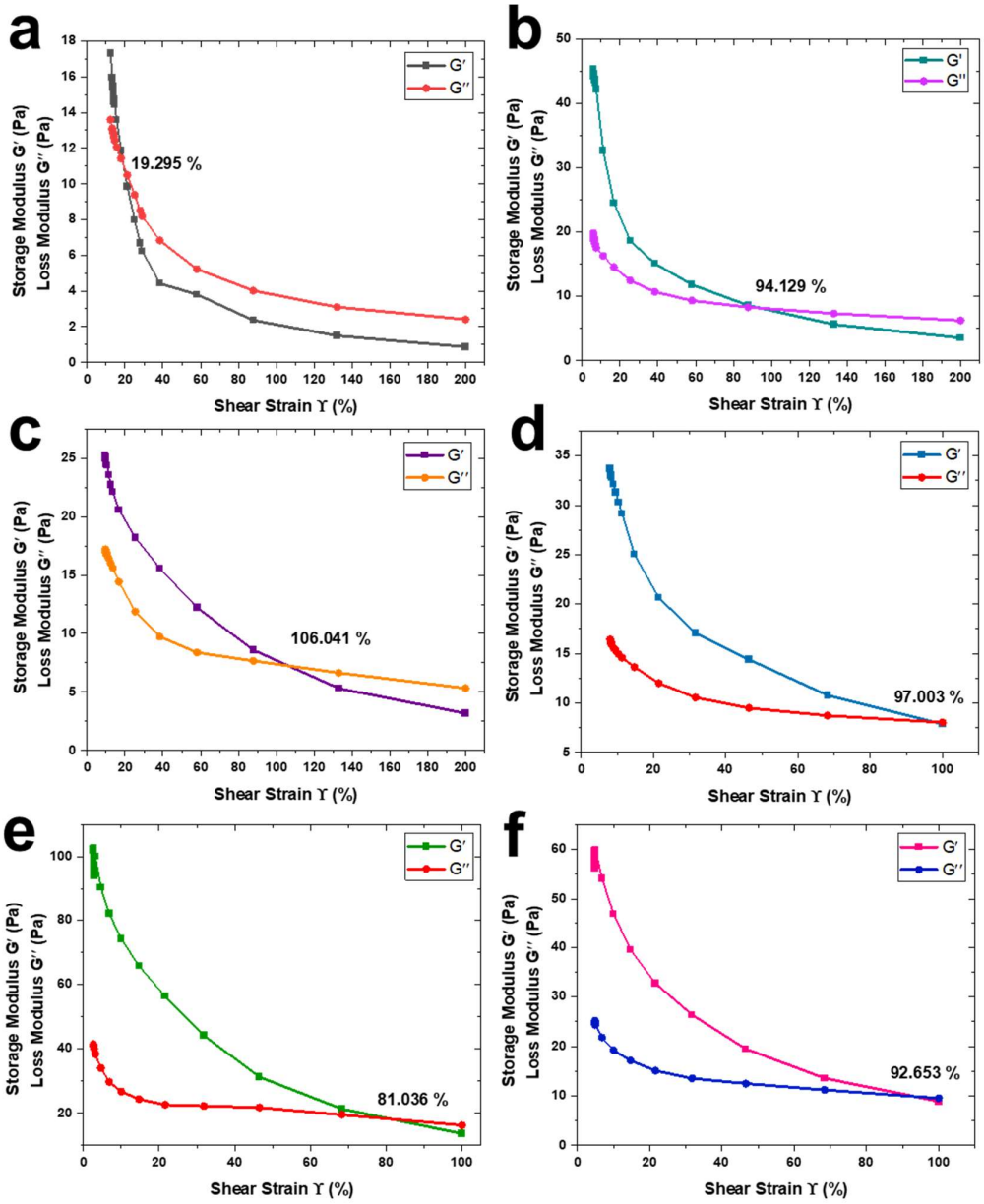

Figure 7. 34 Amplitude sweep curve of (a) TFG F1, (b) TFG F2, (c) TFG F3, (d) marketed Omnigel, (e) plain gel, and (f) placebo TFG F2 gel

7.4.4.7 Drug content and content uniformity determination

The drug content was found to be within 97.899 ± 2.237 to 98.647 ± 1.124% (Table 7. 13), and the content % relative standard deviation (% RSD) of the samples withdrawn from various regions of the container was found to be <2%, reflecting the

homogeneous distribution of the drug throughout the gel matrix and content uniformity.

7.4.4.8 Syneresis

Syneresis is an unwanted natural phenomenon of hydrogel in which unbound excess water is pressed out from the gel matrix due to shrinkage, which can be controlled by the selection of an appropriate gelling agent at optimum concentration. The outcomes of % synersis of various gels are represented in Table 7. 13. The TFG F1 showed high synersis vaslue (1.834 ± 0.012%) compared to other gels due to low concentration of gelling agent. The % syneresis value of TFG F2 (0.671 ± 0.001%) was found to be well comparable with the marketed gel (0.604 ± 0.001%). Such a low synersis value represents the consistency of the prepared gel.

7.4.4.9 Compatibility study

Figure 7. 35 and Figure 7. 36 represent the ATR- FTIR spectra of gel formulations and physical mixture. The peaks of PLFEE (as stated under 7.4.3.3.1.) were found to be retained in the physical mixture and gel formulations.

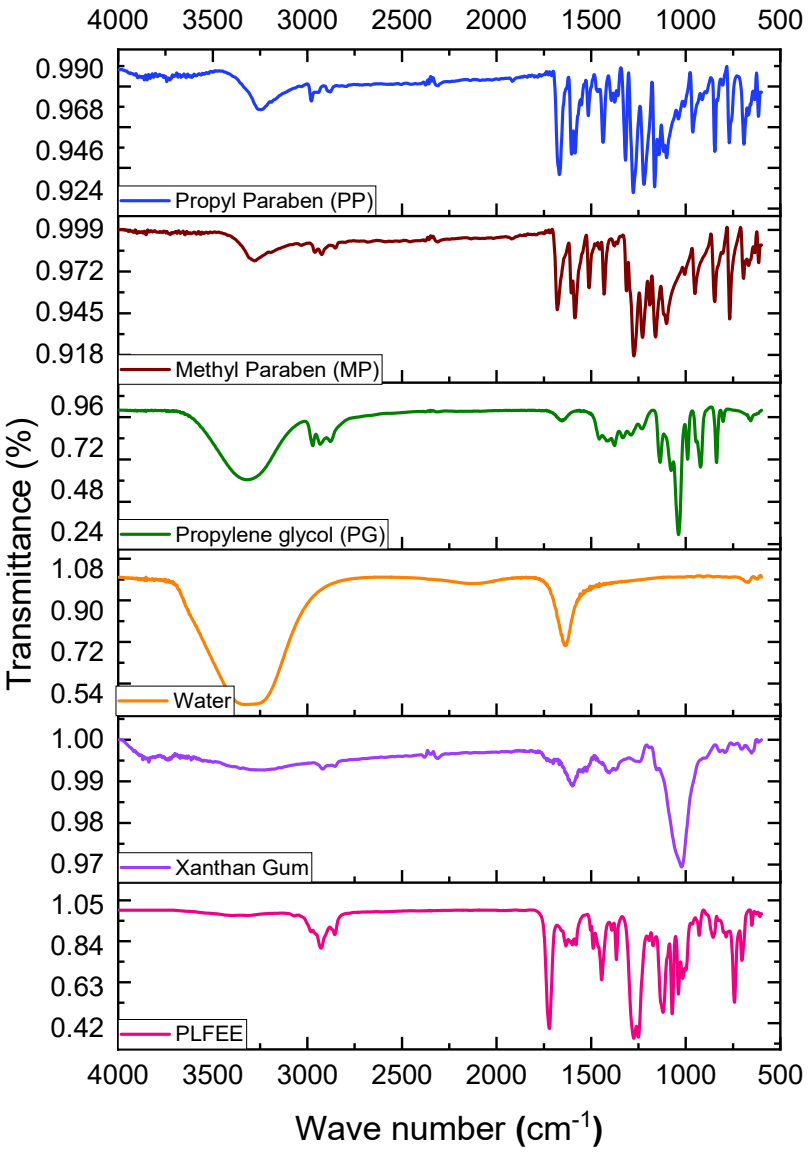

Figure 7. 35 Drug excipient compatibility via ATR-FTIR: FTIR spectra of gel formulation components (PLFEE, xanthan gum, water, propylene glycol, methyl paraben, and propyl paraben)

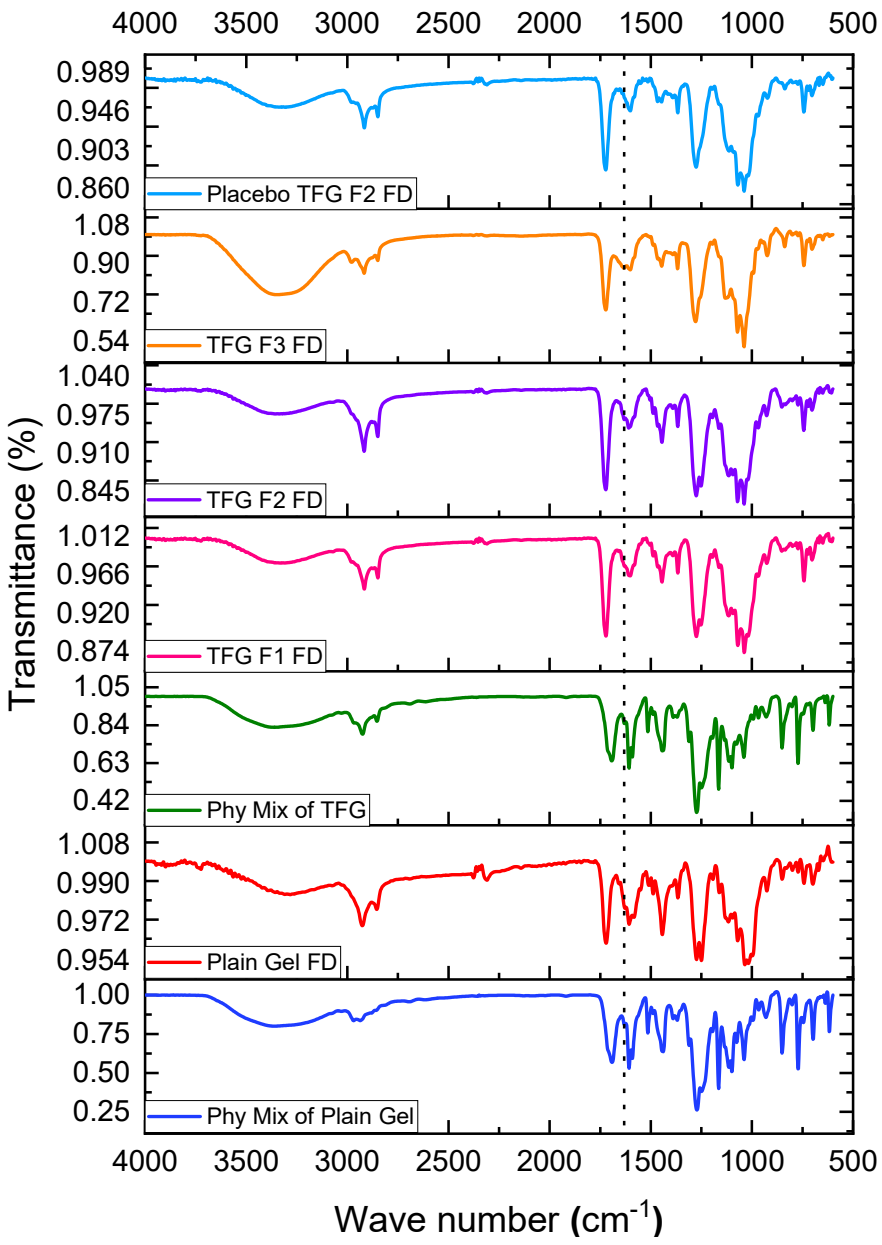

Figure 7. 36 Drug excipient compatibility via ATR-FTIR: FTIR spectra of physical mixture of gel formulations (physical mixture of plain gel and physical mixture of TFG) and gel formulations (freeze dried TFG F1-F3, plain gel, and placebo gel TFG F2)

7.4.4.10 *In-vitro* release study and release kinetics

Based on spreadability, extrudability, syneresis, and rheological outcomes, the TFG F2 was found to be close and well comparable with the marketed gel; hence, it was used in further studies. Figure 7. 37 shows the drug release profile from PLFEE solution, optimized TFs, plain gel, and TFG F2.

The PLFEE solution showed faster drug release in the first 2 h (75.482 ± 1.426%), whereas the optimized TFs showed sustained release (32.908 ± 2.546%). The drug release from the PLFEE solution attained the plateau after 5 h, whereas the optimized TFs continuously released the drug. The optimized TFs showed a biphasic release profile, in which the initial rapid release is ascribed to the release of surface-associated/adsorbed drug followed by a sustained release profile due to the release of entrapped drug [185, 186, 197, 198]. The limited accommodation capacity of the phospholipid bilayer to a larger quantity of the drug leads to the deposition of the free drug at the surface [186]. The un-entrapped drug reached the release medium rapidly while the entrapped drug diffused slowly from the nanovesicles [185]. The sustained release of drug from the optimized TFs is ascribed to the vesicular encapsulation, which acts as a drug reservoir to release the entrapped medicament in a sustained manner, hence having the benefit over conventional dosage forms [198, 199].

The drug release from the plain gel and transgelosome (TFG F2) was found to be remarkably low than that of the PLFEE solution and optimized TFs. The relatively low % drug release from the plain gel and transgelosome (TFG F2) compared to PLFEE solution and optimized TFs are ascribed to the polymeric network of the hydrogel that hinders the drug diffusion [199].

The Kinetics of drug release from optimized TFs and TFG F2 were shown in Table 7. 14. The release profile of optimized TFs best fitted Higuchi diffusion kinetics due to the highest linearity regression coefficient (R^2) compared to the other kinetic models (Table S7). The diffusion-controlled mechanism was found to be the predominant driving force, which is in good agreement with the previous reports on transferosomes [169, 185, 198]. The value of (release exponent) "n" obtained from the Korsemeyer Peppas model was found to be 0.541, representing anomalous diffusion [90], which is mainly mediated by diffusion and matrix erosion [169]. In the case of TFG F2, the maximum R^2 value was found to be associated with Higuchi kinetics (Table S7) [184]. In addition, the value of n (0.338) was <0.45, implying the Fickian diffusion of the transgelosome.

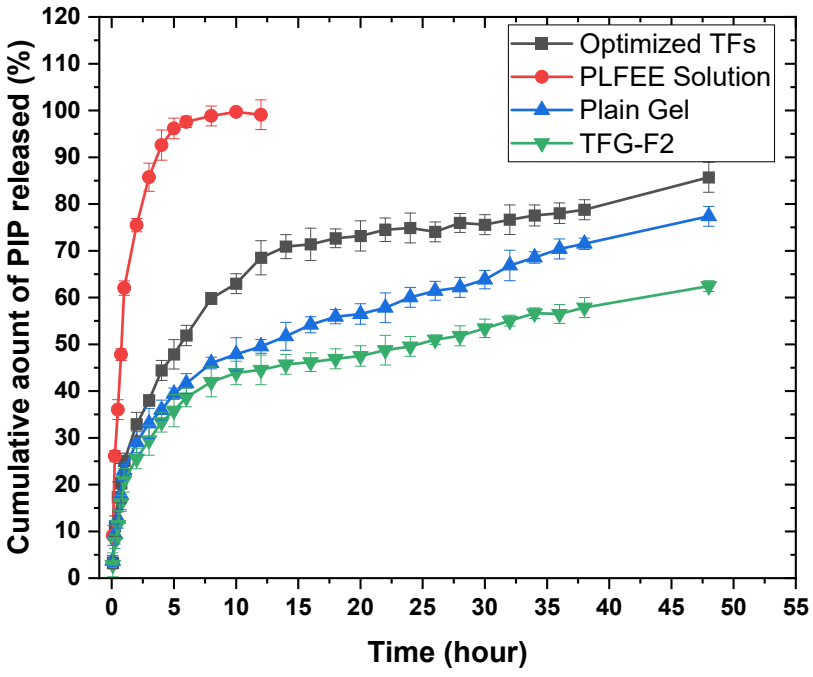

Figure 7. 37 *In-vitro* release study of optimized TFs, PLFEE solution, plain gel and TFG F2 through dialysis bag

Table 7. 14 Kinetics of drug release from optimized TFs and TFG F2

Kinetic Models	Kinetic constants and correlation coefficient	Optimized TFs	TFG F2
Zero-order	K_0	1.420	0.998
	R^2	0.726	0.763
First-order	K_1	0.015	0.007
	R^2	0.878	0.857
Higuchi Model	K_H	11.115	7.686
	R^2	**0.901**	**0.916**
Korsmeyer-Peppas model	K_{kp}	0.408	0.338
	R^2	0.898	0.906
Hixson-Crowell model	K_{HC}	0.038	0.033
	R^2	0.558	0.578
Mechanism of drug release	N	0.541	0.388
	R^2	0.913	0.906

7.4.4.11 Stability study

The stability study results of TFG F2 and plain gel under long-term stability conditions (5 ± 3°C) are presented in Table 7. 15 and Table 7. 16, respectively. The stability study results of TFG F2 and plain gel under accelerated conditions (25 ± 2°C/60 ± 5% RH) are presented in Table 7. 17, and Table 7. 18, respectively. The stability study results of the prepared gel reflected no significant changes in the evaluated parameters over time, indicating the long-term storage potential under refrigerated and room temperature. However, considering the stability of TFs vesicles at 5°C ± 3°C, the storage of transgelosome is preferred in refrigerated conditions.

Table 7. 15 Long-term stability study of TFG F2 under refrigerated conditions (5 ± 3°C)

Formulations	**TFG F2**			
	0 month	**6 months**	**9 months**	**12 months**
Appearance	White color			
Consistency and homogeneity	Gel-like consistency with smooth and homogeneous properties			
Spreadability (cm)	5.034 ± 0.048	5.012 ± 0.014	4.998 ± 0.079	4.986 ± 0.035
Extrudability (g)	154.372 ± 1.428	153.751 ± 1.547	155.368 ± 1.764	157.2 ± 1.258
pH	6.736 ± 0.018	6.657 ± 0.038	6.773 ± 0.024	6.623 ± 0.014
Viscosity (mPa.s) at a Shear rate of 25.1/sec	450.042 ± 3.464	452.034 ± 2.346	452.132 ± 2.657	450.3344 ± 3.214
Drug content (%)	98.647 ± 1.124	98.253 ± 1.233	98.147 ± 1.243	97.221 ± 1.225
Syneresis (%)	0.671 ± 0.001	0.682 ± 0.002	0.686 ± 0.001	0.693 ± 0.003
Drug-excipient compatibility	Compatible			

Results are presented as Mean ± SD

Table 7. 16 Long-term stability study of plain gel under refrigerated conditions (5 ± 3°C)

Formulations	**Plain Gel**			
	0 month	**3 months**	**6 months**	**12 months**
Appearance	Pale yellow			
Consistency and homogeneity	Gel-like consistency with smooth and homogeneous properties			
Spreadability (cm)	5.23 ± 0.089	5.211 ± 0.057	5.167 ± 0.037	5.087 ± 0.033
Extrudability (g)	146.125 ± 2.147	147.284 ± 1.234	147.873 ± 1.354	148.325 ± 1.359
pH	6.652 ± 0.035	6.643 ± 0.134	6.653 ± 0.032	6.623 ± 0.072
Viscosity (mPa.s) at a Shear rate of 25.1/sec	407.73 ± 2.137	407.123 ± 3.211	406.357 ± 2.244	407.133 ± 3.338
Drug content (%)	98.436 ± 1.159	98.124 ± 1.287	97.369 ± 1.118	97.123 ± 2.134
Syneresis (%)	0.941 ± 0.003	0.944 ± 0.002	0.953 ± 0.001	0.986 ± 0.002
Drug-excipient compatibility	Compatible			

Results are presented as Mean ± SD

Table 7. 17 Accelerated stability study of TFG F2 at 25 ± 2°C/60 ± 5% RH

Formulations	**TFG F2**		
	0 month	**3 months**	**6 months**
Appearance	White color		
Consistency and homogeneity	Gel-like consistency with smooth and homogeneous properties		
Spreadability (cm)	5.034 ± 0.048	4.987 ± 0.035	4.873 ± 0.037
Extrudability (g)	154.372 ± 1.428	156.545 ± 2.334	158.357 ± 1.887
pH	6.736 ± 0.018	6.735 ± 0.075	6.686 ± 0.055
Viscosity (mPa.s) at a Shear rate of 25.1/sec	450.042 ± 3.464	455.754 ± 2.117	457.454 ± 2.786
Drug content (%)	98.647 ± 1.124	97.754 ± 2.225	97.346 ± 1.633
Syneresis (%)	0.671 ± 0.001	0.697 ± 0.003	0.712 ±0.002
Drug-excipient compatibility	Compatible		

Results are presented as Mean ± SD

Table 7. 18 Accelerated stability study of plain gel at 25 ± 2°C/60 ± 5% RH

Formulations	Plain Gel		
	0 month	**3 months**	**6 months**
Appearance	Pale yellow		
Consistency and homogeneity	Gel-like consistency with smooth and homogeneous properties		
Spreadability (cm)	5.23 ± 0.089	5.156 ± 0.027	5.024 ± 0.044
Extrudability (g)	146.125 ± 2.147	147.317 ± 2.753	149.354 ± 1.738
pH	6.652 ± 0.035	6.655 ± 0.103	6.631 ± 0.047
Viscosity (mPa.s) at a Shear rate of 25.1/sec	407.73 ± 2.137	410.557 ± 3.154	412.857 ± 2.244
Drug content (%)	98.436 ± 1.159	97.368 ± 1.354	96.843 ± 2.433
Syneresis (%)	0.941 ± 0.003	0.988 ± 0.001	0.997 ± 0.003
Drug-excipient compatibility	Compatible		

Results are presented as Mean ± SD

7.4.5 Ex-vivo skin permeation study and permeability kinetics

Figure 7. 38 represents the cumulative drug permeated from the plain gel and TFG F2 across the C57BL/6 mice skin. The TFG F2 showed significantly ($p<0.05$) higher cumulative drug permeation than that of standardized PLFEE-loaded plain gel. The results of the permeability coefficient (Kp), steady state flux (Jss), enhancement ratio

(Er), and maximum flux (J_{max}) were shown in Table 7. 19. The Kp was found to be higher in the case of TFG F2 (0.0026 $h^{-1}.cm^{-2}$) compared to plain gel (0.0012 $h^{-1}.cm^{-2}$). The steady-state flux (Jss) of the drug from the plain gel and transgelosome (TFG F2) was found to be 1.935 ± 0.057 µg. $h^{-1}.cm^{-2}$ and 4.332 ± 0.243 µg. $h^{-1}.cm^{-2}$, respectively, achieving an enhancement ratio of 2.238. The permeation profile of the optimized TFG F2 showed a maximum flux (Jmax) value (i.e., 13.489 ± 0. 753 µg. $h^{-1}.cm^{-2}$) over plain gel (6.791 ± 0. 645 µg. $h^{-1}.cm^{-2}$). The significant improvement ($p<0.05$) of drug permeation from TFG F2 compared to the plain gel reflects the ability of vesicular hydrogel (TFG F2) to enhance drug permeation across the skin.

The improved skin permeation of various drugs (e.g., raloxifene hydrochloride [175], aceclofenac [167], 5-fluorouracil [176], ketoconazole [196], risperidone [170], diflunisal [199], and deferoxamine [164]), bioactive phytoconstituents (e.g., Colchicine, tocopherol, epigallocatechin-3-gallate, resveratrol, paeonol, and apigenin) [34], and plant extracts (e.g., flavonoids and phenolics from *Parkia speciosa*, antioxidants from *Rosmarinus officinalis*, asiaticoside from *Centella asiatica*, epigallocatechin from green tea leaf, berberine from *Berberis aristate*) [34] via TFG was reported previously.

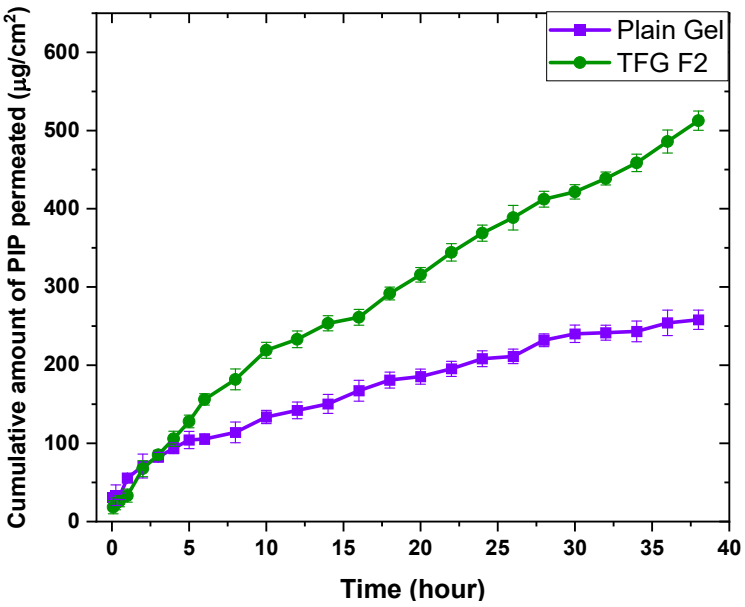

Figure 7. 38 *Ex-vivo* skin permeability of plain gel and TFG F2 through C57BL/6 female mice

Table 7. 19 *Ex-vivo* skin permeability of plain gel and TFG F2

Gel	Permeability coefficient (K_p)	Steady-state Flux (J_{ss})	Enhancement Ratio (ER)	Maximum Flux (J_{max})
	($h^{-1}.cm^{-2}$)	(µg. $h^{-1}.cm^{-2}$)		(µg. $h^{-1}.cm^{-2}$)
Plain gel	0.0012	1.935 ± 0.057	--	6.791 ± 0. 645
TFG F2	0.0026	4.332 ± 0.243	2.238	13.489 ± 0. 753

Results were represented as mean ± standard deviation (n = 3)

The stratum corneum comprises proteins and lipids layers, which are structurally arranged as "bricks and mortar" that obstruct the deeper entry of drug candidates across the skin (Figure 7. 39a). However, in the case of ultradeformable vesicular gel, the enhanced permeation of the drug was attributed to two identified mechanisms viz. (i) the maintenance of a transdermal osmotic gradient and (ii) the elastomechanics principle of ultradeformable TFs vesicles [34, 185, 199] (Figure 7. 39b). The variance of the water content between the relatively dehydrated (~15%) skin surface and the hydrated epidermis (~75%) acts as a driving force [34]. TFs have the inherent property to avoid dry surroundings (i.e., xerophobia); thus, to remain fully swollen, they tend

to move towards relatively hydrated deeper layers of skin. Further, due to their self-optimizing deformability behavior and utilizing the principle of elastomechanics, they deform/squeeze and penetrate through the tight junctions of the stratum corneum easily and rapidly by changing their shape and size [34]. Further, the edge activator (i.e., Tween® 80) also acts as a penetration enhancer that causes the architectural alteration of skin lipids by solubilization, leading to enhanced permeation of drug molecules [34, 167]. Moreover, the phospholipids possess high affinity towards the biological membrane, and along with the edge activators, they decreased the interfacial tension at the surface of the skin [198]. Also, the small size of the transferosomal vesicles increases the surface area of the formed film in contact with the skin surface which improves penetration [174].

The Kinetics of the drug permeated from TFG F2 through C57BL/6 mice skin is shown in Table 7. 20. The kinetic analysis of the drug permeated from TFG F2 through the skin revealed the Higuchi diffusion kinetics as demonstrated by the highest correlation coefficient (R^2) of the model. The obtained value (0.599) of release exponent (n) revealed the non-Fickian diffusion, anomalous transport (0.46-0.88). A similar outcome was reported elsewhere [200].

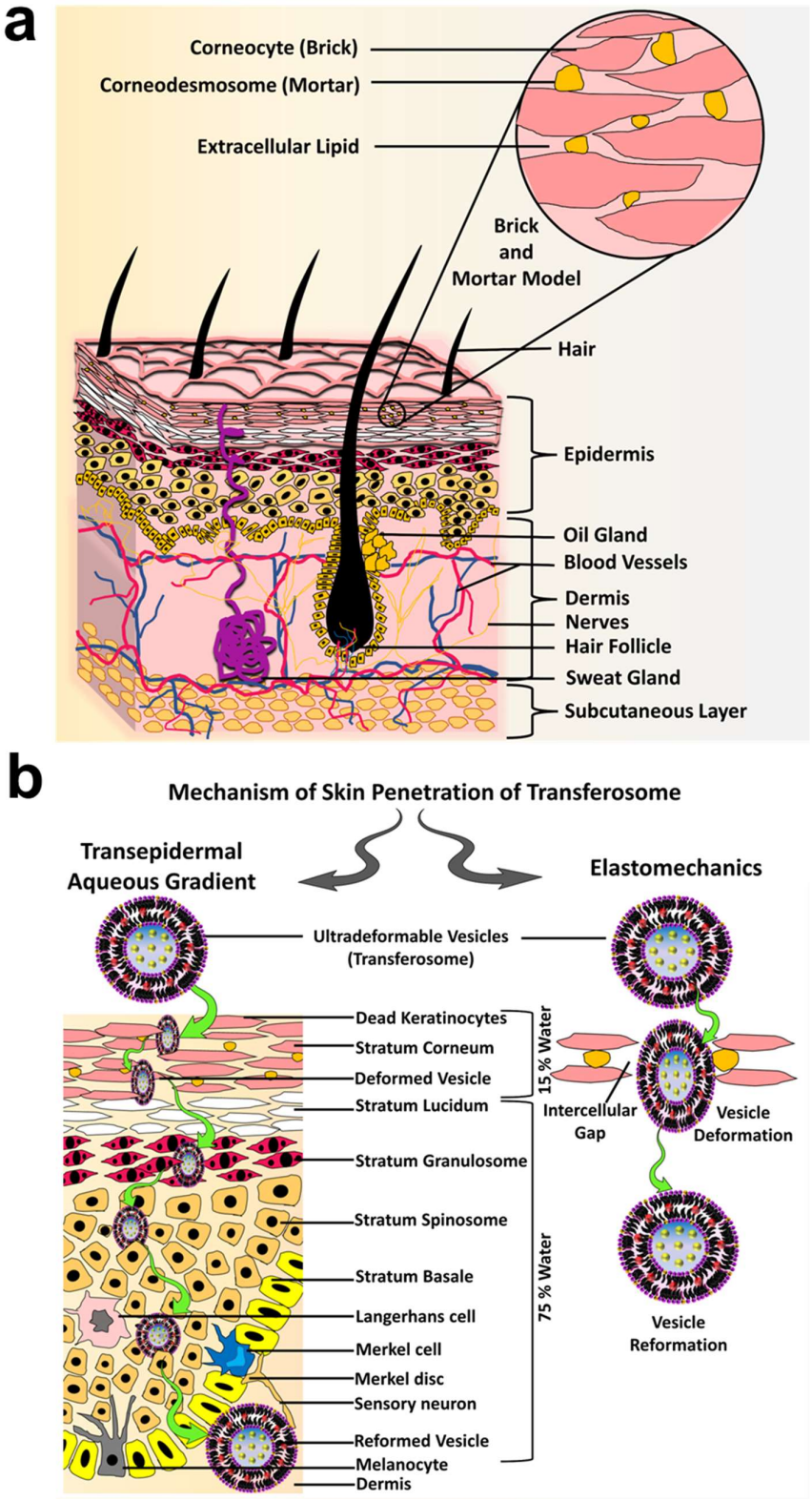

Figure 7. 39 Structure of skin and the penetration mechanism of transferosome across the skin (a) anatomy of the skin and (b) mechanism of skin penetration of ultradeformable transferosome

Table 7. 20 Kinetics of drug permeated from TFG F2 through C57BL/6 mice skin

Kinetic Models	Kinetic constants and correlation coefficient	Skin permeability of TFG F2
Zero-order	K_0	1.993
	R^2	0.980
First-order	K_1	0.016
	R^2	0.983
Higuchi Model	K_H	13.466
	R^2	0.987
Korsmeyer-Peppas model	K_{kp}	0.613
	R^2	0.977
Hixson-Crowell model	K_{HC}	0.067
	R^2	0.861
Mechanism of drug release	n	0.599
	R^2	0.970

7.4.6 Depth of skin penetration via confocal laser scanning microscopy (CLSM)

The plain gel showed very low fluorescence intensity at the deeper layer of the skin (Figure 7. 40); in contrast, the vesicular transgelosome resulted in intense fluorescence intensity, especially in the deep layers of the skin (Figure 7. 41). The transgelosome loaded with CU-6 reflect improved transdermal permeation potential and deeper skin accumulation of CU-6 than the plain gel, which is in accordance with the *ex-vivo* skin permeation results. Similar results have been observed by various researchers [35, 178, 184, 201].

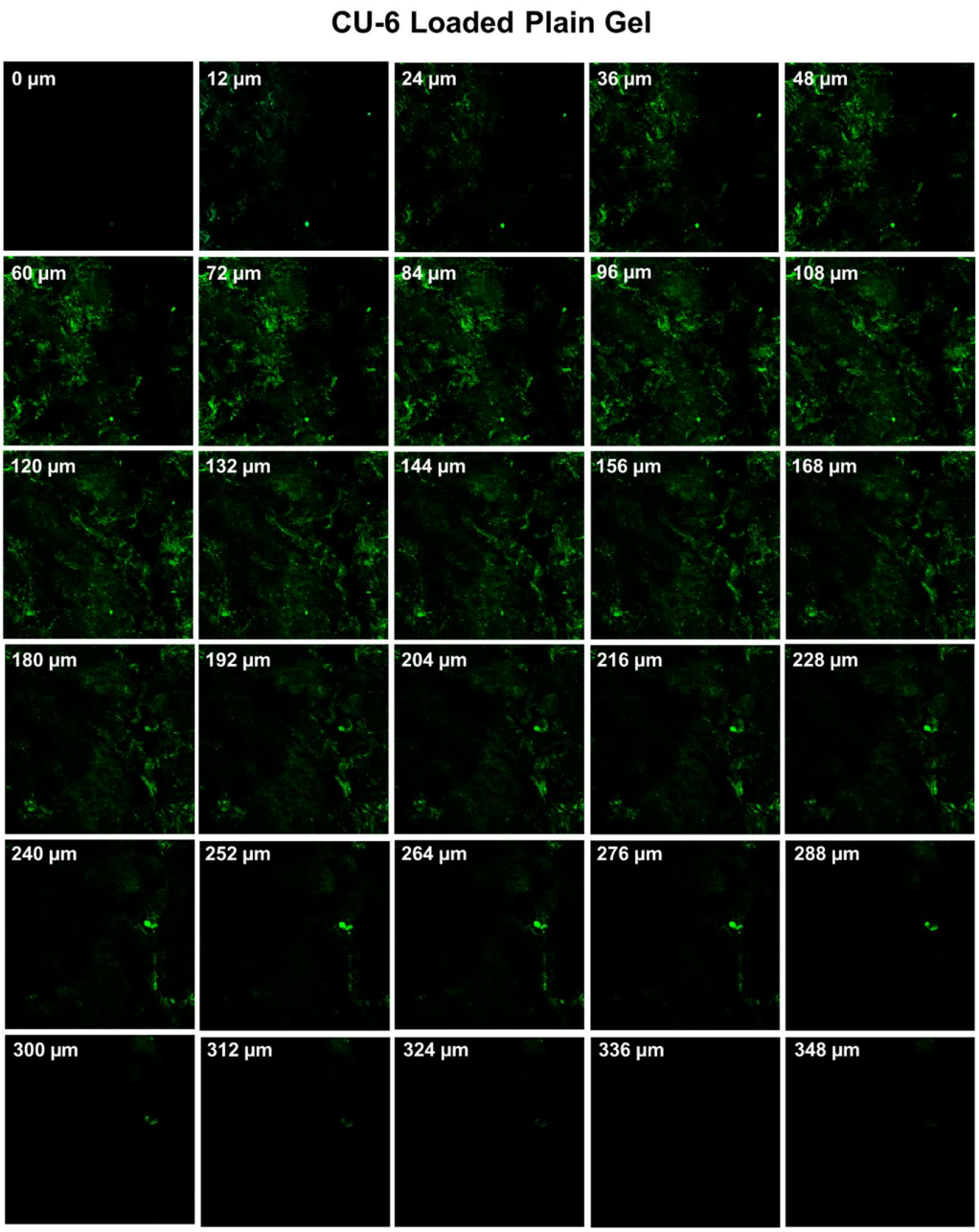

Figure 7. 40 CLSM study for the depth of CU-6 penetration into C57BL/6 skin from plain gel loaded CU-6. Each photomicrograph was captured by optical slicing of the skin from the epidermis to subcutaneous tissue by the Z-stacking feature of CLSM and the depth of each layer is marked in the figure.

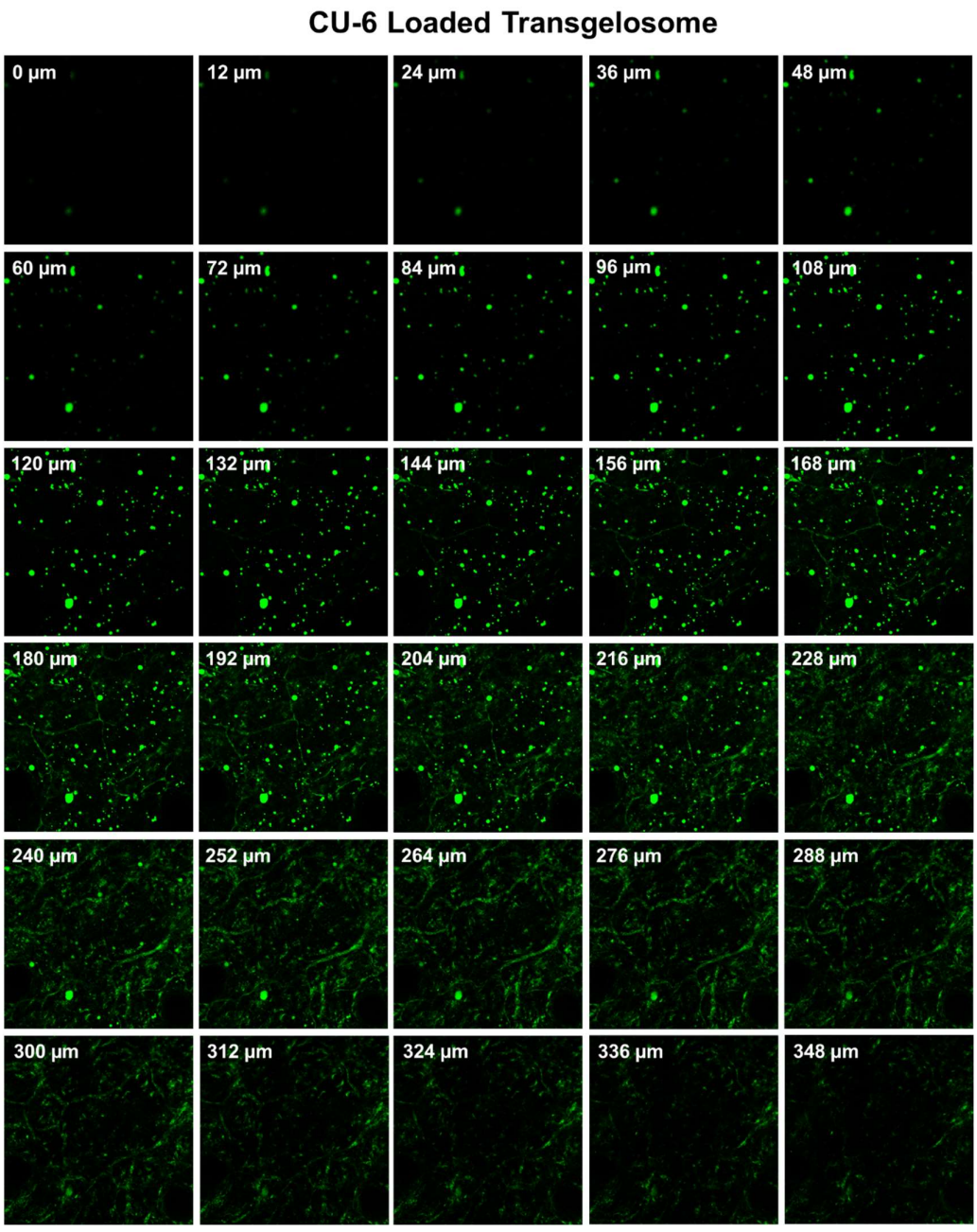

Figure 7. 41 CLSM study for the depth of CU-6 penetration into C57BL/6 skin from TFG F2 loaded CU-6. Each photomicrograph was captured by optical slicing of the skin from the epidermis to subcutaneous tissue by the Z-stacking feature of CLSM and the depth of each layer is marked in the figure.

7.4.7 Acute dermal toxicity of standardized PLFEE

The outcomes of the dermal toxicity study of standardized PLFEE were reported based on survival or death, skin color (Draize criteria), change in body weight, behavioral alterations, hematological parameters, biochemical parameters, and histopathology. No death of animals was noticed at any topical dose (200, 1000, and 2000 mg/kg) of standardized PLFEE after 14 days. The photographs of vehicle-applied control C57BL/6 female mouse and standardized PLFEE (2000 mg/kg) applied C57BL/6 mouse are shown in Figure 7. 42a and Figure 7. 42b, respectively. After topical application (after 30 min) of standardized PLFEE, a disagreeable rapid movement of animals was observed without any visual sign of skin irritation (erythema or edema). The disagreeable behavior was ascribed to the pungent principle of standardized PLFEE. Table 7. 21 represents the grading values for the primary skin irritation test and the corresponding response categories as per Draize criteria. The values (zero) of the average primary irritation index (PII) by the standardized PLFEE (2000 mg/kg) are the same as those of the vehicle-treated C57BL/6 group (Table 7. 22), representing its non-irritancy nature. The skin histopathological observations of vehicle-applied control C57BL/6 female mouse (Figure 7. 42c) and standardized PLFEE (2000 mg/kg) applied C57BL/6 mouse (Figure 7. 42d) showed no alterations of the skin anatomy. The changes in the body weight between the vehicle (water) control group (21.843 ± 2.658 g) and standardized PLFEE (2000 mg/kg) treated animals (22.138 ± 1.157 g) were found to be statistically insignificant ($p<0.05$) on 14^{th} day.

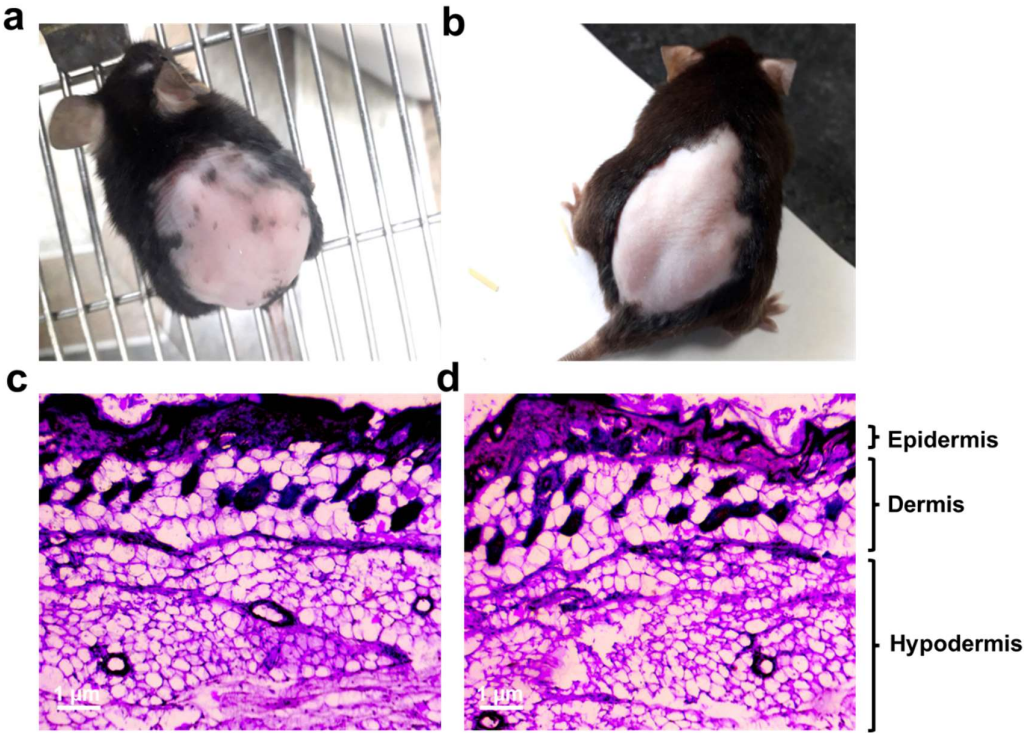

Figure 7. 42 Acute dermal toxicity study for estimation of skin irritancy (a) photograph of vehicle applied control C57BL/6 female mouse, (b) photograph of standardized PLFEE (2000 mg/kg) applied C57BL/6 mouse, (c) histopathology of vehicle applied control C57BL/6 female mouse, and (d) histopathology of standardized PLFEE (2000 mg/kg) applied C57BL/6 mouse observed at 10X magnification

Table 7. 21 Grading values for the primary skin irritation test and response categories

Skin responses	Score of primary irritation index (PII)
Erythema and Eschar Formation	
• No Erythema	0
• Very slight erythema (barely perceptible)	1
• Well-defined erythema	2
• Moderate to severe erythema	3
• Severe erythema (beet-redness) to slight eschar formation (injuries in depth)	4
Edema formation	
• No edema	0
• Very slight edema (barely perceptible)	1
• Slight edema (edges of area well-defined by definite raising)	2
• Moderate edema (raised approximately 1.0 mm)	3

• Severe edema (raised more than 1.0 mm and extending beyond the area of exposure)	4
Total possible score for irritation	8
Primary irritation index (PII)	**Category**
• 0 - 0.4	Negligible
• 0.5 - 1.9	Slight irritation
• 2.0 - 4.9	Moderate irritation
• 5.0 - 8.0	Severe irritation

Table 7. 22 Reaction on skin and score of vehicle-applied control C57BL/6 female mice, and standardized PLFEE (2000 mg/kg) applied C57BL/6 mice

Formulation	Response	After time interval (h)	C57BL/6 mice				PII Score	Category
			i	ii	iii	iv		
Vehicle applied	Erythema	24	0	0	0	0	0	Negligible
		48	0	0	0	0	0	
		72	0	0	0	0	0	
	Edema	24	0	0	0	0	0	Negligible
		48	0	0	0	0	0	
		72	0	0	0	0	0	
Standardized PLFEE (2000 mg/kg) applied	Erythema	24	0	0	0	0	0	Negligible
		48	0	0	0	0	0	
		72	0	0	0	0	0	
	Edema	24	0	0	0	0	0	Negligible
		48	0	0	0	0	0	
		72	0	0	0	0	0	

PII: Primary irritation index

The biochemical parameters (Table 7. 23) and hematological parameters (Table 7. 24) of the aforementioned groups, studied after 14 days, reflected a non-significant difference ($p<0.05$).

Table 7. 23 Biochemical parameters of topically applied vehicle control C57BL/6 group and standardized PLFEE (2000 mg/kg) treated C57BL/6 group

Serum biochemical parameters	**Vehicle control C57BL/6 group**	**PLFEE (2000 mg/kg) treated C57BL/6 group**
Creatinine (mg/dL)	0.31 ± 0.031	0.34 ± 0.018
Urea (mg/mL)	40.37 ± 3.158	41.48 ± 3.163
ALP (U/L)	46.23 ± 3.784	44.55 ± 2.436
SGPT (U/L)	35.85 ± 3.565	36.132 ± 2.463
SGOT (U/L)	138.7 ± 0.312	136.2 ± 0.372
Total Cholesterol (mg/dL)	90.46 ± 3.466	92.513 ± 2.371
Triglyceride(mg/dL)	105.2 ± 2.498	103.72 ± 3.617
Glucose (mg/dL)	220 ± 9.748	222 ± 6.751
Total protein (g/dL)	6.892 ± 0.131	7.134 ± 0.533

ALP: alkaline phosphatase, SGPT: serum glutamic pyruvic transaminase, SGOT: serum glutamic-oxaloacetic transaminase. Students t-test was performed at $p<0.05$ using GraphPad Prism 5 (GraphPad Software, Inc., San Diego, California).

Table 7. 24 Hematological parameters of topically applied vehicle control C57BL/6 group and standardized PLFEE (2000 mg/kg) treated C57BL/6 group

Hematological parameters	**Vehicle control C57BL/6 group**	**PLFEE (2000 mg/kg) treated C57BL/6 group**
TLC/ WBC ($*10^3$/µL)	4.2 ± 0.732	3.9 ± 0.563
Hemoglobin (gm/dL)	13.1 ± 2.435	12.3 ± 2.498
Monocytes (%)	6 ± 1.247	7 ± 1.023
Lymphocytes (%)	57 ± 8.123	57 ± 7.423
Neutrophils (%)	35 ± 2.336	34 ± 3.643
Eosinophils (%)	2 ± 0.435	2 ± 0.543
Basophils (%)	0	0
TRBCs ($\times10^6$/ µL)	9.27 ± 0.425	9.17 ± 0.373
PCV (%) or HCT (%)	40.3 ± 4.753	41.369 ± 5.356
RDW (%)	15.7 ± 3.243	15.643 ± 2.46
MCV (fL)	44.0 ± 5.776	43.5 ± 4.147
MCH (pg)	13.5 ± 3.436	14.3 ± 2.435
MCHC (g/dL)	32.6 ± 4.573	31.5 ± 3.363
Platelet ($\times10^5$/ µL)	5.34 ± 0.382	4.956 ± 0.283

TLC: total leucocyte count, WBC: white blood cells, TRBCs: total red blood cell counts, PCV: packed cell volume or HCT: hematocrit test, RDW: red cell distribution width, MCV: mean corpuscular volume, MCH: mean corpuscular haemoglobin, MCHC: mean corpuscular haemoglobin concentration. Students t-test was performed at $p<0.05$ using GraphPad Prism 5 (GraphPad Software, Inc., San Diego, California).

The vital organs' histology of the vehicle-treated group (Figure 7. 43a) and standardized PLFEE (2000 mg/kg) applied C57BL/6 group (Figure 7. 43b) displayed branching myocytes (BM) of the heart, glomerulus (G) of the kidney, central vein (CV), and hepatic portal vein (HPV) of the liver; bronchioles (B) of the lungs, red pulp (RP) and white pulp (WP) of the spleen.

No histological changes of the vital organs were observed from the histological photomicrographs of the vehicle-applied control C57BL/6 mice group (Figure 7. 43a) and standardized PLFEE (2000 mg/kg) applied C57BL/6 mice group (Figure 7. 43b).

The overall outcomes of the acute dermal toxicity study revealed no sign of dermal toxicity in the C57BL/6 animals after topical application of standardized PLFEE, even at a higher dose (2000 mg/kg), signifying its possible pre-clinical applicability.

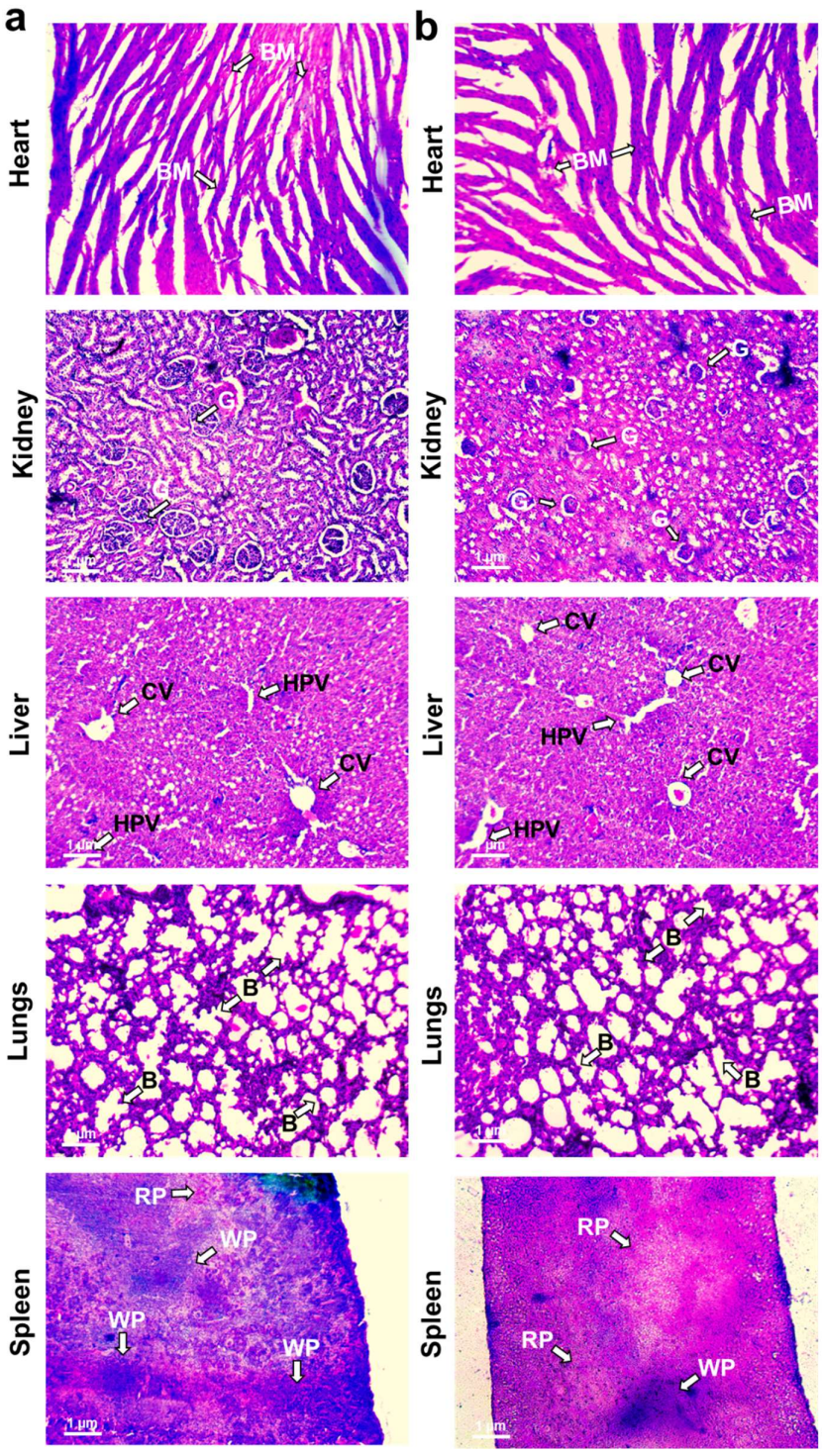

Figure 7. 43 Histopathology of heart, kidney, liver, lungs, and spleen of (a) vehicle control C57BL/6 group and (b) PLFEE (2000 mg/kg) topically treated C57BL/6 group at 10X magnification for acute dermal toxicity assessment. PLFEE: *Piper longum* fruits ethanolic extract; BM: branching myocytes; G: glomerulus; CV: central vein; HPV: hepatic portal vein; B: bronchioles: RP: and red pulp; and WP: white pulp

7.4.8 Skin irritation study

The visual outcomes of the skin irritation study were represented in Figure 7. 44, and the corresponding erythema and edema scores of the study observed at 24, 48, and 72 h were shown in Table 7. 25. The standard irritant (0.8% w/v aqueous formalin solution) showed a noticeable sign of skin irritation (Figure 7. 44a) in C57BL/6 mice. The total PII scores (erythema + edema) indicate moderate to severe irritation by the standard irritant (Table 7. 25). In contrast, the placebo gel (TFG F2) and all other gel formulations did not show any sign of skin irritation (Figure 7. 44b-d). In the case of standardized PLFEE-loaded plain gel, a rapid moment of animals was observed after 30 minutes of topical application without any visual sign of skin irritation. Such behavior of the animals is ascribed to the pungency principle of PLFEE owing to the direct contact with the skin. However, in the case of vesicular gel (TFG F2), such behavior was not noticed, which is due to the entrapment of PLFEE inside the transferosomal vesicle.

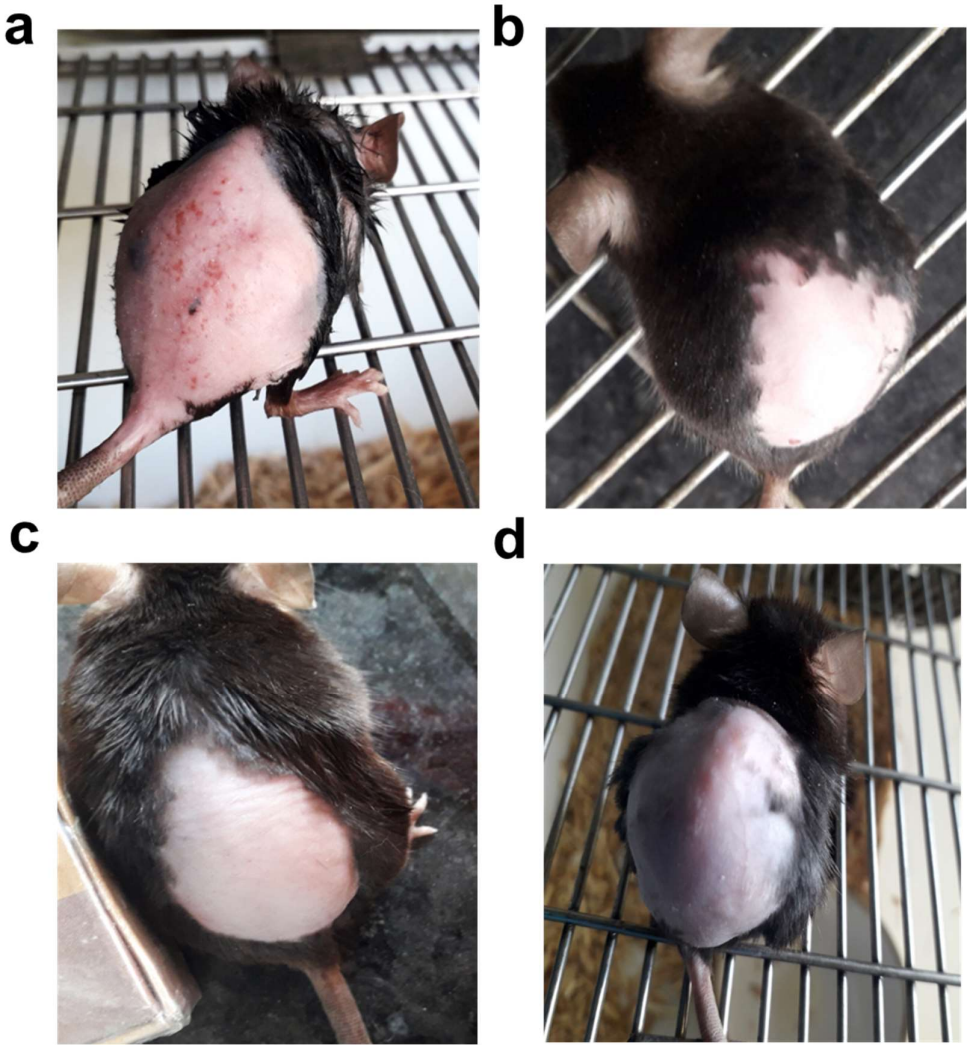

Figure 7. 44 Skin irritation study of (a) standard irritant (0.8% w/v aqueous formalin solution), (b) placebo TFG F2, (c) TFG F2, and (d) plain gel. Placebo TFG F2: Placebo transgelosome formulation TFG F2; TFG F2: Transgelosome containing optimized transferosome

Table 7. 25 Reaction on skin and score of standard irritant (0.8% v/v aqueous formalin solutions), placebo TFG-F2 (vehicle control), TFG-F2, and plain gel on femaleC57BL/6 mice

Formulation	Time (h)	PII of Erythema				Average PII score of Erythema (a)	PII of Edema				Average PII score of Edema (b)	Total irritation score (a+ b)	Category
		i	ii	iii	iv		i	ii	iii	iv			
Standard irritant	24	3	3	4	3	3.250	2	2	1	2	1.750	5	Severe irritation
	48	2	2	3	2	2.250	1	1	1	0	0.750	3	Moderate irritation
	72	2	2	2	1	1.75	1	1	0	0	0.500	2.250	Moderate irritation
Placebo TFG F2	24	0	0	0	0	0	0	0	0	0	0	0	Negligible
	48	0	0	0	0	0	0	0	0	0	0	0	
	72	0	0	0	0	0	0	0	0	0	0	0	
TFG F2	24	0	0	0	0	0	0	0	0	0	0	0	Negligible
	48	0	0	0	0	0	0	0	0	0	0	0	
	72	0	0	0	0	0	0	0	0	0	0	0	
Plain Gel	24	0	0	0	0	0	0	0	0	0	0	0	Negligible
	48	0	0	0	0	0	0	0	0	0	0	0	
	72	0	0	0	0	0	0	0	0	0	0	0	

PII: Primary irritation index

The histopathological photomicrograph of skin treated with standard irritant showed ruptured anatomy (Figure 7. 45a). In contrast, the photomicrographs of skin topically applied with placebo TFG F2, TFG F2, and plain gel showed intact skin architecture of distinct layers of skin (epidermis, dermis, and hypodermis) with no deterioration or anatomical alterations (Figure 7. 45b-d). A topical product with higher acidity or alkalinity affects the natural environment of the skin [163-165]. All the formulated gels possess a pH towards neutrality, hence having very less chance of skin irritation due to acidity and alkalinity. The overall results indicated the acceptable skin tolerability of the prepared gels. The overall skin irritation results of investigated PLFEE-loaded plain gel, TFG F2, and placebo gel showed no sign of skin irritation, demonstrating acceptable skin tolerability.

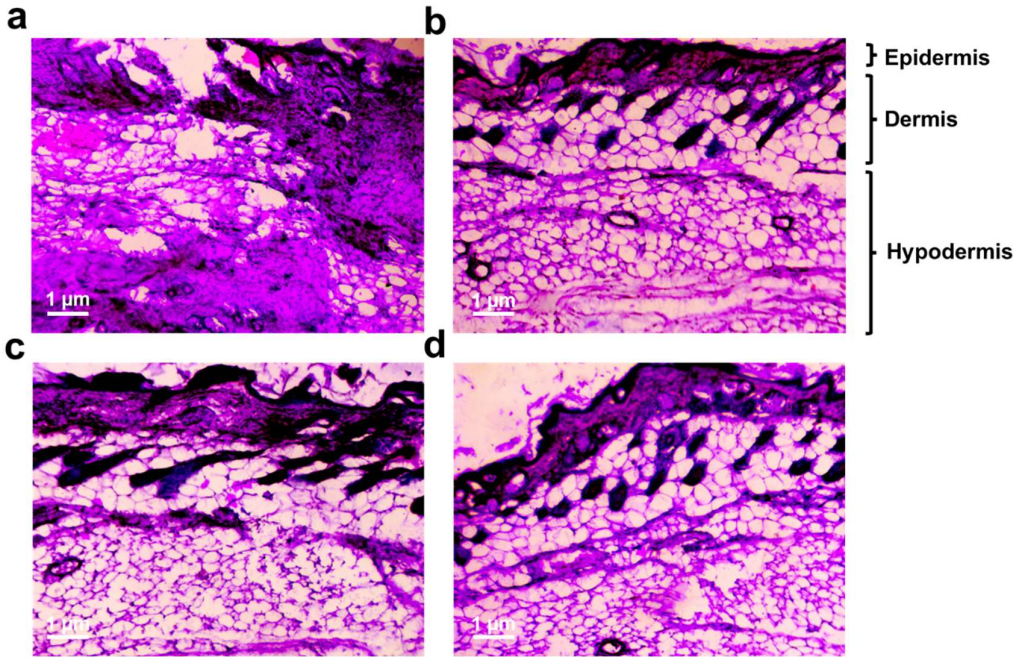

Figure 7. 45 Histopathological photomicrographs of C57BL/6 mice skin after skin irritation studies of (a) standard irritant (0.8% w/v aqueous formalin solution), (b) placebo TFG F2, (c) TFG F2, and (d) plain gel

7.4.9 *In-vivo* anticancer activity against melanoma

The *in-vivo* tumor growth was examined from the changes in body weight. The body weight of the "normal control group" was found to be increased up to the 30th day. The tumor control group displayed an early weight loss followed by rapid weight gain than normal control group and various treated groups (Figure 7. 46a). An early weight loss followed by rapid weight gain in the case of "tumor control group" than other groups is due to uncontrolled cell proliferation and tumor growth. At the end of the study, the body weight of the "tumor control group" was found to be significantly higher ($p<0.05$) than that of all treated groups. Compared to "tumor control group", all the treatment groups showed growth of body weight close to the "normal control group" due to the treatment effects.

On the 30th day, the TV of all treatment groups was found to be significantly decreased ($p<0.05$) compared to the tumor control group (Figure 7. 46b and Figure 7. 46c). The obtained tumor volume (TV) was in the order of "tumor control group" > "Plain gel group" > "TFG F2 group" > "DTIC group" > "DTIC + Plain gel" > "DTIC + TFG F2" group. The TFG F2 significantly decreased ($p<0.05$) the tumor volume in "Plain gel" and "Tumor control" groups. The DTIC showed a significant reduction ($p<0.05$) of the TV compared to the "Tumor control" group. Further, a significant reduction ($p<0.05$) of the TV was observed in the case of "DTIC + Plain gel" group compared to the DTIC alone. In the case of the "DTIC + TFG F2" treated group, a significant reduction ($p<0.05$) of TV was noticed compared to the "DTIC + Plain gel," DTIC, and "Tumor control group" group.

The volume doubling time (VDT) of tumors in various treatment groups was prolonged compared to the "tumor control" group (Figure 7. 46d). The VDT in the

case of the TFG F2-applied group was found to be significantly increased ($p<0.05$) compared to the "Plain gel" and "Tumor-control" groups. The "DTIC + Plain gel" group displayed a significant increase in VDT compared to the DTIC and "Tumor control" groups. A further significant improvement ($p<0.05$) of the VDT was noticed in the case of the "DTIC + TFG F2" group than in the "DTIC + Plain gel," DTIC, and "Tumor control group."

The tumor weight on the 30^{th} day was shown in Figure 7. 46e. All the treatment groups displayed a significantly lower ($p<0.05$) tumor weight than the "Tumor control" group and are in accordance with the TV of the respective groups.

The % tumor growth inhibition (TGI) was found to be significantly improved ($p<0.05$) in the case of treated groups compared to the tumor control group (Figure 7. 46f). The TFG F2-applied group exhibited a significant improvement ($p<0.05$) of % TGI compared to the plain gel-applied group. The "DTIC + Plain gel" group showed a significant improvement of % TGI compared to DTIC alone. Further, the "DTIC + TFG F2" group showed a significant enhancement of % TGI compared to the "DTIC + Plain gel" and DTIC group. All the treatment groups demonstrated a % TGI of more than 50%, and a value >50% was perceived to be meaningful [48].

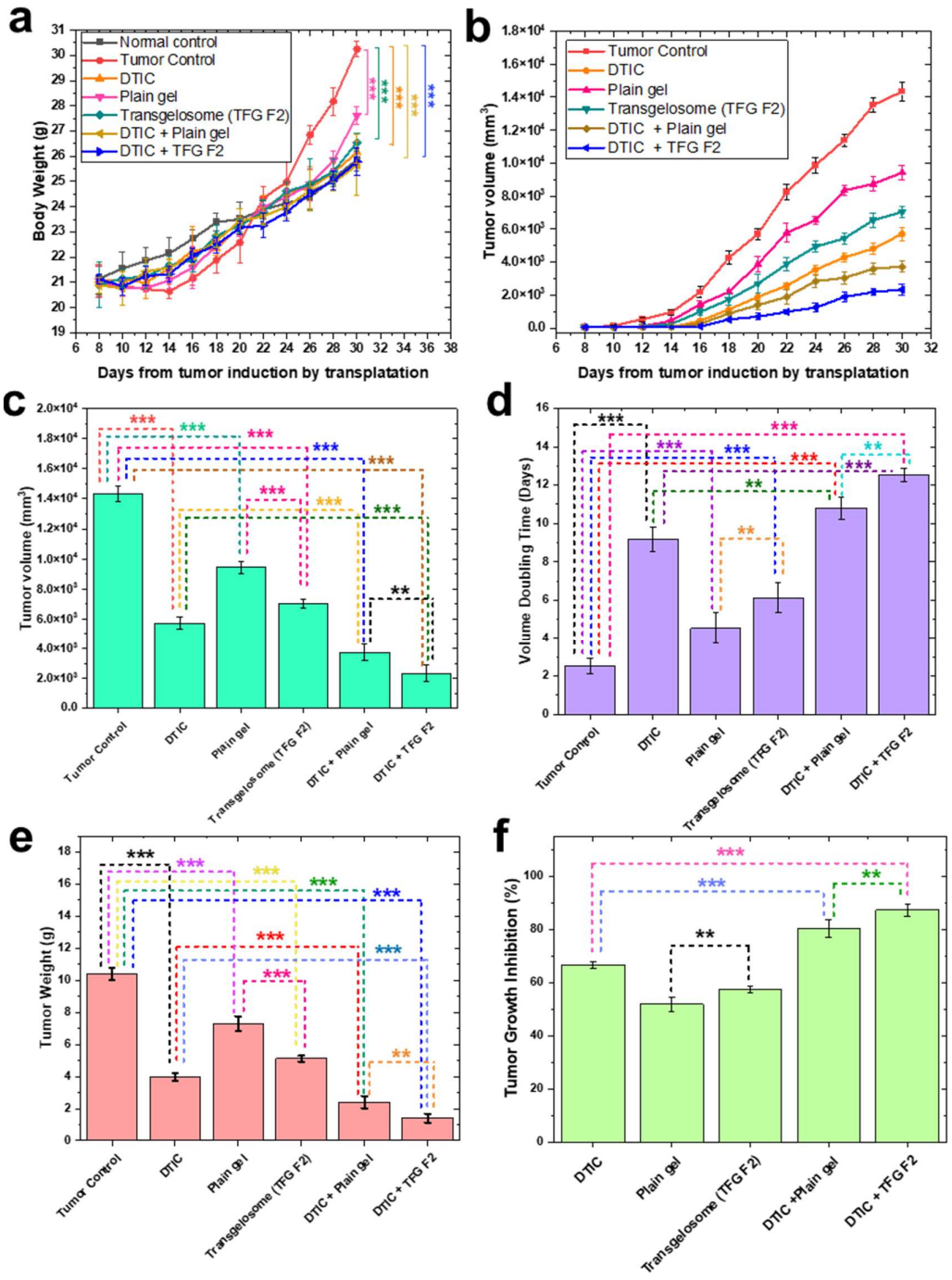

Figure 7. 46 Tumor regression analysis (a) changes in body weight, (b) tumor volume at an interval of two days after developed palpable tumor, (c) tumor volume on 30th day, (d) tumor volume doubling time (VDT) of various group, (e) tumor weight at 30th day, and (f) percent tumor growth inhibition (% TGI) of various groups at 30th day. The asterisks marks (*) represent the level of significance at $p<0.05$ in all cases. The statistical analysis was performed using one way ANOVA at followed by Tukey's test $p<0.05$ using GraphPad Prism 5 (GraphPad Software, Inc., San Diego, California).

Photograph of isolated melanoma tumors from various groups of female C57BL/6 mice on 30th day is shown in Figure 7. 47a. The TV of all treatment groups was found to be decreased compared to the "tumor control group".

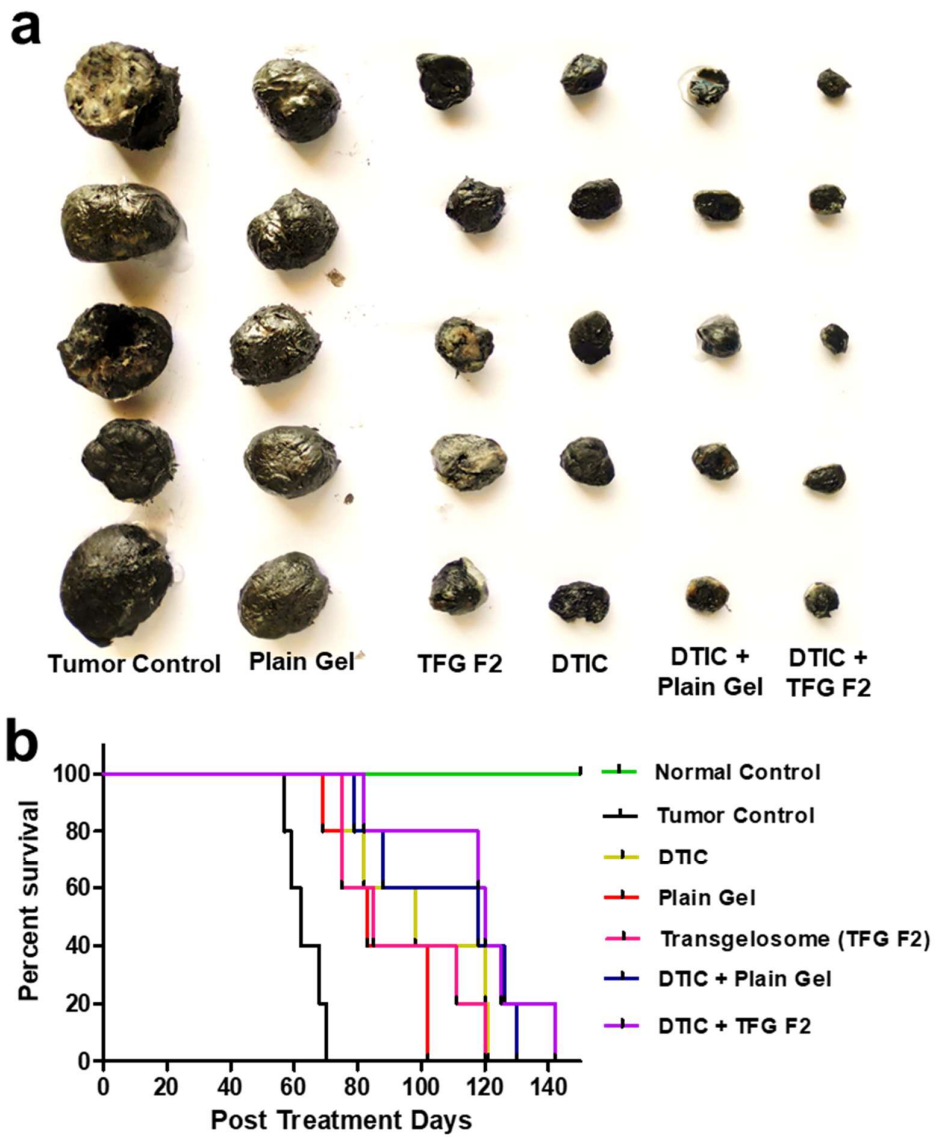

Figure 7. 47 Photographs of isolated tumor and life expectancy study (a) photograph of representative tumors from each group on 30th day, (b) life expectancy study

The life span of all treated groups was prolonged compared to the “Tumor control” group. The percent survivorship of different groups was represented as a Kaplan-Meier survival plot (Figure 7. 47b). The % ILS of “DTIC,” “Plain gel,” “TFG F2”, “DTIC + Plain gel,” and “DTIC + TFG F2” were found to be 56.962, 36.392, 47.468, 71.202, and 85.759%, respectively. The prolongation of the life span by 25% or more over that of tumor control was considered an effective antitumor activity [48].

The histopathological photomicrographs of healthy skin, skin over melanoma tumor, and tumor tissues from female C57BL/6 mice of tumor control and various treatment groups were shown in Figure 7. 48. The histology of healthy skin (Figure 7. 48a) represented distinct layers of epidermis, dermis, and hypodermis, representing the normal anatomy of the skin. However, the photomicrograph of skin over melanoma (Figure 7. 48b) displayed destroyed anatomy and the presence of live tumor cells (LTC). The “Tumor control” group presented a larger population of LTC (Figure 7. 48c). In contrast, all the treatment groups displayed a reduced population of the LTC and a higher population of necrotic regions (Figure 7. 48d-h).

The DTIC alone caused a noticeable decrease in the LTC population as an antineoplastic drug (Figure 7. 48d). The “Plain gel” group displayed few necrotic regions (NR) with a reduction of LTC (Figure 7. 48e). The TFG F2 applied group showed a marked reduction of LTC with a relatively higher population of NR (Figure 7. 48f). A marked reduction of the LTC was observed in the case of the “DTIC + Plain gel” group with a relatively larger necrotic area (Figure 7. 48g). The “DTIC + TFG F2” group demonstrated a very low population of LTC and larger NR compared to the “DTIC + Plain gel” group (Figure 7. 48h). The overall histological outcomes presented the higher anticancer activity of standardized PLFEE-loaded TFG F2 compared to the

plain gel. Further, TFG F2 as an adjuvant treatment will improve the activity of DTIC for melanoma therapy.

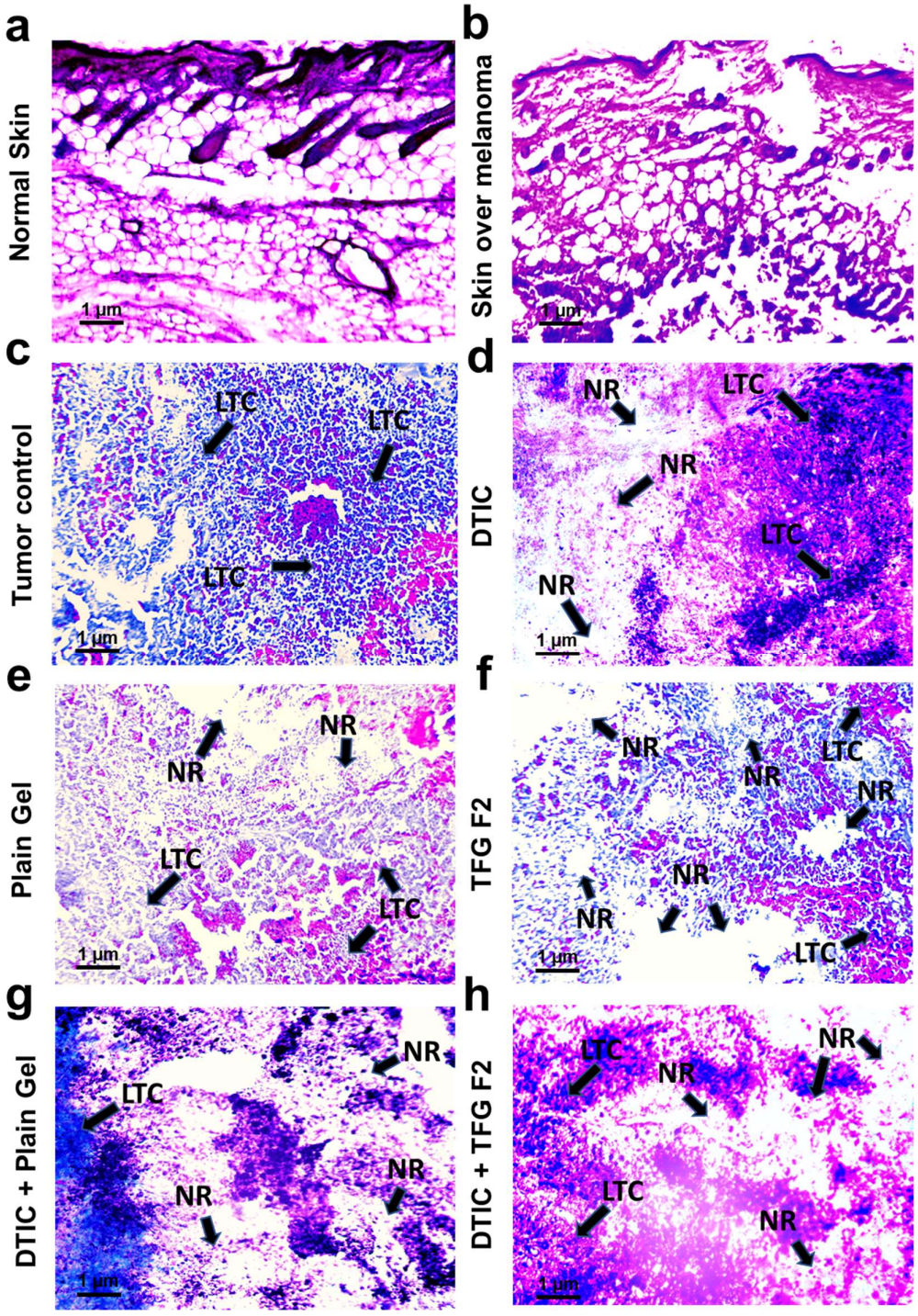

Figure 7. 48 Histopathology study of skin and melanoma tumor: histology of (A) normal skin, (B) skin over melanoma tumor, (C) tumor of tumor control, (D) tumor of DTIC treated, (E) tumor ofplain gel, (F) tumor of TFG F2treated, (G) tumor of DTIC

+ Plain geltreated, and (H) tumor of DTIC + TFG F2treated group. NR: necrotic region; LTC: live tumor cell

Overall, the *in-vivo* anticancer study revealed the potential anticancer activity of TFG F2 compared to standardized PLFEE-loaded plain gel. The significant ($p<0.05$) tumor regression results on the 30th day in the case of TFG F2 were ascribed to its improved transdermal permeability compared to the plain gel. Utilizing the circumstances of transepidermal aqueous gradient and the principle of elastomechanics, the nanovesicular ultradeformable TFs within the TFG easily permeate through the skin compared to plain gel.

7.5 Conclusions

The thin-film hydration technique was employed for the development of standardized PLFEE-loaded ultradeformable vesicles (TFs) and optimized by the QbD approach. The response surface analysis and optimization were carried out by Design-Expert® software to obtain the best TFs with good % EE, acceptable vesicle size, and flexibility. The optimized TFs demonstrated amorphous nature, nano size, excellent % EE, drug loading, flexibility, low PDI, drug-excipient compatibility, prolonged stability, *in-vitro* cytotoxicity, and uptake in B16F10 melanoma cells. Due to their low viscosity, the optimized TFs were incorporated into Xanthan gum-based hydrogel to develop transgelosome for transdermal application. The transgelosome (TFG F2) showed excellent organoleptic possessions, consistency, homogeneity, spreadability, extrudability, rheological properties, syneresis, drug content, content uniformity, drug excipient compatibility, and stability. The *ex-vivo* skin permeability and CLSM revealed the improved skin permeability of TFG F2 compared to the plain gel.

The acute dermal toxicity study (OECD 402) via skin irritation, biochemical, hematological, and histopathological observations revealed the nontoxic nature of the

standardized PLFEE. The skin irritation study revealed the nonirritating nature of TFG F2.

The *in-vivo* anticancer activity of standardized PLFEE-loaded plain gel was studied and compared with that of the PLFEE-loaded ultradeformable vesicular TFG F2 gel. The results of the tumor regression study in melanoma (B16F10) bearing C57BL/6 mice model revealed improved therapeutic activity of TFG F2 compared to plain gel. Moreover, the TFG F2 also enhanced the anticancer activity of DTIC as an adjuvant therapy. The overall outcome revealed the potential of formulated PLFEE-loaded vesicular transgelosome (TFG F2) for melanoma cancer therapy either alone or as an adjuvant therapy with DTIC.

7.6 Summary points

- Melanoma is one of the most aggressive and deadly forms of skin cancer, and plant-based therapeutics have shown their therapeutic potential against melanoma.
- Skin, mainly the stratum corneum (SC), averts the deeper entry of therapeutics as well as harmful substances from the outer milieu.
- Novel ultradeformable phospholipid-based transferosomal vesicles (TFs) containing standardized *Piper longum* fruits ethanolic extract (PLFEE) were successfully prepared by thin film hydration method through Quality-by-Design (QbD) approach.
- Central Composite Design (CCD)-based response surface analysis and optimization was carried out by Design-Expert® software for obtaining optimal TFs formula with high % EE, acceptable vesicle size, and flexibility.
- Compared to unformulated plain PLFEE, the PLFEE-loaded optimized TFs showed excellent pharmaceutical possessions with improved *in-vitro* cytotoxicity against B16F10 melanoma cells. The Coumarin-6 (CU-6) loaded optimized TFs also revealed intense fluorescence and

enhanced *in-vitro* cellular uptake compared to neat CU-6 in the B16F10 cell line.

- To improve the topical applicability, the optimized TFs were successfully incorporated into xanthan gum-based hydrogel to develop transgelosome.
- The transgelosome (TFG F2) demonstrated excellent pharmaceutical possessions, non-irritant, with improved *ex-vivo* skin permeability and deeper depth of penetration compared to the plain gel.
- The tumor regression analysis in melanoma (B16F10) bearing C57BL/6 mice model revealed improved therapeutic activity of TFG F2 compared to plain gel.
- The TFG F2 also enhanced the anticancer activity of the standard anticancer drug dacarbazine (DTIC) as an adjuvant therapy. The overall outcome revealed the potential of vesicular transgelosome (TFG F2) for melanoma cancer therapy.